

FROM HAYABUSA TO HAYABUSA2: PRESENT STATUS AND PLANS OF CURATORIAL WORKS FOR JAXA'S ASTEROIDAL SAMPLE RETURN MISSIONS.

T. Yada¹, K. Sakamoto¹, M. Yoshitake¹, K. Kumagai², M. Nishimura², K. Yogata¹, Y. Nakano⁴, S. Furuya¹, M. Abe¹, T. Okada¹, S. Tachibana³, H. Yurimoto^{1,4}, and M. Fujimoto^{1,5}, ¹Astromat. Sci. Res. Group, Inst. Space Astronaut. Sci., Japan Aerosp. Explor. Agency, 3-1-1 Yoshinodai, Chuo, Sagamihara, Kanagawa 252-5210, Japan (yada@planeta.sci.isas.jaxa.jp), ²Marine Works Japan Ltd., 3-54-1 Oppamahigashi, Yokosuka 237-0063 Japan, ³Dept. Earth Planet. Sci., Grad. Sch. Science, Univ. Tokyo, 7-3-1 Hongo, Bunkyo, Tokyo 113-0033, Japan, ⁴Dept. Earth Science, Grad. Sch. Science, Hokkaido Univ., Kita 8, Nishi 5, Kita, Sapporo, Hokkaido 060-0808, Japan, ⁵Earth-Life Sci. Inst., Tokyo Inst. Tech., 2-12-1-1E-1 Ookayama, Meguro, Tokyo 152-8550, Japan.

Introduction: The new era of sample return missions had started since the Stardust returned samples from comet 81P/Wild 2 in 2006 [1], followed by the Hayabusa spacecraft from the near-Earth S-type asteroid 25143 Itokawa in 2010 [2,3]. In this year, Hayabusa2 will reach its target body, the near-Earth C-type asteroid 162173 Ryugu [4], and also OSIRIS-REx toward the near-Earth B-type asteroid 101955 Bennu [5]. Additionally, several other sample return missions have been planned recently, such as the Martian Moons eXplorer (MMX) for the Phobos and/or Deimos [6], the CAESAR for 67P/Churyumov-Gerasimenko [7], and the HELACLES for the Moon [8]. Therefore, returned-sample curation is increasing its importance in those sample return missions, in order to maximize scientific gains of their missions. The Astromaterial Science Research Group (ASRG) of JAXA has been managing curatorial works of Hayabusa-returned samples since its return in 2010, and preparing for sample curation of Hayabusa2 samples, which is planned to be returned in 2020.

Present status of curatorial works for Hayabusa-returned samples: Major advantages of the returned samples by missions compared with meteorites and cosmic dust found on the Earth are contamination control against the terrestrial environment and identification of their sampling bodies and positions. In order to keep these advantages of Hayabusa-returned samples, the ASRG developed the clean chambers in ultra-pure nitrogen or ultra-high vacuum conditions not to expose samples to the terrestrial atmosphere and contaminate them with the terrestrial detritus grains. They are installed in a cleanroom of class better than 1,000 in Fed. Std. 209E [3]. Environments of both the cleanroom and clean chambers have been monitored periodically by silicon wafers exposure method assisted by chemical analyses with a thermal decomposition GC-MS and a vapor-phase decomposition ICP-MS [9]. We installed an electrostatically controlled micro-manipulator in the clean chamber, which have been used for handling particles of 10-300 μ m in size, recovered from the sample container returned by Hayabusa. Additionally, the particles have been transfer to the FE-SEM/EDS for initial description using a sealable sample holder without exposing to air. Then they have been given their own ID numbers and listed on the database, which is open in public on the website of the ASRG (<https://curation.isas.jaxa.jp/curation/hayabusa/index.html>). More than 700 particles have been given IDs so far, and most of them are available for the international announcement of opportunity of research, which had started since 2012 and is still going on. We plan to finish initial descriptions of whole the Hayabusa-returned samples until 2020.

Preparation status of curation for Hayabusa2-returned samples: In parallel with the curatorial works mentioned above, the ASRG has developed clean chambers for Hayabusa2-returned samples in cooperation with advisory committee of specification of curation facility for Hayabusa2-returned samples. A new cleanroom of class 1,000 had been established in last summer, in where new clean chambers for Hayabusa2-returned samples will be handled. The new clean chambers (CCs) are basically composed of five components; CC3-1, 3-2, 3-3, 4-1, and 4-2, the former three for vacuum processes and the latter two for those in purified nitrogen conditions. We plan to unclosethe sample container of Hayabusa2 and extract the sample catcher in the CC3-1, then transfer to the CC3-2 to unclosethe catcher and obtain some fraction of the samples inside the catcher in vacuum. Then the catcher will be transferred to the CC3-3 to be purged in purified nitrogen condition and further sent to CC4-1 and 4-2 to be observed by an optical microscope, weighed by a balance, and the samples in there to be extracted for further descriptions. The final parts of CCs (CC3-3, 4-1, and 4-2) are now under installation. Then the ASRG will start their functional checks after their installations, followed by a series of rehearsals for initial processes of the returned samples, which will continue until the Hayabusa2 sample return in 2020, in cooperation with the sampler team and the initial analyses team of the Hayabusa2 mission.

References: [1] Brownlee D. et al. (2006) *Science* 314, 1711. [2] Abe M. et al. (2011) *LPS XLII*, Abstract #1638. [3] Yada T. et al. (2014). *Meteoritics & Planetary Science* 49, 135. [4] Watanabe S. et al. (2017) *Space Sci. Rev.* 208, 3. [5] Lauretta D. et al. (2017) *Space. Sci. Rev.* 212, 925. [6] Fujimoto M. et al. (2017) *EPSC2017*, Abstract #136. [7] Squyres S. W. et al. (2018) *LPS XLIX*, Abstract #1332. [8] Karouji Y. et al. (2018) *New Views of the Moon 2 – Asia*, Abstract #6053. [9] Karouji Y. et al. (2014) *Chikyukagaku (Geochemistry)* 48, 211.

PHYSICAL PROPERTIES OF SILICATE-RICH REGOLITH PARTICLES FROM ITOKAWA ASTEROID

S. Tanbakouei^{1,2}, J.M. Trigo-Rodríguez^{1,2}, and J. Sort^{3,4}

¹*Institute of Space Sciences (ICE-CSIC), Campus UAB, Carrer de Can Magrans s/n, 08193 bellaterra(Barcelona), Catalonia, Spain,*

²*Institut d'Estudis Espacials de Catalunya (IEEC), C/ Gran Capità, 2-4, Ed. Nexus, desp. 201, 08034 Barcelona, Catalonia, Spain,*

³*Departament de Física, Universitat Autònoma de Barcelona, E-08193 Bellaterra, Spain,*

⁴*Institució Catalana de Recerca i Estudis Avançats, Passeig Lluís Companys 23, E-08010 Barcelona, Spain.*

Introduction: The Hayabusa spacecraft rendez-voused with asteroid 25143 Itokawa in 2005 and brought regolith samples, collected during two touchdowns carried out on 19 and 25 November 2005 in its smooth terrain (MUSES-C), and returned to Earth in a sample-return capsule in 2010 [1]. The Itokawa reflectance spectrum corresponds to that of S-type asteroids, and its bulk mineralogy is consistent with the LL group of ordinary chondrites [2]. The surface of Itokawa consists of non-uniformly distributed boulders and regolith [3]. Cratering structures on Itokawa of meter- to hundred-meter sizes have been identified [3]. Evidence of a re-arrangement of boulders and migration of regolith, possibly owing to impact or tidal shaking, has also been identified on Itokawa [3-4]. Here we concentrate in studying the mechanical and magnetic properties of three regolith particles returned by Hayabusa mission using the nano-indentation technique. Our methodology, first applied to meteorites in a previous work [5], could be used in a next future to study the properties of Ryugu materials to be returned by Hayabusa 2.

Technical Procedure: Three Itokawa particles provided by JAXA, embedded in epoxy resin and polished to mirror-like appearance, with numbers RA-QD02-0014, RA-QD02-0023 and RA-QD02-0047 (hereafter designated as S14, S23 and S47 for simplicity) were investigated. First three samples were analyzed by optical microscopy and scanning electron microscopy (SEM). A scanning electron microscope FEI Quanta 650 FEG is working in a low-vacuum BSED mode. An EDX Inca 250 SSD XMax20 detector with an active area of 20 mm² is applied for elemental analysis of the samples. Micro-Raman spectra with a spot size of approximately 1 μm and laser power below 0.6 mW were obtained in order to study the shock experienced by the samples and give us chemical and structural information of different phases. Backscatter measurements were done at room temperature using the 5145 Å line of an Argon-ion laser with a Jobin-Yvon T-64000 Raman spectrometer attached to an Olympus microscope which equipped with a liquid nitrogen-cooled CCD detector. The Raman spectrometer is working in windows between 100 and 1400 cm⁻¹ to acquire high resolution spectra.

The mechanical properties (hardness and reduced Young's modulus) were evaluated by the method that Oliver and Pharr (1992) first used. We choose the maximum applied forces of 5 mN and 10 mN in order to keep the maximum penetration depth below one fifth of the overall thickness of the sample. We applied some necessary corrections for the contact region and adoption of the instrument. We also kept the thermal drift below 0.05 nm·s⁻¹. The contact stiffness, was defined as:

$$S = dP/dh \quad (1)$$

P denotes the applied load and h means the penetration depth during nanoindentation. P_{max} is the maximum load applied in the surface area A. Hence Hardness was calculated from the following equation:

$$S = \frac{P_{max}}{A} \quad (2)$$

The elastic recovery calculated as the ratio between the elastic energy, U_{el} -estimated from the area between the unloading indentation segment and the x-axis- and U_{tot} (U_{el}+U_{pl}, where U_{pl} is the plastic energy)- estimated as the area between the loading indentation segment and the x-axis.

We also determined the reduced Young's modulus, E_r, defined as:

$$\frac{1}{E_r} = \frac{1-\nu^2}{E} + \frac{1-\nu_i^2}{E_i} \quad (3)$$

The elastic displacements occur in all three samples, with Young's modulus E and Poisson's ratio ν, and the indenter, with elastic constants E_i and ν_i. Representative nanoindentation curves for one of the studied particles are shown in Fig. 1, from which the mean mechanical properties resulted from the analyzed region, can be extracted (Table 1).

As the hardness values are not remarkably different at 5 and 10 mN, it seems that the hardness has not affected by amount of the indentation load. It means that with our chosen loads, the strain-hardening phenomena that could happen due to the indentation size effect was avoided.

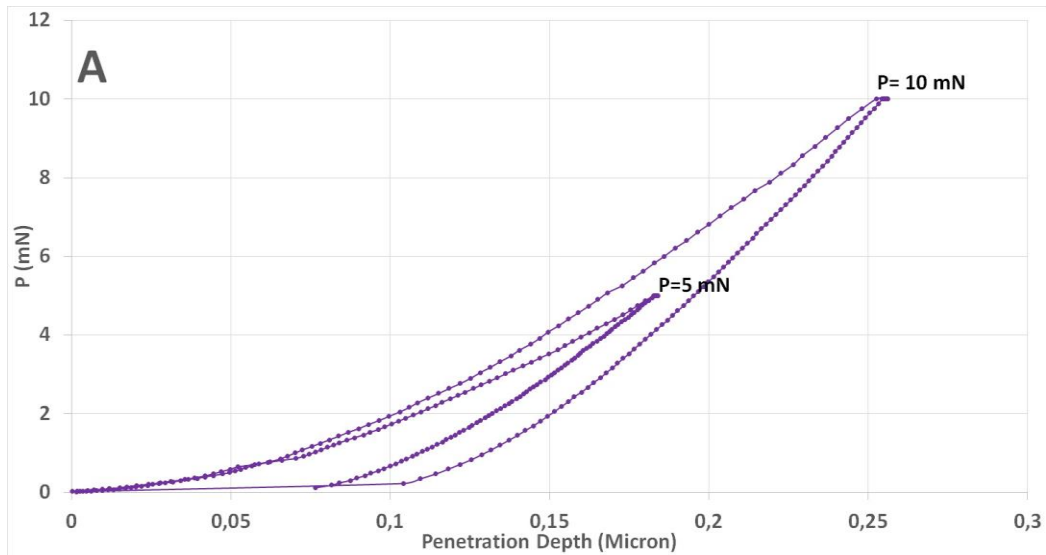


Figure 1. Indentation curve obtained for S14 sample.

Table 1. Average mechanical properties for three silicate-rich regolith particles of asteroid Itokawa. Reduced Young's modulus (E_r), hardness (H), constant stiffness (S), elastic recovery (U_{el}/U_{tot}) and plasticity index (U_{pl}/U_{tot}) were calculated by averaging the results from two lines of indentations from the maximum applied force of 5 mN.

E_r (GPa)	H (GPa)	S (mN/ micron)	U_{el}/ U_{tot}	U_{pl}/ U_{tot}
93.0 ± 0.20	10.33 ± 0.03	77.0 ± 0.20	0.75 ± 0.07	0.25 ± 0.07

Conclusions: Itokawa regolith is made of fractured particles produced by the collisional gardening of its surface along the eons. Their forming silicates are shocked, annealed and chemically homogenized, as we have also demonstrated using Raman spectroscopy [4]. This is consistent with regolith particles created by disaggregation, primarily as a response to impacts, but thermal fatigue cannot be ruled out in some cases [5]. In general, the mechanical properties of Itokawa regolith particles are comparable with silicates forming LL chondrites like e.g. Chelyabinsk. In any case, the elastic recovery of Chelyabinsk meteorite minerals exhibit lower values than these measured for Itokawa regolith grains. Despite of the homogeneous composition, we have discovered that some particles have distinctive areas that have been preferentially shocked. The induced drift in the positions of the olivine Raman peaks is due to changes in the olivine structure, typically associated with a structural rearrangement of the lattice. On the other hand, the reduced Young's modulus values obtained here for the Itokawa meteorite are above the measured for Chelyabinsk meteorite [6]. There is difference in the Young's modulus but hardness values are similar. Concerning the magnetic properties, we have found a soft magnetic behavior with a coercivity of around 70 Oe. The observed magnetic properties are consistent with the presence of tiny Fe and Ni inclusions in the samples, as was detected by energy-dispersive X-ray (EDX) analyses, leading to the formation of FeNi, FeO or FeS₂, among others.

Acknowledgements: This study was supported by the Spanish grant AYA 2015-67175-P, and ST made this study in the frame of a PhD. on Physics at the Autonomous University of Barcelona (UAB). We also thank Dr. Toru Yada and the Hayabusa curation staff of JAXA for providing the samples analyzed here.

References

- [1] Yano et al. (2006) *Science* 312, 1350–1353. [2] Abe M. et al. (2006) *Science* 312, 1334–1338. [3] Saito J. et al. (2006) *Science* 312, 1341–1344. [4] Tanbakouei S. et al. (2018) submitted [5] Matsumoto et al. (2016) *GCA* 187, 195–217. [6] Moyano-Camero C.E. et al. (2017) *ApJ* 835:157, 9 pp.

Establishing Itokawa's water contribution to Earth

Ziliang Jin¹ and Maitrayee Bose¹

¹ *Center for Isotope Analysis, School of Earth and Space Exploration, Arizona State University, Tempe, AZ 85287.*

Japan's Hayabusa mission returned with more than 1500 particles from the S-type asteroid 25143 Itokawa and provided us with a plethora of information on small (≤ 20 km) undifferentiated bodies. Different from C-type asteroids, S-type asteroids are supposed to have originated in the inner solar system [1]; and we asked the question: Could Earth have acquired its volatiles from S-type asteroid bodies like Itokawa? Water, as we know, is critical to the formation of terrestrial planets and the origin of life. Most of the inner solar system objects contain at least 200 ppm water [2-4]. Earth is unique and contains abundant liquid water with 330–1200 ppm in its primitive mantle [4]. The origin of water on Earth is highly debated. To shed light on this issue, we measured water contents and D/H ratios in low-calcium pyroxenes (LPx) from Itokawa collected from Muses sea.

The water concentrations of two Itokawa grains are 700 ± 50 ppm (2σ) and 988 ± 50 ppm (2σ). These numbers have been corrected for galactic-cosmic-ray spallation events based on the reported 8 Ma exposure age of Itokawa [5], and the H and D production rates [6, 7]. We developed a thermal-diffusion model based on the one-dimensional Fick's law to correct for water-loss events, namely thermal metamorphism and impacts [8]. Based on the mineral proportions in Itokawa (67.2 wt.% olivine, 18.1 wt.% LPx and 2.6 wt.% high calcium pyroxene) [9], the estimated water content of Bulk Silicate Itokawa (BSI) ranges from 330 to 1570 ppm. The δD values of the Itokawa LPx grains after galactic-cosmic-rays spallation correction are -61 ± 16 ‰ (2σ) for RA-QD02-0057 and -35 ± 12 ‰ (2σ) for RA-QD02-0061. The Itokawa D/H ratio is indistinguishable from those of terrestrial and lunar samples, ordinary chondrites, carbonaceous chondrites, and meteorites from Vesta and Mars. Therefore, based on the estimated BSI water contents and δD values of Itokawa, we infer that the original planetesimals, e.g. S-type asteroids, in inner solar system are hydrous and could be a potential contributor to the total water budget of Earth or inner solar system bodies.

We will present the H isotope data on Itokawa particles and LL6 LAR12036 and LL5 LAR12241 ordinary chondrites, introduce our new thermal diffusion model, and discuss the implications of these results at the meeting.

References

[1] Walsh K. J. et al. 2011. *Nature* 475: 206. [2] McCubbin F. M. et al. 2012. *Geology* 40: 683. [3] Hauri E. H. et al. 2015. *Earth and Planetary Science Letters* 409: 252. [4] Peslier A. H. et al. 2017. *Space Science Reviews* 212: 743. [5] Nagao K. et al. 2011. *Science* 333: 1128. [6] Füri E. et al. 2017. *Earth and Planetary Science Letters* 474: 76. [7] Merlivat L. et al. 1976. *Lunar and Planetary Science Conference Proceedings* 7: 649. [8] Ingrin J. and Blanchard M. 2006. *Reviews in Mineralogy and Geochemistry* 62(1): 291. [9] Tsuchiyama A. 2014. *Elements* 10 (1):45.

The origin of hydrogen in space weathered rims of Itokawa regolith particles.

L. Daly¹, M. R. Lee¹, L. J. Hallis¹, P. A. Bland², S. M. Reddy^{2,3}, D. W. Saxey³, W. D. A. Rickard³, D. Fougere^{2,3}, N. E. Timms², F. Jourdan², M. A. Cox², T. Salge⁴, H.A. Ishii⁵, J.P. Bradley⁵, J. Aguiar⁶, K. Hattar⁷, L.P. Keller⁸, M.S. Thompson⁸, R. Christoffersen⁸

¹*School of Geographical and Earth Sciences, University of Glasgow, Glasgow, G12 8QQ, UK. (luke.daly@glasgow.ac.uk).*

²*Department Earth and Planetary Science, Curtin University, GPO Box U1987, Perth, WA 6102, Australia.*

³*Geoscience Atom Probe Facility, Advanced Resource Characterisation Facility, John de Laeter Centre, Curtin University, GPO Box U1987, Perth, WA 6845, Australia.*

⁴*Imaging and Analysis Centre, Natural History Museum, Cromwell Road, London, SW7 5BD, UK.*

⁵*Hawaii Institute of Geophysics and Planetology, University of Hawaii at Manoa, Honolulu, HI, 96822.*

⁶*Idaho National Lab, Idaho Falls, Idaho, USA.*

⁷*Sandia National Laboratories, PO Box 5800, Albuquerque, New Mexico, 87185, USA.*

⁸*Robert M Walker Laboratory for Space Science, Code KR, Astromaterials Research and Exploration Science, NASA Johnson Space Center, Houston, TX, 77058, USA.*

Introduction: Space weathering is the combined action of the solar wind, solar flares, micrometeorite impacts, and galactic cosmic rays [1]. These processes alter the physical and chemical properties of surfaces exposed to the vacuum of space. Within Itokawa particles, space weathering features include 20–40 nm thick amorphous and vesiculated rims and Fe nanoparticles (n_p) [2, 3], as well as ~100–300 nm diameter micrometeorite impact craters [4]. Space weathering also implants elements contained within the solar wind, in particular the noble gases, He and Ne [5], as well as H [6]. Hydrogen is particularly important as it may react with Itokawa silicates to produce OH and H₂O; OH has been observed in space weathered rims of interplanetary dust particles [6]. The possibility of generating water through the interaction of solar wind with silicate minerals may have significant implications for the origin of water in the inner solar system. Therefore, it is important to quantify the abundance and distribution of these elements across these space weathering features, but also to ensure that such features are related to space weathering processes and not terrestrial contamination. Here we have combined field emission scanning electron microscopy (FE-SEM), transmission electron microscopy (TEM), time of flight secondary ion mass spectrometry (TOF-SIMS) and, for the first time, atom probe tomography (APT), to the study of space weathered rims in Itokawa regolith particles. For comparison, analyses were performed on San Carlos olivine reference materials that had been irradiated with low energy He or deuterium (D).

Methods: Itokawa particle RA-QD02_0279 was mounted on a glass rod (Figure 1) and particles RA-QD02_0278 and RB-CV-0087 were mounted on carbon tape. RA-QD02_0278 and RB-CV-0087 were initially characterised at the Natural History Museum to identify mineral phases and space weathering features such as micrometeorite impact craters (Figure 2) using an FEI Quanta 650 FE-SEM with an annular Bruker energy dispersive X-ray spectrometer (EDS) inserted between the pole piece and the sample. This geometry allows non-destructive analysis at sub-micron resolution of uncoated samples with substantial surface topography by using ultra low beam current (25 pA) and low accelerating voltage (6kV) under high vacuum. The particles were then sputter coated with 200 nm of Cr to protect the sample from FIB-SEM sample preparation. Using a TESCAN LYRA3 FIB-SEM at Curtin University, APT needles were extracted by focussed ion beam (FIB) techniques [7], and TOF-SIMS ion maps were acquired from RA-QD02_0279 using both a negative and positive ion beam. The resulting 100 nm diameter APT needles were analysed at the geoscience atom probe facility (Cameca LEAP 4000X HR) at Curtin

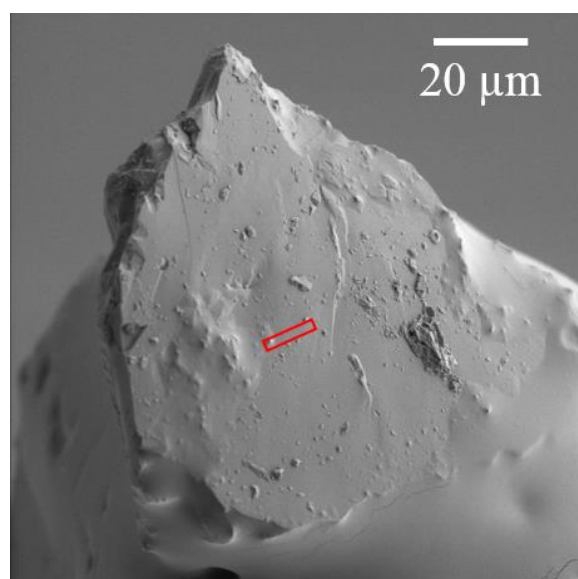


Figure 1: SE image Itokawa particle RA-QD02-0293. Atom probe specimens were extracted from the red box

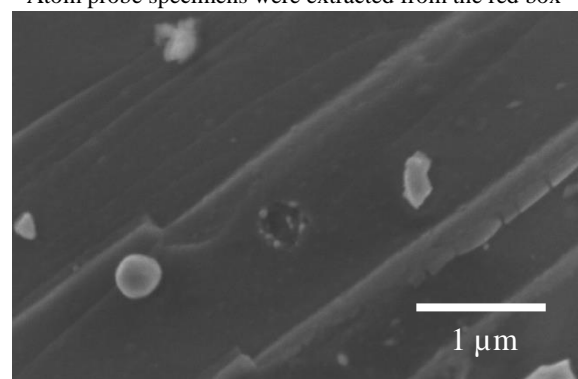


Figure 2: A SE image of a micrometeorite impact crater in Itokawa particle RA-QD02-0278.

University. Using a TESCAN LYRA3 FIB-SEM at Curtin University, APT needles were extracted by focussed ion beam (FIB) techniques [7], and TOF-SIMS ion maps were acquired from RA-QD02_0279 using both a negative and positive ion beam. The resulting 100 nm diameter APT needles were analysed at the geoscience atom probe facility (Cameca LEAP 4000X HR) at Curtin

University. Electron-transparent foils were also extracted from regions of the particles adjacent to the atom probe needles for correlative high resolution TEM and EDS. APT needles were also extracted from San Carlos olivine, both from pristine grains and from samples that had been implanted with He and D using a 10 kV Colutron accelerator.

Results and discussion: SEM imaging indicates that particle RA-QD02_0278 has several circular features on its surface that we interpret as micrometeorite impact structures (Figure 2), whereas RA-QD02_0279 and RB-CV-0087 lack such structures (Figure 1). EDS maps collected from the circular features in RA-QD02_0278 indicate that they have a similar chemical composition to the host olivine grain and so are likely to have been formed by secondary impact ejecta. Four APT datasets, each containing over 50 million ions, were collected from RA-QD02_0279 and one APT data set through a micrometeorite impact crater was collected from RA-QD02_0278. In all APT datasets evaporation commenced in the Cr coating, giving confidence that the outermost surfaces of the particles were measured, which have been potentially altered by space weathering features. The bulk chemistry derived from the APT data from RA-QD02_0279 indicate it is olivine (Fe_{30}). He and Ne were not observed in the mass spectrum and no Fe_{np} were detected. However, nanoscale domains of heterogeneous densities were observed in the outermost 20-30 nm (Figure 3). The high-density regions are enriched in Mg. Three of the four RA-QD02_0279 APT datasets show an enrichment of up to ~1.2 at. % in OH and H_2O ions that extends inwards for ~50 nm from the outer surface of the olivine particle. None of these features were observed in the pristine San Carlos olivine. TEM measurements of Itokawa, and APT data collection from the irradiated San Carlos olivine reference materials are ongoing and these results along with the implications of these new atomic scale observations will be presented at the meeting.

TEM measurements of Itokawa, and APT data collection from the irradiated San Carlos olivine reference materials are ongoing and these results along with the implications of these new atomic scale observations will be presented at the meeting.

References:

- [1] Chapman C.R., (2004) *Ann. Rev. of Earth & Planet. Sci.*, 32, 539-567. [2] Noguchi T., et al., (2011), *Science*, 333, 6046, 1121-1125. [3] Noguchi T. et al., (2014) *MAPS*, 49, 2, 188-214. [4] Harries D., et al., (2016), *EPSL*, 450, 337-345. [5] Nagao K., et al., (2011) *Science*, 333, 6046, 1128-1131. [6] Bradley J.P., et al., (2014) *PNAS*, 111, 5, 1732-1735. [7] Thompson K., et al., (2007), *Ultramic.*, 107(2), 131-139.

Acknowledgements: This work is funded by UKSTFC and a UAE seed grant. This work was performed, in part, at the Center for Integrated Nanotechnologies, an Office of Science User Facility operated for the U.S. Department of Energy (DOE) Office of Science. Sandia National Laboratories is a multi-mission laboratory managed and operated by National Technology and Engineering Solutions of Sandia, LLC., a wholly owned subsidiary of Honeywell International, Inc., for the U.S. DOE's National Nuclear Security Administration under contract DE-NA-0003525. The views expressed in the article do not necessarily represent the views of the U.S. DOE or the United States Government.

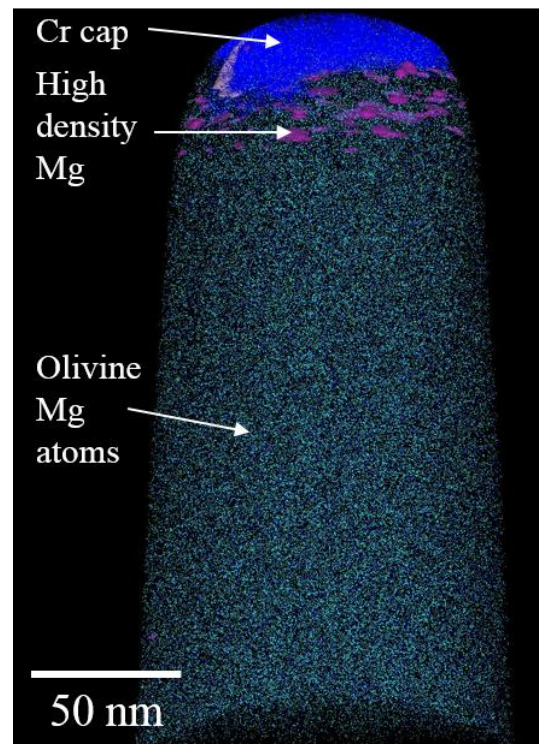


Figure 3: Atom probe needle of a space weathered rim of Itokawa. The blue and teal dots represent individual atoms of Cr and Mg, respectively. The protective Cr cap is clearly visible where the blue atoms are concentrated at the top of the needle. Pink isosurfaces depict Mg-rich, high-density regions close to the surface of the olivine grain.

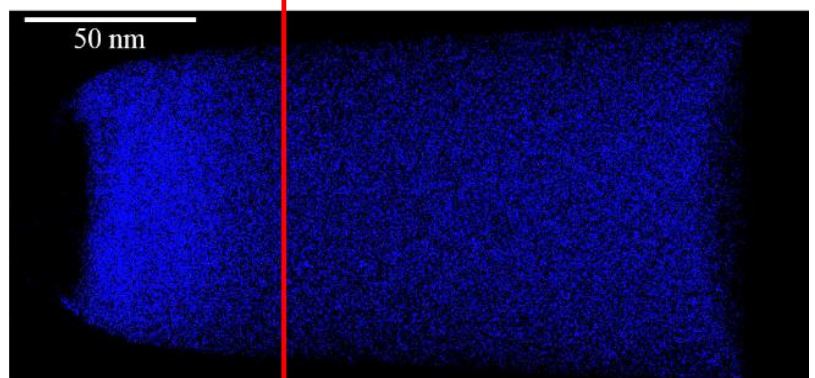
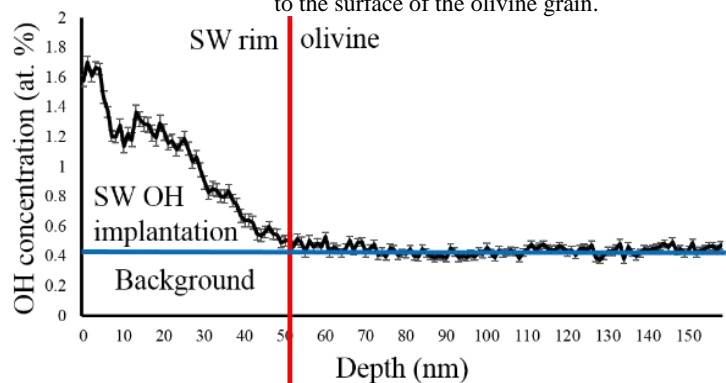


Figure 4: Atom probe needle of a space weathered rim of Itokawa. The blue dots represent OH ions, which are enriched up to 1.2 at. % in the outer 50 nm of the particle (left hand side).

Synchrotron Nanoprobe Analysis of Space Weathered Itokawa Grains

L. J. Hicks¹, J. C. Bridges¹, T. Noguchi², T. Ireland³, A. Miyake⁴, and J. D. Piercy¹

¹University of Leicester, UK (ljh47@le.ac.uk)

²Kyushu University, Japan; ³Australian National University, Australia; ⁴Kyoto University, Japan

Space weathering on Itokawa is largely the result of the bombardment by electrons and protons from the Solar Wind. Its effects are manifested by darkening and reddening of the affected surfaces [1]. In order to make the most detailed and accurate mineralogical analyses possible of space weathering effects in grains of Asteroid Itokawa, returned by the *Hayabusa* mission, we perform a multi technique characterisation of their mineralogy and isotopes at the sub-micron scale.

Five Itokawa grains allocated to this study are RB-QD04-0063, RB-QD04-0080, RB-CV-0089, RB-CV-0011, RB-CV-0148. Each were embedded in epoxy resin and ultramicrotomed for ultra-thin (~100 nm) sections which were observed using a JEOL JEM-ARM200F at the Ultramicroscopy Research Center, Kyushu University. The original potted butts were embedded again in epoxy resin to prepare polished samples 8 mm in diameter for SHRIMP analysis by using Leica EM TXP. From these embedded grains, FIB-SEM sections were obtained for TEM analyses and X-ray synchrotron nanoprobe analyses.

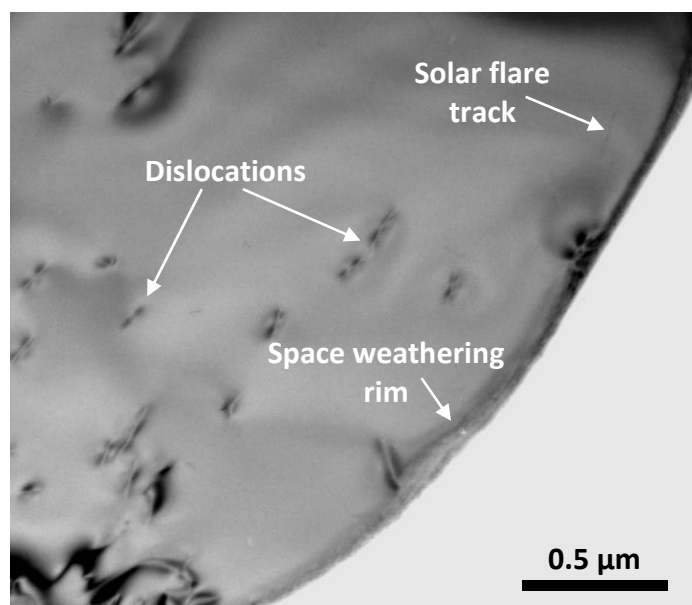


Figure 1. Bright-Field TEM image of RB-CV-0089, a low-Ca pyroxene grain featuring a <1 μm thick space weathering rim.

TEM-EDS chemical composition measurements have been performed on the FIB sections using a JEOL JEM-3200 FSK. Four of the five Itokawa grains are olivines, whereas RB-CV-0089 (shown in Figure 1) is a low-Ca pyroxene featuring high-Ca pyroxene inclusions. RB-QD04-0063 olivine grain also features plagioclase inclusions. All of the FIB sections have space weathering rims.

X-ray synchrotron analyses will be performed using the I-14 nanoprobe Beamline at *Diamond Light Source*, UK. The I-14 Beamline is capable of measuring a wide energy range (5-23 keV) down to a spatial resolution of 50 nm, and raster scanning to produce XRF/XANES mapping. Based on Fe-K X-ray Absorption Spectroscopy (XAS), we obtain high resolution XRF/XANES maps, XAS spectra, and ptychography imaging, analysing the five Itokawa grains in detail, with particular emphasis in the Fe redox changes and associated textures of space weathering. A typical Fe-K XAS measurement, for analysing the Fe redox, ranges from

7000 to 7300 eV with a higher resolution range of energy increments over the XANES features (~7100-7150 eV). The raw XAS and XANES data is then processed using *Athena 0.8.056* and *DAWN 1.9* [2]. Analysing the shifts in the Fe-K absorption edge and $1s \rightarrow 3d$ pre-edge peak centroid, and comparing to ferromagnesian silicate reference materials of known ferric-ferrous content, it is possible to semi-quantitatively deduce the oxidation state of our samples, similarly to previous studies of Itokawa, Comet Wild 2, and martian meteorite samples [3,4,5,6]. The high spatial resolution of I-14 will allow us to map the variation in Fe oxidation state across Itokawa grains and relate this to metallization associated with potential space weathering in the grains.

This X-ray nanoprobe analysis of Itokawa samples will reveal new insights into the redox changes associated with space weathering, informing further studies of other airless Solar System bodies such as the returned samples of asteroids Ryugu and Bennu from the *Hayabusa 2* and *OSIRIS-REx* missions.

References

- [1] Binzel R. P. et al. 2001. *Meteoritics & Planetary Science*, 36, 1167-1172.
- [2] Basham M. et al. 2015. *Journal of Synchrotron Radiation*, 22, 853-858.
- [3] Noguchi T. et al. 2014. *Earth, Planets and Space*, 66, 124-133.
- [4] Hicks L.J. et al. 2017. *Meteoritics & Planetary Science*, 52, 2075-2096.
- [5] Changela H. G. 2012. *Geochimica et Cosmochimica Acta*, 98, 282-294.
- [6] Hicks L.J. et al. 2014. *Geochimica et Cosmochimica Acta*, 136, 194-210.

Collisional fragmentation of an olivine-enstatite-rich Itokawa particle

Agnese Fazio¹, Dennis Harries¹ and Falko Langenhorst^{1,2}

¹*Analytical Mineralogy of Nano- and Microstructures, Institute of Geosciences, Friedrich Schiller University Jena, Germany*

²*Hawai'i Institute of Geophysics and Planetology, School of Ocean and Earth Science and Technology, University of Hawai'i at Manoa, USA (Falko.Langenhorst@uni-jena.de)*

Introduction: The regolith grains sampled and returned to Earth by the spacecraft Hayabusa from asteroid 25143 Itokawa allowed for the second time – after the Apollo missions – the direct study of space weathering effects [1] and confirmed the link between ordinary chondrites and the S-type asteroid [2]. The reported space weathering effects are due to both solar wind irradiation and impacts of micrometeoroids. They include nanocrystalline and amorphous layers [2-6], melt- and vapor-deposited layers [3, 5], and shock metamorphic features (e.g., lattice defects) [7]. In this work, we present the results of a study on grain RB-QD04-0092. This particle documents the complex dynamic evolution of the asteroid surface by impact gardening.

Sample and methods: In the context of the 4th International Announcement of Opportunity for Hayabusa sample investigation, we have received five Itokawa particles. Currently, we have focused on the investigation of particle RB-QD04-0092, which was sliced into five subsamples by focused ion beam (FIB) on a scanning electron microscope (SEM) and then studied by analytical transmission electron microscopy (TEM), following the procedure described by [6].

Observations and discussion: RB-QD04-0092 is a flat grain (29 x 25 x 8 μm) consisting of enstatite (En75-80) and olivine (Fo71-78). Numerous mineral fragments are attached to its surface (Fig. 1). They are mainly made of Mg-rich olivine, troilite, and plagioclase.

TEM reveals that the entire particle possesses a polycrystalline rim (maximum thickness 70 nm) and incipient vesicle/blister formation, indicating a moderate solar wind exposure [8]. Contrary to other observations [2], no (sulfur)-iron nanoparticles and amorphized rims were found. Solar flare tracks were observed in both enstatite and olivine with a density comparable to previously reported data ($10^8 - 10^9 \text{ cm}^{-2}$; [4, 6]).

In addition to these features, olivine and enstatite show typical shock effects known for shocked meteorites, that is: (1) screw dislocations with Burgers vector [001] in olivine and (2) (100) clinoenstatite lamellae in orthoenstatite. This is the first report of clinoenstatite lamellae in Hayabusa-returned samples. Dislocations in olivine occur localized in at least three separate sites, suggesting more than just one impact event. We found a maximum length of the [001] dislocations of 2.5-3 μm . Taking the estimated dislocation velocity in experimentally shocked olivine [9], their time of propagation and, hence, shock duration can be approximated to be of the order of 1.5 ns. This short time indicates that the multiple collisions that RB-QD04-0092 underwent must have occurred with other tiny particles or fragments in the regolith of Itokawa. Clinoenstatite lamellae are relatively short, which is also in agreement with such small-scale grain-grain collisions. However, impact microcraters are absent on the surfaces of sites with the aforementioned shock effects.

Conclusions: The absence of a well-developed amorphous rim containing nanoparticles and the occurrence of at least four sites with shock effects and no microcraters indicate that RB-QD04-0092 was involved in active regolith gardening. This collisional gardening has the effect of reducing the effective exposure time of regolith grains.

Acknowledgements

We are grateful to JAXA for providing Itokawa particles. FIB-TEM facilities at FSU Jena were funded by the Gottfried-Wilhelm-Leibniz award to FL (LA 830/14-1). AF thanks the Alexander von Humboldt Foundation for a postdoctoral grant.

References

- [1] Bennett C.J., et al. 2013 *Chemical Reviews* 113:9086. [2] Noguchi T., et al. 2011 *Science* 333:1121. [3] Thompson M.S., et al. 2014 *Earth Planets and Space* 66:89. [4] Keller L.P. and Berger E.L. 2014 *Earth Planets and Space* 66:71. [5] Noguchi T., et al. 2014 *Meteoritics & Planetary Science* 49:188. [6] Harries D. and Langenhorst F. 2014 *Earth Planets and Space* 66:163. [7] Langenhorst F., et al. 2014 *Earth Planets and Space* 66:118. [8] Harries D., et al. 2018 Abstract #368. EPSC 2018. [9] Langenhorst F., et al. 1999 *Earth and Planetary Science Letters* 173:333.

Measuring Shock Stage of Itokawa and Other Asteroid Regolith Grains by Electron Back-Scattered Diffraction

Michael Zolensky¹, James Martinez¹, Scott Sitzman², Takashi Mikouchi³, Kenji Hagiya⁴, Kazumasa Ohsumi⁵, Yasuko Terada⁵, Naoto Yagi⁵, Mutsumi Komatsu⁶, Hikaru Ozawa⁴, Yuta Taki⁴, Yuta Yamatsuta⁴, Atsushi Takenouchi³, Hikari Hasegawa³, Haruka Ono³, Kotaro Higashi³, Masaki Takata⁵, Arashi Hirata⁴, Ayaka Kurokawa⁴, Shoki Yamaguchi⁴.

¹ARES, NASA JSC, Houston, TX (USA); ²Aerospace Corporation, El Segundo, CA, (USA); ³School of Science, Univ. of Tokyo (Japan); ⁴Graduate School of Life Science, Univ. of Hyogo (Japan); ⁵Japan Synchrotron Radiation Research Institute (Japan); ⁶SOKENDAI (Japan).

Introduction: One of the fundamental aspects of any astromaterial is its shock history, since this factor elucidates critical historical events, and also because shock metamorphism can alter primary mineralogical and petrographic features, and reset sample chronologies [1-3]. Failure to take shock history into proper account during characterization can result in seriously incorrect conclusions being drawn regarding the formation and geological history of a body. Thus the Hayabusa Preliminary Examination Team (HASPET) made shock stage determination of the Itokawa samples a primary goal. However, we faced several difficulties in this particular research. The shock state of ordinary chondrite materials is generally determined by simple optical petrographic observation of standard thin sections, sometimes doubly polished but always of a uniform, set thickness. The Itokawa samples available to the analysis team were sometimes attached to carbon fibers, but more generally mounted into plastic blocks which were polished on only one side, and were of non-standard and greatly varying thickness, all of which significantly complicated petrographic analysis (but did not prevent it).

Shock State by EBSD: We made determination of the sample shock state of several Itokawa regolith grains by electron back-scattered diffraction (EBSD) [1-5]. Since EBSD is probably going to become the tool of choice for shock determination of regolith grains, we made a special effort to provide a solid foundation for this technique. Thus one goal of this work is to devise a bridge between shock determinations by standard light optical petrography, crystal structures as determined by electron and X-ray diffraction techniques [1-4]. We are comparing the Itokawa samples to L and LL chondrite meteorites chosen to span the shock scale experienced by Itokawa, specifically Chainpur (LL3.4, Shock Stage 1), Semarkona (LL3.00, S2), Kilabo (LL6, S3), NWA100 (L6, S4) and Chelyabinsk (LL5, S4). In this presentation we will concentrate on the EBSD work.

An important subtask of the EBSD work was to determine if shock state “standards” (meteorite samples of accepted shock state) show strain measurements that may be statistically differentiated, using a sampling of particles (number and size range) that may be expected from an asteroid sample-return mission. We are initially seeking “Indirect” evidence of impact shock since we are not seeking actual strain values, rather indirect strain-related measurements such as extent of intra-grain lattice rotation.

Our ultimate goal is to establish and then to apply the EBSD method, in particular, to regolith grains from near-earth asteroid Itokawa returned to Earth by the Hayabusa spacecraft, and ultimately add this capability to the planetary science tool kit for subsequent missions and their resultant returned astromaterial particles.

Our research will improve our understanding of how small, primitive solar system bodies formed and evolved, and improve understanding of the processes that determine the history and future of habitability of environments on other solar system bodies. The results will directly enrich the ongoing asteroid and comet exploration missions by NASA and JAXA, and broaden our understanding of the origin and evolution of small bodies in the early solar system, and elucidate the nature of asteroid and comet regolith.

Techniques: This work was begun under the auspices of the Hayabusa Sample Preliminary Examination Team (HASPET) activity, where many analyses were made in carefully planned sequential order, under very severe time constraints. One effect of the time constraint was that we frequently had only one opportunity to see a particular sample before it was partially or entirely consumed by a subsequent analysis. Since EBSD requires exceptionally well-polished samples we had to find a new procedure for the final polish. Rather than using water and colloidal silica, as is traditional for EBSD, we used a mixture of ethylene glycol, ethanol, glycerol, and 0.05 μm alumina, as recommended by George Vander Voort (personal communication, 2010). The resulting sample finish was slightly inferior to what could have been achieved using colloidal silica, but was adequate for our purposes.

We employed JSC’s Supra 55 variable pressure FEG-SEM and Bruker EBSD system. We were not seeking actual strain values, but rather indirect strain-related measurements such as extent of intra-grain lattice rotation, and

determining whether shock state “standards” (meteorite samples of accepted shock state, and appropriate small grain size) show strain measurements that may be statistically differentiated, using a sampling of particles (number and size range) typical of asteroid regoliths.

In order to usefully obtain and compare EBS patterns from astromaterial samples, we had to undergo a rather extensive optimization program for sample preparation and analysis settings. Unfortunately, we anticipate that each EBSD user must perform a similar procedure, especially for different SEM models. Using our system we determined that a column pressure of 9 Pa and no C-coating on the sample was optimal. We varied camera exposure time and gain to optimize mapping performance, concluding that 320x240 pattern pixilation, frame averaging of 3, 15 kV, and low extractor voltage yielded an acceptable balance of hit rate (>90%), speed (11 fps) and map quality using an exposure time of 30 ms (gain 650). We found that there was no strong effect of step size on Grain Orientation Spread (GOS) and Grain Reference Orientation Deviation angle (GROD-a) distribution; there was some effect on grain average Kernel Average Misorientation (KAM) (reduced with smaller step size for the same grain), as expected. We monitored GOS, Maximum Orientation Spread (MOS) and GROD-a differences between whole olivine grains and sub-sampled areas, and found that there were significant differences between the whole grain dataset and subsets, as well as between subsets, likely due to sampling-related “noise”. Also, in general (and logically) whole grains exhibit greater degrees of cumulative lattice rotation. Sampling size affects the *apparent* strain character of the grain, at least as measured by GOS, MOS and GROD-a. There were differences in the distribution frequencies of GOS and MOS between shock stages, and in plots of MOS and GOS vs. grain diameter. These results are generally consistent with those reported by A. Ruzicka [5]. However, it is unknown whether the differences between samples of different shock states exceeds the clustering of these values to the extent that shock stage determinations can still be made with confidence. We are investigating this by examination of meteorites with higher shock stage 4 to 5.

Grain size vs. GOS/MOS distribution: We compared the grain size vs GOS and MOS distributions for Semarkona and Chelyabinsk, which have significantly different shock histories. Significant differences between plots of GOS and MOS vs grain size are apparent, and can be proposed as factors to be used to discriminate between different shock histories. It remains to be proven that these are due to differences in the inherent properties of these samples rather than due to differences in settings used for data acquisition, or to deconvolve these two and other potential sources. Notably, MOS shows considerably less difference in “illegal zone” limit position.

Conclusions: A major question we are addressing is: Do small fragments properly represent the strain state of larger rocks? And if so, how to measure that strain? Along these lines there are some important factors to consider. Subsets of larger grains generally don’t fully represent the full range of strain behaviors exhibited by the largest grains in our EBSD maps by the strain-related measurements we’re using (GOS, MOS, GROD-a, KAM and grain averaged KAM). There is not a 100%, completely clear relationship between grain size and GOS/MOS. However, a very preliminary comparison between Semarkona and Chelyabinsk indicated a significant strain difference, using GOS. Therefore, it appears that GOS can be used to reveal the impact shock histories of asteroidal samples, assuming that a sufficient number of samples or map areas are interrogated. Since there’s no strong effect of grain size on some of the most important strain-related measures (e.g., GOS and GROD-a), perhaps small particles are may be reasonably characterized by relatively pixelated maps. Our results suggest that shock strain can be best elucidated by collection of especially slow, high quality EBSD maps (e.g., 640 x 480 camera binning, >1 frame averaging), even if they’re only incrementally better than the standard balanced settings we used (320x240, 1 frame). The best results are obtained when completely comparable maps are collected. This means using identical (1) sample preparation techniques, (2) identical instrument and instrument conditions, (3) identical map settings, (4) similar mapping areas and/or number of grains. Since there are numerous SEM models being used by meteoriticists, it would be a best for a set of standard materials to be prepared and distributed in “round robin” fashion to all interested labs.

Acknowledgements: We thank JAXA for the Hayabusa samples. MEZ was supported by the NASA Hayabusa and Hayabusa2 Participating Scientist Programs.

References: [1] Zolensky et al. (2012) *Lunar and Planetary Science*, XLIII, #1477, Lunar Planet. Inst., Houston (CD-ROM); [2] Zolensky et al. (2014) *Hayabusa 2014: 2nd Symposium of Solar System Materials. Abstracts.*; [3] Zolensky et al. (2016) *Hayabusa 2016 Abstracts*; [4] Hagiya et al. (2016) *Abstracts, 79th Annual Meeting of the Meteoritical Society*; [5] Ruzicka and Hugo (2017) *80th Annual Meeting of the Meteoritical Society*, 6368.

U-Pb systematics of Hayabusa particles: Constraints on the thermal and impact histories of 25143 Itokawa

K. Terada^{1*}, Y. Sano², N. Takahata², A. Ishida³, A. Tsuchiyama⁴, T. Nakamura³, T. Noguchi⁵, Y. Karouji⁶,
M. Uesugi⁷, T. Yada⁶, M. Nakabayashi¹, K. Fukuda⁸, H. Nagahara⁸

¹ Graduate School of Science, Osaka University, Toyonaka 560-0043, Japan.

² Atmosphere and Ocean Research Institute, The University of Tokyo, Chiba 277-8564, Japan.

³ Graduate School of Science, Tohoku University, Sendai 980-8578, Japan.

⁴ Graduate School of Science, Kyoto University, Kyoto 606-8502, Japan.

⁵ Faculty of Arts and Science, Kyushu University, Fukuoka 819-0395, Japan.

⁶ JAXA, Sagami-hara 252-5210, Japan.

⁷ JASRI/SPring-8, Hyogo, 679-5198, Japan.

⁸ Graduate School of Science, The University of Tokyo, Bunkyo-ku 113-0033, Japan.

Understanding the origin and evolution of near-Earth asteroids (NEAs) is an issue of scientific interest and practical importance because NEAs are potentially hazardous to the Earth. However, when and how NEAs formed and their evolutionary history remain enigmas. Here, we report the U-Pb systematics of Itokawa particles for the first time. Ion microprobe analyses of seven phosphate grains from a single particle provide an isochron age of 4.64 ± 0.18 billion years (1σ). This ancient phosphate age is thought to represent the thermal metamorphism of Itokawa's parent body, which is identical to that of typical LL chondrites [1]. In addition, the incorporation of other particles suggests that a significant shock event might have occurred 1.51 ± 0.85 billion years ago (1σ), which is significantly different from the shock ages of 4.2 billion years of the majority of shocked LL chondrites [2] and similar to that of the Chelyabinsk meteorite [3]. Combining these data with recent Ar-Ar studies on particles from a different landing site [4], we conclude that a globally intense impact, possibly a catastrophic event, occurred ca. 1.4 Ga ago. This conclusion enables us to establish constraints on the timescale of asteroid disruption frequency, the validity of the crater chronology and the mean lifetime of small NEAs [5].

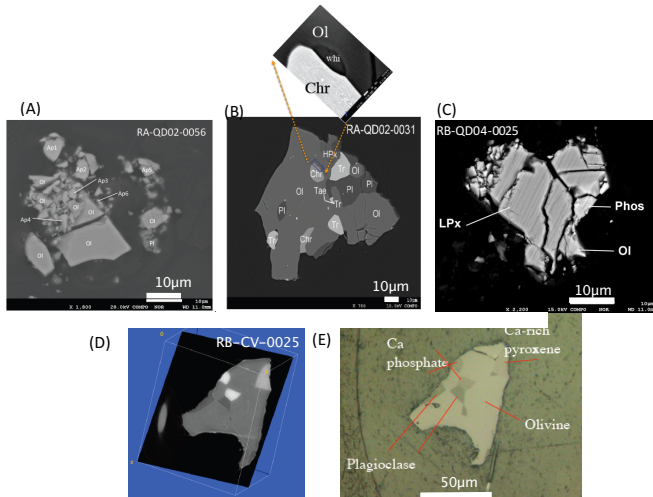


Figure 1. Cross sections of the Itokawa particles.

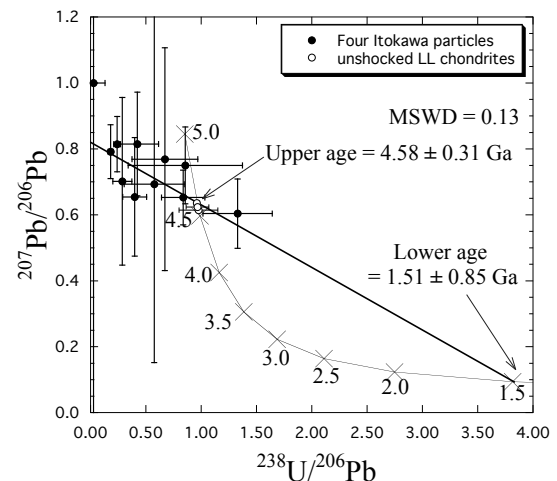


Figure 2. Tera-Wasserburg diagram of four Itokawa particles.

References

- [1] Göpel C. et al. 1944. *Earth Planet. Sci. Lett.* **121**, 157-171.
- [2] Swindle T. D. and Kring D. A. 2008. In: Workshop on Early Solar System Impact Bombardment, Lunar & Planetary Institute (abstract #3004).
- [3] Righter K. et al. (2015) *Meteoritics & Planetary Science* **50**, 1790–1819.
- [4] Park J. et al. 2015. *Meteoritics and Planetary Science* **50**, 2087-2098.
- [5] Terada et al. 2018. *Scientific Reports* **8**: 11806.

Itokawa, a >4.2 Ga old rubble pile asteroid

F. Jourdan¹, N.E. Timms¹, T. Nakamura², W.D.A. Rickard¹, E. Eroglu¹, C. Mayers¹, P.A. Bland¹, R. Oike² and T. Yada³

¹*Curtin University, Perth, GPO Box U1987, WA, Australia*

²*Tohoku University, Aoba, Sendai, Miyagi 980-8578, Japan*

³*Institute of Space and Astronautical Science, JAXA, Sagami-hara, Kanagawa 252-5210, Japan*

Asteroid 25143 Itokawa is a rubble pile asteroid consisting of reaccumulated fragments from a catastrophically disrupted monolithic parent asteroid, and from which regolith dust particles have been recovered by the Hayabusa space probe. When and how did the collision that resulted in the initial breakup of Itokawa's parent body occur? In a previous study [1], we obtained an age of 2291 ± 139 Ma on a single particle (#0013). Equilibration near the time of formation implies that this particle was formed deep inside the parent asteroid, yet a full reset of the K/Ar suggests that the particle was then close to the surface at 2.3 Ga. We then developed a novel temperature-pressure-porosity model, coupled with diffusion models to show that the relatively low pressure and high temperature involved in the impact process can be reconciled only if the asteroid was already made of porous material at ~ 2.3 Ga and thus, if asteroid Itokawa was already formed, thereby providing a *minimum* age for catastrophic asteroid breakup. In this study, we present SEM, EBSD, ToF-SIMS and $^{40}\text{Ar}/^{39}\text{Ar}$ dating results from four more particles (RA-QD02-0010, RA-QD02-0288, RB-CV-0082 and RB-QD04-1159). Unlike Particle #0013 [1], EBSD analyses show that none of these particles exhibit any noticeable sign of shock deformation, except perhaps one grain of troilite in particle #1159 which shows evidence of crystal-plastic deformation. Yet, $^{40}\text{Ar}/^{39}\text{Ar}$ analyses show the K/Ar system in all these particles has been reset at various ages.

Particle #0288 and #1159 yielded two well-defined plateau ages of 4219 ± 35 Ma ($P=0.58$) and 4149 ± 41 Ma ($P=0.27$), respectively best interpreted as recording a high temperature, yet very low shock impact event. Considering that the parent planetesimal of Itokawa is unlikely to have had an internal source of heat for ~ 340 Ma after formation, the equilibrated particles must have been by then close to the surface to be exposed to any impact related thermal event. The very low level of shock indicated by EBSD analysis (<10 GPa) suggest a high porosity of 35-40 % to allow the particle to reach the level of post-shock temperature required to reset plagioclase (cf. models by Jourdan et al., [1]). This suggests that Itokawa (probably a larger version at the time) was already formed by 4.2 Ga, almost twice as long as previously estimated.

Particle #0082 is a melt rock particle which petrography has been described by Nakamura et al. [2] and Timms et al. ([3]: this meeting). EBSD analysis shows no sign of shock in the pyroxene and olivine phenocrysts present amongst the glass. Unfortunately, $^{40}\text{Ar}/^{39}\text{Ar}$ analyses did not yield any resolvable plateau age but is consistent with recoil redistribution, an artifact caused by the neutron-activation of ^{39}Ar , thus suggesting an age of age of 4.4 – 4.5 Ga. Whereas initially considered as an impact melt rock, our preferred interpretation is currently that it is a fragment of a mesostasis-bearing porphyritic chondrule produced at the birth of the solar system (Timms et al., this meeting).

Particle #0010 did not yield any plateau age but a single hump-shaped age spectrum. ToF-SIMS compositional analyses of the plagioclase revealed the presence of sub-micrometer-wide K-feldspar exsolution lamellae (antiperthite). An argon diffusion model suggests that a brief yet high temperature heating event at ~ 500 Ma is able to decouple the K-feldspar and plagioclase $^{40}\text{Ar}^*$ reservoirs and reproduce the observed single hump-shape spectrum.

Conclusions: Plagioclase-bearing equilibrated particles have recorded a series of impact events $\{\sim 500$ Ma, 1350 ± 250 Ma (multi-particles, [3]), 2291 ± 139 Ma [1], 4149 ± 41 Ma and 4219 ± 35 Ma $\}$ best interpreted as occurring at / or near the surface of Itokawa, which implies a larger version of the rubble pile was already formed by at least ~ 4.2 Ga. This suggests that rubble pile asteroids can survive ambient solar system bombardment for extremely long periods. Such a long-term survival makes sense considering that the “cushiony” rubble pile nature of an asteroid makes it more prone to absorb shock during impacts without further breaking apart due to a drastically reduced radius of the impact-induced shock zone in porous media.

References

[1] Jourdan et al., 2017. *Geology* 45. [2] Nakamura et al., 2017. Hayabusa symposium 2017. [3] Timms et al., 2018. Hayabusa symposium 2018. [4] Park et al., 2015. *Meteoritics & Planetary Science* 50.

Itokawa chondrule fragment preserves evidence of proto-planetary disk processing

N.E. Timms¹, F. Jourdan¹, W.D.A. Rickard¹, T. Nakamura², D.W. Saxey¹, D. Fougereuse¹, S.M. Reddy¹, L. Daly³, P.A. Bland¹, Z. Qadir¹, R. Oike² and T. Yada⁴

¹*Curtin University, Perth, GPO Box U1987, WA, Australia*

³*Tohoku University, Aoba, Sendai, Miyagi 980-8578, Japan*

²*University of Glasgow, Glasgow, G12 8QQ, UK*

⁴*Institute of Space and Astronautical Science, JAXA, Sagamihara, Kanagawa 252-5210, Japan*

(*correspondence: n.timms@curtin.edu.au)

Particles brought back from Itokawa provide a unique opportunity to study unaltered material in their original context (i.e. without glass hydration). Here we combine time of flight secondary ion mass spectrometry (ToF-SIMS), electron backscatter diffraction (EBSD), transmission electron microscopy (TEM), energy dispersive spectroscopy (EDS), ⁴⁰Ar/³⁹Ar geochronology, and Atom Probe Tomography (APT) to examine one of the few melt rock particles recovered from the Itokawa asteroid by the Hayabusa mission [1]. This particle (RB-CV-0082) comprises 5-30 µm long crystals of high-Ca Cr-bearing pyroxene, olivine within a quenched emulsion of variable composition silicate glass. The olivine (Fa = 26.7% via APT; 27.9% via EDS) is similar in composition to other olivine from equilibrated Itokawa particles. EBSD mapping reveals that the olivine and high-Ca pyroxene phenocrysts are crystalline and do not show any evidence of shock metamorphism or deformation. Furthermore, the high-Ca pyroxene form elongate clusters of grains that have a strong crystallographic and shape preferred orientation.

TEM imaging, EBSD and TOF-SIMS (≤50 nm spatial resolution) maps show two dominant glass compositions form interconnected globules, much of which is amorphous. These segregations are Si-Al-Na-K-O-rich and Ca-Fe-Mg-Ti-O-rich, and are plagioclase and pyroxene normative, respectively. Locally, nebulous segregations of Si-Al-Na-O-rich and crystalline Mg-Fe-Si-O-rich material are associated with partially- to totally-digested olivine grains. The glass also contains ~5%vol nano-vesicles (typically 10-300 nm across), and minor nano-scale crystals of troilite and merrillite. Within the Si-Al-Na-K-O-rich regions of the glass, the alkalis (including K relevant to ⁴⁰Ar/³⁹Ar dating) are further segregated into even finer lamellae, alternating over 100 nm length scales. Further nanoscale analyses by APT constrain the compositions of fine-scale domains within the particle, demonstrating that lamellae within Si-Al-Na-K-O domains comprise end-member orthoclase and albite normative compositions, consistent with antiperthite lamellae. The ⁴⁰Ar/³⁹Ar analysis of particle RB-CV-0082 indicates an approximate age of 4.5 Ga. However, the data show that the ⁴⁰Ar/³⁹Ar analysis is likely to be affected by recoil, precluding resolution of a precise age.

The texture of RB-CV-0082 is consistent with incipient flash melting, with complete digestion of feldspar and partial digestion of olivine and pyroxene. The various glass compositions are consistent with phase separation into conjugate immiscible liquids formed by spinodal decomposition upon cooling below the upper critical solution temperature in a multicomponent oxide system, preserved by rapid quenching [2]. Subsequent crystallization of the plagioclase-normative immiscible domains to plagioclase was followed by exsolution of Na and K- rich (antiperthite) lamellae upon cooling below the feldspar solvus.

It has been reported that the regolith from the Itokawa asteroid underwent long-term thermal annealing and subsequent impact shock [4]. It is possible that an impact event could have caused flash melting and quenching of a metamorphosed olivine-pyroxene-plagioclase parent rock responsible for the texture of this particle. This melting mechanism would help explain why the relict olivine composition is similar to that of normal Itokawa olivine while preserving interstitial fine-scale glass textures. However, the lack of shock microstructures in olivine and pyroxene grains, the crystallographic alignment of elongate (barred?) pyroxene, and extremely old ⁴⁰Ar/³⁹Ar age are more consistent with a porphyritic chondrule with mesostasis origin for the particle rather than an impact melt origin. As such, this particle provides more insight into chondrule formation within the proto-planetary disk than the history of the Itokawa parent body. Nevertheless, the preservation of such fine-scale microstructures and compositional variations in this particle imply that it has not been extensively texturally equilibrated via recrystallisation and grain growth at high temperatures associated with thermal metamorphism on the initial Itokawa parent body (as interpreted for the majority of the Itokawa particles). Therefore, this fragment was likely to have been sourced from near the surface of the Itokawa parent body prior to breakup. The preservation of nano-vesicles indicates that the timescales of flash heating and quenching were very short and did not result in the complete loss of volatiles, which has implications for volatile retention

through chondrule formation and processing within the proto-planetary disk, as well as accretion, processing and breakup of the asteroid parent body.

References

- [1] Nakamura. T. et al. 2014. Abstract at Hayabusa 2014. [2] Hamann et al. (2017). *Meteoritics & Planetary Science* 1-39. [3] Jourdan. F. et al. 2017. *Geology* 45:819-822. [4] Nakamura. T. et al. 2011. *Science* 333:6046.

Searching for Volatiles in Space Weathered Grains

Katherine D. Burgess¹ and Rhonda Stroud¹

¹ U.S. Naval Research Laboratory, Washington, DC, USA

Space weathering alters the physical, chemical, and optical characteristics of materials on the surfaces of airless bodies. In our current understanding, solar wind ion irradiation and micrometeoroid bombardment, along with other processes, lead to the formation of thin amorphous coatings and nanophase metallic iron inclusions (npFe^0) that in turn are the main causes of darkening and reddening in the visible to near infrared wavelength region [1]. While we have been able to study lunar rocks and soils for the past almost 50 years and have gained an understanding of the main processes and effects of space weathering there, open questions about the rates at which alteration occurs and how various space weathering processes interact with each other remain. The return of samples from asteroid Itokawa has provided a new avenue for understanding the effects of space weathering and how the dominant processes can vary in different regions of the Solar System. Additionally, advances in scanning transmission electron microscopy (STEM) instrumentation and associated techniques have enabled new measurements and analyses of old and new samples and can provide new insights about space weathering processes and features [2,3].

Recent work on space weathered grains from the Moon and asteroid Itokawa have demonstrated that the phase of the substrate or host grain plays a significant role in how materials are altered by solar wind irradiation and micrometeoroid bombardment [2,4]. Vesicles and/or surface blisters are observed to be present in or on some phases but not others that are directly adjacent. The presence (or lack of) vesicles in some materials, as well as whether they contain hydrogen (or water) or helium provides key information about how space weathering progresses in different phases and the relative rates of alteration.

We used focused ion beam microscopy (FIB) to prepare samples for analysis using an aberration-corrected Nion STEM equipped with detectors for electron energy loss spectroscopy (EELS) and energy dispersive X-ray spectroscopy (EDS). Spectrum image data cubes were collected in order to map changes in oxidation state, presence of volatiles, and elemental composition. FIB allows for preparation of site-selected regions of grains and allows us to maintain context and spatial relationships across phase boundaries and features of interest.

Using these methods, we have identified helium in vesicles in the rims of ilmenite grains from two different lunar soils. Figure 1 shows a small ilmenite grain attached to a larger plagioclase grain. The exposed surface of the ilmenite has a well-developed space weathered rim with npFe^0 inclusions and small vesicles. Planar defects are seen in this rim up to 135 nm from the surface. In comparison to a rim on an ilmenite grain from sub-mature lunar soil 71501 [2], the defects in the rim have high areal density. As was noted for that grain, helium implanted by the solar wind can be identified in some vesicles using EELS. The energy of the helium K-edge measured for these vesicles, 22.8 eV, is consistent with $n_{\text{He}} \sim 40 \text{ nm}^{-3}$, similar to what was seen in [2]. Thus far, helium has been identified only in vesicles or defects in oxides, not silicates, from the Moon.

Figure 2 shows scanning electron microscope (SEM) images of the surface of a multi-phase lunar grain. As noted for some Itokawa particles [4], the two phases show different surface morphology features, including blisters present on the Mg-, Fe-rich silicate phase (either olivine or pyroxene) but not the Al-rich (plagioclase) surface. The number of small (<100 nm) adhered spherical particles is also higher on the mafic grain. FIB/STEM can be used to determine if these blisters indicate the presence of vesicles and how the rim differs between these two phases across this boundary, as well as if any volatiles remain trapped in the vesicles.

The careful work on the Itokawa particles examined to date have shown the significant scientific value in each single grain through detailed comparisons with other grains, both asteroidal and lunar. Understanding how and when hydrogen and helium implanted by the solar wind coalesce into larger defects and vesicles

requires an understanding of which phases host the most vesicles, whether or not there are other features associated with these vesicles, and what other processes, such as heating, might be necessary for vesicle formation. Detailed comparisons between samples from the Moon and from Itokawa will allow for a better understanding of how location in the Solar System may affect vesicle formation and volatile trapping and how the important space weathering processes vary between those locations.

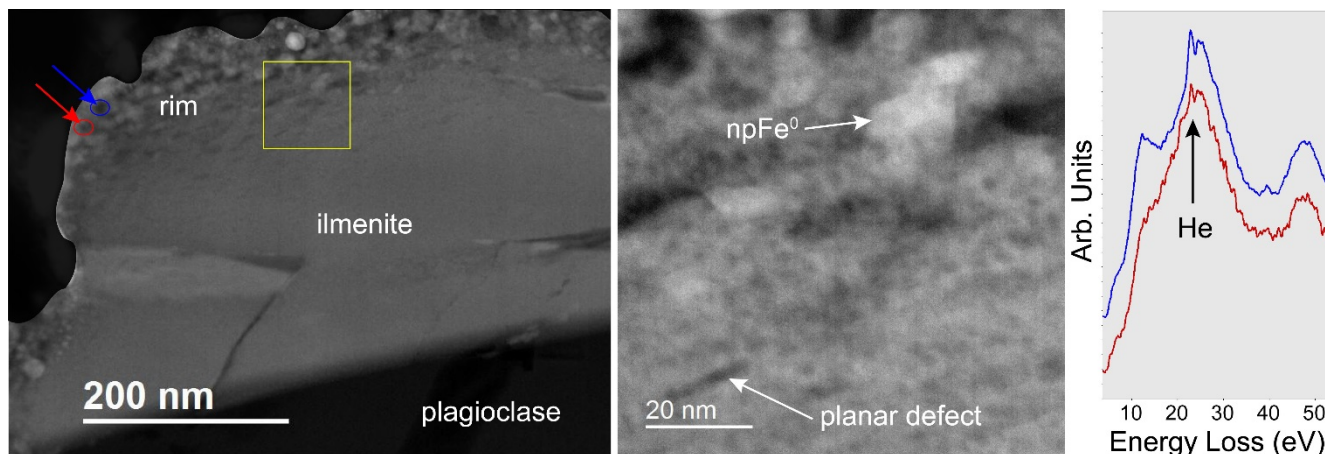


Figure 1. An ilmenite grain attached to a plagioclase grain in mature lunar soil 79221 has a well-developed space weathered rim on the exposed surface. Some of the vesicles in the rim contain trapped helium from the solar wind that can be measured using EELS.

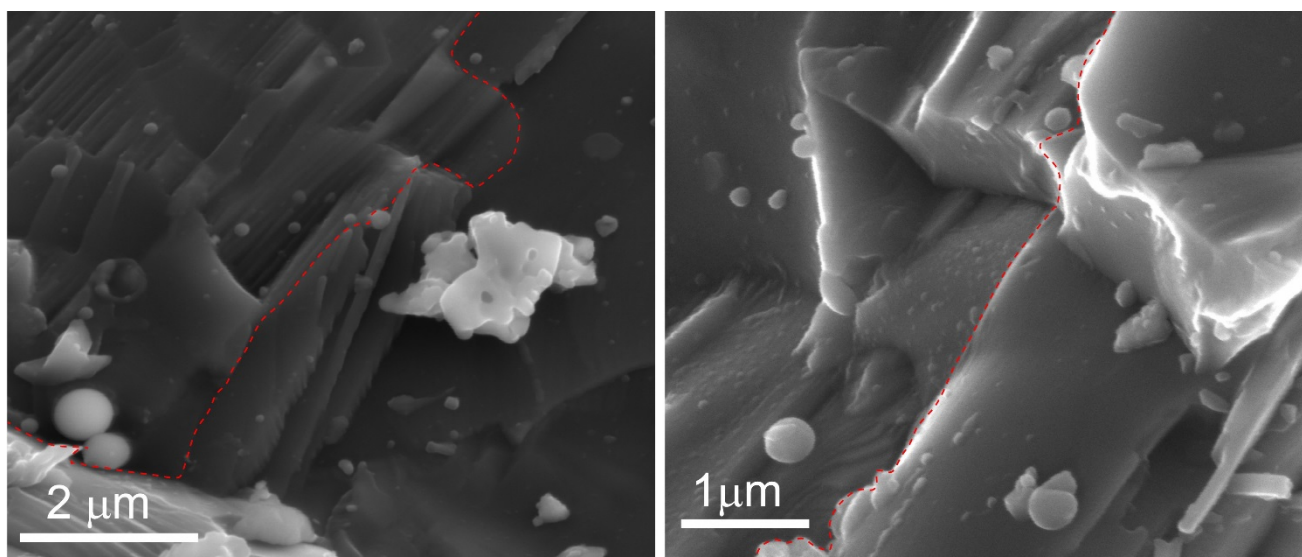


Figure 2. Different phases react very differently to the same space weathering exposure and thus are likely to have different rates of vesicle formation or have vesicles from through different mechanisms. (a) SEM secondary electron image shows the Mg-rich phase (left) is fractured in a different pattern than the Al-rich phase (right) and has more <100 nm adhered surface nanoparticles. (b) The Mg-rich silicate has numerous apparent blisters, while the Al-rich silicate lacks the blister-like features.

References

- [1] Pieters, C.M., and S.K. Noble (2016) *JGR*, 121, 1865.
- [2] Burgess, K.D., and R.M. Stroud (2018) *GCA*, 224, 64.
- [3] Thompson, M.S., et al. (2016) *M&PS*, 51, 1082.
- [4] Matsumoto, T., et al. (2016) *GCA*, 187, 195.

Preliminary results from sulfide Hayabusa particle RB-CV-0234

Devin L. Schrader¹ and Thomas J. Zega²

¹Center for Meteorite Studies, School of Earth and Space Exploration, Arizona State University, Tempe, AZ 85287-1404, USA
(devin.schrader@asu.edu),

²Lunar and Planetary Laboratory, University of Arizona, Tucson, Arizona 85721, USA (tzega@lpl.arizona.edu)

Introduction: We performed initial analyses of the sulfide Hayabusa particle RB-CV-0234, and compared it to our results from LL3–6 chondrite sulfides [1,2], with the goal of further constraining the formation and alteration conditions of asteroid Itokawa. Preliminary analysis by JAXA's Hayabusa examination team via scanning electron microscope (SEM) determined that RB-CV-0234 (25.9 μm in diameter) consists of FeS, Fe, FeNiS, and CuS, making it an ideal target potentially containing both pyrrhotite group sulfides [(Fe,Ni,Co,Cr)_{1-x}S] and the rare Ni-rich sulfide, pentlandite [(Fe,Ni,Co,Cr)_{9-x}S₈].

Sulfides are important to study as their compositions, textures, and crystal structures can be used to constrain oxygen fugacity of formation, shock stage, and aqueous-, thermal-, and cooling-histories [e.g., 3–8]. The pyrrhotite group sulfides are largely nonstoichiometric and have a range of compositions ($0 < x < 0.125$) and distinct crystal structures (polytypes). The stoichiometric end members are 2C (troilite; FeS, hexagonal) and 4C (Fe₇S₈, monoclinic) pyrrhotite. There are also pyrrhotites of intermediate compositions with $0 < x < 0.125$ (all hexagonal); including the non-integral NC-pyrrhotites and the integral 5C (Fe₉S₁₀), 6C (Fe₁₁S₁₂), and 11C (Fe₁₀S₁₁) pyrrhotites [e.g., 9–11]. Geothermometry of pyrrhotite-pentlandite intergrowths in meteorites shows that most formed via primary cooling from high temperature or thermal metamorphism [e.g., 12–14]. Sulfides in the LL4 to LL6 chondrites typically equilibrated between 600 and 500°C, consistent with formation during cooling after thermal metamorphism [14]. However, geothermometry of pyrrhotite-pentlandite intergrowths from an LL5–6 impact melt-breccia indicated that the sulfides were annealed at $\leq 230^\circ\text{C}$, likely after an impact event [12]. Analyses of Hayabusa particles have identified asteroid 25143 Itokawa as LL4–6 chondrite material ($\sim 10\%$ LL4 and $\sim 90\%$ LL5–6) [e.g., 15–18] that was thermally metamorphosed between ~ 780 and 840°C [15]. Itokawa particles were found to record shock stages between S2 and S4, with most particles around S2 [19,20]. Sulfides in Hayabusa particles [e.g., 15,21,22] may record additional and/or complementary information on the formation conditions of asteroid Itokawa.

Samples and Analytical Procedures: We mounted RB-CV-0234 on an epoxy bullet, following the methods of [21], and microtomed the sample in preparation for analysis and sample extraction using the FEI Helios NanoLab 660 focused-ion-beam-SEM (FIB-SEM) at the University of Arizona (UAz). The visible particle surface was $25.0 \times 10.2 \mu\text{m}$ after microtoming. X-ray element maps and high-resolution images of the microtomed RB-CV-0234 were obtained with the FIB-SEM prior to extraction of a $\sim 12.4 \times 11.2 \mu\text{m}$ section from one end of the whole particle, which was then thinned to electron transparency ($< 100 \text{ nm}$) following the methods of [23]. The FIB section was then analyzed using the 200 keV aberration-corrected Hitachi HF5000 scanning transmission electron microscope (TEM) at UAz.

Results: FIB-SEM X-ray element maps showed that the microtomed surface of RB-CV-0234 consisted entirely of pyrrhotite. However, X-ray element maps of the extracted FIB section, determined via TEM analysis, revealed a grain of pentlandite ($4.8 \times 1.3 \mu\text{m}$) at the bottom of the section (Fig. 1). The FIB section contains a single large grain of pyrrhotite and a single smaller grain of pentlandite. Selected-area electron-diffraction (SAED) patterns of the pyrrhotite and pentlandite grains index to 2C pyrrhotite (troilite) and pentlandite along the [110] zone axis (i.e., they are crystallographically oriented), respectively.

Discussion: The preliminary results from the first FIB section from RB-CV-0234 are most consistent with it being a sulfide from an LL6 chondrite, similar to the sulfides from Saint-Séverin studied by [1]. We infer this because, based on results from the LL3–6 chondrite sulfides we previously studied via FIB-TEM [1,2], only sulfide grains in Saint-Séverin (LL6, S2 [24]) contain a similar pentlandite/pyrrhotite morphology (i.e., blocky pentlandite in pyrrhotite) and 2C pyrrhotite (troilite) with pentlandite [1]. The other LL chondrites we studied contained either a distinct morphology (e.g., pentlandite lamellae) and/or multiple polytypes of pyrrhotite [1,2]; perhaps indicating higher degrees of shock as troilite in ordinary chondrites is known to display shock indicators, such as fized and polycrystalline troilite [e.g., 8]. This conclusion is

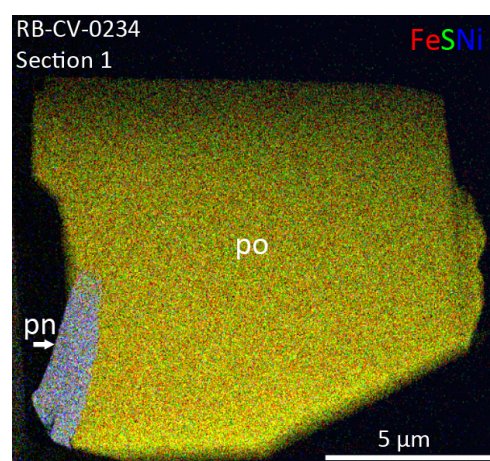


Fig. 1. Composite TEM X-ray element map (RGB=FeSNi) of RB-CV-0234 FIB Section 1; where po = pyrrhotite and pn = pentlandite.

consistent both with the petrographic types represented in Hayabusa particles (10% LL4 and 90% LL5–6 [15,17,18]) and the most likely shock stage of Hayabusa samples (S2; [19,20]). Additional planned FIB section extractions from RB-CV-0234 will allow us to test this conclusion and investigate if the sulfide contains any evidence of space weathering [e.g., 22]. We plan to determine the compositions of both the pentlandite and the pyrrhotite via quantitative energy-dispersive X-ray spectroscopy with the TEM at UAz [25], and determine the sulfide's geothermometry to constrain its thermal history (i.e., if the sulfide was annealed at low temperature, or cooled from high temperature [e.g., 12,14]).

Acknowledgements: We thank JAXA for the loan of the Hayabusa particle used in this study through the 5th International Announcement of Opportunity, and NASA grant NNX17AE53G (DLS PI, TJZ Co-I) for funding this research.

References

- [1] Schrader D. L. and Zega T. J. 2017. Abstract #6347. 80th MetSoc. [2] Schrader D. L. and Zega T. J. 2018. Abstract #2621. 49th LPSC. [3] Arnold R. G. 1967. *Can. Min.* 9:31. [4] Kissin S. A. and Scott S. D. 1982. *Econ. Geol.* 77:1739. [5] Raghavan V. 2004. *J. Phase Equilib.* 25:373. [6] Wang H. et al. 2006. *J. Sulfur Chem.* 27:1. [7] Harries D. and Langenhorst F. 2013. *Meteorit. Planet. Sci.* 48:879. [8] Bennet M. E. and McSween Jr. H. Y. 1996. *Meteorit. Planet. Sci.* 31:255. [9] Morimoto N. et al. 1975. *Econ. Geo.* 70:824. [10] Wang H. et al. 2006. *J. Sulfur Chem.* 27:1. [11] Harries D. et al. 2011. *Am. Min.* 96:716. [12] Jamsja N. and Ruzicka A. 2010. *Meteorit. Planet. Sci.* 45:828. [13] Schrader D. L. et al. 2015. *Meteorit. Planet. Sci.* 50:15. [14] Schrader D. L. et al. 2016. *Geochim. Cosmochim. Acta* 189:359. [15] Nakamura T. et al. 2011. *Science* 333:1113. [16] Noguchi T. et al. 2014. *Earth, Planets, and Space* 66:124. [17] Tsuchiyama A. et al. 2011. *Science* 333: 1125. [18] Tsuchiyama A. et al. 2014. *Meteorit. Planet. Sci.* 49:172. [19] Noguchi T. et al. 2011. *Science* 333:1121. [20] Zolensky M. E. et al. 2012. Abstract #1477. 43rd LPSC. [21] Berger E. L. and Keller L. P. 2015. *Microscopy Today* 23:18. [22] Harries D. and Langenhorst F. 2014. *Earth, Planets, and Space* 66:163. [23] Zega T. J. et al. 2007. *Meteorit. Planet. Sci.* 42:1373. [24] Rubin A. E. 2004. *Geochim. Cosmochim. Acta* 68:673. [25] Zega T. J. et al. 2018. Abstract #2084. *Microsc. Microanal.* 24 (Suppl. 1).

Exploring the potential of Xe⁺ Plasma FIB for minimum mass-loss sectioning of meteoritic analogs of coarse-grained (0.2-1 mm) asteroidal samples from the JAXA Hayabusa 2 sample return mission to asteroid Ryugu.

A.J. Brearley¹, R.H. Jones², T. L. Burnett³, J. Donoghue³, and T. Nakamura⁴

¹*Department of Earth and Planetary Sciences, 1University of New Mexico, Albuquerque, NM 87131, USA*

²*School of Earth and Environmental Sciences, University of Manchester, Oxford Road, M13 9PL, UK*

³*School of Materials, University of Manchester, Oxford Road, M13 9PL, UK*

⁴*Department of Earth and Planetary Materials Science, Tohoku University, Aramaki, Aoba, Sendai, Miyagi 980-8578, Japan.*

Introduction: The JAXA Hayabusa 2 sample return mission will collect samples of Ryugu, a spectral type Cg asteroid, in autumn 2018 and return them to Earth in December 2020. It is expected that a significant component of the material collected will be regolith particles that are ~0.2-1 mm in diameter. These comparatively large carbonaceous chondrite fragments will be the focus of research of the Coarse-grained Sample Analysis Team. Samples in this size range present significant challenges for sample preparation. It is highly desirable that the samples can be cut into two or more subsamples for analysis using different techniques, while leaving material that can be archived for future study. Typical cutting techniques such as wafering saws using wires or blades are highly wasteful in terms of mass. In preparation for these challenges, we are exploring the application of Xe⁺ plasma FIB (P-FIB) techniques as a potential methodology for sectioning coarse-grained Hayabusa 2 particles, with minimum mass loss.

Background: Focused ion beam techniques have become the method of choice for the site-specific sample preparation of a wide range of synthetic and natural materials. Ga⁺ FIB has become an established tool for the preparation of small volume samples for cross sectional imaging and TEM analysis [1]. However, the relatively low beam currents which can be obtained from Ga⁺ ion sources limit their ability to section materials that are more than a few 10s of microns in size. The more recent development of P-FIB technology utilizing Xe⁺ ions, delivers much higher beam currents and enhanced sputtering rates (10-30% higher and up to 300% for some materials [2]), has revolutionized the field of large area cross-sectional analysis, as well as enabling the extraction of large volumes of material for ex-situ analysis.

Methodology: A Thermo Fisher Dualbeam® Xe⁺ P-FIB at the University of Manchester was used as a proof of concept instrument for our preliminary studies. A sample of the Murray CM2 chondrite was used as an analog material with properties that are likely to be a good match to samples that will be returned by the mission. Murray is a complex, heterogeneous meteorite with materials of diverse densities and grain sizes that sputter at different rates and represent a significant challenge. A chip of Murray, ~1x2 mm in size, was secured to an aluminium SEM stub using Superglue and was examined uncoated in the P-FIB.

Results: The first order sputtering behavior of Murray was determined by carrying out a cleaning cross section on a relatively flat surface of the sample. At instrumental conditions of 30 kV, 0.47 μA, a 50 x 50 μm² cleaning cross section depth of 30 μm (the calculated cutting depth for Si) sputtered to a measured depth of ~56 μm in 2 minutes. Sample sputtering was quite homogeneous across the whole area, except for an inclusion with much lower sputtering rates that was removed after a second cleaning cross section. A satisfactory surface was produced in approximately 3 minutes. A second experiment was performed to determine the viability of cutting larger regions of sample. A regular cross section was set up on the edge of the fragment with dimensions 316 μm (L), 66 μm (W) and 120 μm (D). Using a beam current of 1.3 μA, the pattern cut through to a depth of ~192 μm in 30 minutes (Fig. 1A). A sputter-resistant particle remained in the lower part of the surface that required three additional cleaning cross sections to reduce in size. These experiments show that sputtering is remarkably fast over large areas, even in regular cross section patterning mode, where the tip of the ion beam is removing material.

In order to section a single, coarse-grained particle, a complete cut across the entire diameter of the particle that maximizes the depth to width ratio of the cut is required. Due to increased re-deposition as the ion beam penetrates deeper into the sample, the sputtering rate will decrease with depth and the width of the cut will also become smaller. We explored two different approaches to cutting the sample to maximize the depth to width ratio of the trench. In the first case, a rectangular pattern 50 μm long, 5 μm wide and 30 μm deep was run at a beam current of 470 nA (40 seconds duration) on a relatively flat region of the sample surface. A regular cross section cut normal to the first rectangular pattern was then run to look at the geometry of the trench, which was

carrot-shaped with a poor depth to width ratio of 2:1 (Fig. 1B, trench 1). A slight improvement in the depth to width ratio was obtained if the trench was open at one end at the start of the pattern (Fig. 1B, trench 2). This result demonstrates that sputtering using a standard rectangular pattern is inefficient and not a viable approach for sectioning this kind of chondritic material. An alternative approach is to take advantage of the higher sputtering rates when the ion beam interacts with the sample at glancing angle and sputtering occurs at the edge of the beam. For this experiment, we utilized a cleaning cross section pattern, but with dimensions that are essentially the reverse of those used typically for polishing a sample surface, i.e. the face that the beam is cutting is very narrow, but the pattern is highly elongate. A pattern with a width of 5 μm (on the cutting face), a depth of 50 μm and a length of 50 μm resulted in a trench in the sample with a depth to surface width ratio of ~ 9 (90 μm deep) (Fig. 1B, trench 3) in 40 seconds.

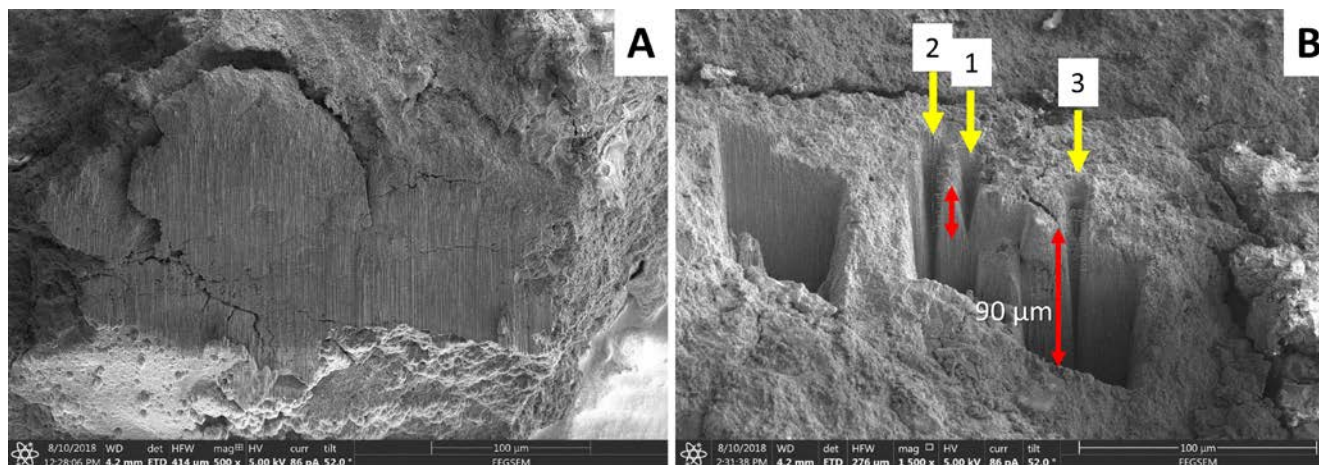


Figure 1 - A) SE image of Xe P-FIB cross section cut on the surface of a fragment of the Murray CM chondrite. The face is over 300 μm in width. B) SE image of trenches cut into Murray sample using different types of patterns. Trench 1 was cut using a rectangular pattern with closed ends that produced a carrot-shaped cross section. Trench 2 was cut using the same pattern, but the trench was open at one end resulting in a deeper trench. Trench 3 was cut using a narrow cleaning cross section, producing a deeper trench with improved depth to width ratio.

Conclusions: Although we have yet to cut an entire particle, these experiments demonstrate that P-FIB has great potential for sectioning Hayabusa 2 particles. Preliminary results show that it should be possible to section 500 μm diameter particles in time periods of ~ 1 -2 hours. However, the heterogeneity of the sample in terms of sputtering rates does require that cutting through more resistant phases must be factored into the milling time. It may be advantageous sectioning the sample in two separate cuts run from opposite sides of the particle. Based on the depth to width ratio (9:1) obtained from the sample of Murray cut using a cleaning cross section, we estimate that the width of the top of the cut would be around 50 μm . Cutting particles larger than 500 μm in diameter in half would be more challenging and time consuming. A better strategy may be to remove serial slices of lower diameter. We are continuing to develop this method, including assessment of the extent of beam damage to the sample, adjacent to the cut.

References: [1] L.A. Giannuzzi, and F.A. Stevie (1999) *Micron*, 30, 197-204. [2] Burnett, T.L. et al. (2016) *Ultramicroscopy* 161, 119-129.

Thermal Infrared Spectra of Heated CM and C2 Chondrites and Implications for Asteroid Sample Return Missions

Helena Bates^{1,2}, Kerri Donaldson Hanna², Ashley King¹, Neil Bowles², Katie Rhodes³ and Sara Russell¹

¹*Earth Science Department, Natural History Museum, London, SW7 5BD, UK*

²*Atmospheric, Oceanic and Planetary Physics, University of Oxford, Oxford, OX1 3PU, UK*

³*Earth Science and Engineering, Imperial College, London, SW7 5BB, UK*

Introduction: JAXA's Hayabusa2 arrived at its target asteroid, the C-type asteroid Ryugu, in June 2018 and NASA's Origins, Spectral Interpretation, Resource Identification and Security Regolith Explorer (OSIRIS-REx) is on its approach to its target, the B-type asteroid Bennu, with arrival due in December 2018. The C- and B-type asteroids are part of the larger C-complex class [1,2], which have been linked to carbonaceous chondrite meteorites, in particular the aqueously altered CM and CI chondrites [3–5]. These meteorites are rich in organics and water, and are considered chemically pristine, so investigating them and their parent body asteroids will tell us about the early evolution of our Solar System.

Some aqueously altered CM and CI chondrites have also experienced thermal metamorphism [6,7]. Previous work has suggested that thermally metamorphosed CM and CI chondrites could be good analogues for the C- and B-type asteroids [8–10] including Ryugu [11,12]. The surfaces of C-complex asteroids might contain a mixture of hydrated and dehydrated materials having experienced a complex history of both fluid and thermal alteration. Unravelling the effects of these processes will be imperative for putting data from Hayabusa2 and OSIRIS-REx into geologic context.

OSIRIS-REx and the Mobile Asteroid Surface Scout (MASCOT) on board Hayabusa2 both carry thermal infrared (TIR) instruments in order to determine surface mineralogy, the OSIRIS-REx thermal emission spectrometer (OTES) and the Mascot Radiometer (MARA). TIR spectra have many diagnostic spectral features associated with rock forming minerals [13]. These include the Christiansen feature (CF), between 7.5 – 9 μm , which is an emissivity maximum diagnostic of composition [13], the reststrahlen bands (RB), which are the fundamental vibrations of silicate minerals between 8 – 12 μm and 15 – 25 μm , and the transparency feature (TF), which is an emissivity minima between 11 – 13 μm caused by volume scattering in optically thin minerals [13]. Laboratory measurements in the TIR are generally made under ambient conditions; however previous work has shown that measuring under the appropriate near-surface asteroid conditions causes shifts in the position of the CF, and increases the spectral contrast between the CF and RBs [14–16]. Therefore, in order to accurately compare between laboratory measurements and data collected from asteroids, it is critical to perform measurements under simulated asteroid environment conditions (SAE).

Here we present TIR emissivity measurements, collected under ambient and SAE conditions, for a number of thermally metamorphosed CM and C2 chondrites. These SAE measurements should be more directly comparable to observations by OSIRIS-REx and Hayabusa2. There have been limited studies of TIR spectra measured under SAE for carbonaceous chondrites [16], and none on thermally metamorphosed CM and CI chondrites, so this offers a new opportunity to investigate the spectral signatures of Bennu and Ryugu.

Samples: Nakamura (2005) defined a heating scale for thermally metamorphosed CM and CI chondrites, from stage I to stage IV. Stage I samples have been heated to peak metamorphic temperatures of <250 $^{\circ}\text{C}$, and show little to no dehydration of hydrous phases. Here we have investigated the sample MacAlpine Hills (MAC) 87300, an ungrouped C2 chondrite which previous work has suggested is a stage I sample, but shows CM and CO affinities [6,17]. Stage II samples have been heated to temperatures of 300 – 500 $^{\circ}\text{C}$, and are mostly composed of a highly disordered phase thought to be dehydrated phyllosilicates. We investigated the CM2 Elephant Moraine (EET) 92069, and the anomalous CM chondrite Wisconsin Range (WIS) 91600, both of which have been suggested to be stage II samples [7,18]. We did not study any stage III samples, which have been heated to temperatures of 500 – 750 $^{\circ}\text{C}$ and show some recrystallization of anhydrous phases, but we did investigate the CM2 chondrites Pecora Escarpment (PCA) 02010 and PCA 02012, which are stage IV samples [19]. Stage IV samples have been heated to >750 $^{\circ}\text{C}$ and have experienced widespread recrystallization of anhydrous phases such as olivine and metal.

Experimental: TIR emissivity measurements were made under ambient and SAE conditions in the Planetary Analogue Surface Chamber for Asteroid and Lunar Environments (PASCALE) within the Planetary Spectroscopy Facility at the University of Oxford [16]. Under ambient conditions the sample was heated from below to ~ 80 $^{\circ}\text{C}$ whilst the chamber was held at an ambient pressure (~ 1000 mbar N_2) and temperature (~ 28 $^{\circ}\text{C}$). Under SAE conditions, the near surface environment of Bennu is simulated by removing atmospheric gases from the chamber so measurements are completed under vacuum ($<10^{-4}$ mbar), cooling the interior of the chamber to <-150 $^{\circ}\text{C}$ using liquid N_2 and heating the samples from above and below until the maximum brightness temperature of the sample is ~ 75 $^{\circ}\text{C}$. This induces a thermal gradient in the upper hundreds of microns of

the sample, which is what we would expect on the surface of Bennu near local midday. Spectra were collected using a Bruker VERTEX 70v Fourier Transform Infrared (FTIR) spectrometer at a resolution of 4 cm^{-1} from $1800 - 200\text{ cm}^{-1}$ ($5.5 - 50\text{ }\mu\text{m}$).

Results: Emissivity spectra are presented in Figure 1. The stage IV PCA 02010 and PCA 02012 samples are spectrally similar with the main diagnostic features located at similar wavelengths, and show a feature near $6\text{ }\mu\text{m}$, which is not present in the stage II samples. This could indicate it is representative of the higher abundances of anhydrous phases in the stage IV samples. The spectra show a steep spectral contrast leading up to the CFs, which are identified near $8.5\text{ }\mu\text{m}$, and emissivity maxima near $9.7\text{ }\mu\text{m}$. The TFs for the stage IV samples are identified near $12.5\text{ }\mu\text{m}$.

The spectral shapes of EET 96029 and MAC 87300 are also similar to each other, with CFs identified near $8.7\text{ }\mu\text{m}$ with additional emissivity maxima near $9.7\text{ }\mu\text{m}$, and TFs at $12.5\text{ }\mu\text{m}$. The similarity between EET 96029 and MAC 87300 requires further investigation, as they not only are classified differently, but also have different thermal histories.

The spectrum of WIS 91600 is different from the other meteorites investigated here. It has a broad emissivity maximum centred near $6.5\text{ }\mu\text{m}$ followed by an emissivity minima, and a CF near $9.4\text{ }\mu\text{m}$. The CF at longer wavelengths suggests it is dominated by a different mineralogy in comparison to the other meteorites investigated here. Its TF is identified at similar wavelengths to the other samples near $12.5\text{ }\mu\text{m}$. The spectra suggests WIS 91600 has a distinct mineralogy when compared with the other stage II samples, and further investigation into its composition is required to determine which mineralogy is dominating the spectra.

There are clear spectral differences between samples that have been heated to different peak metamorphic temperatures. In order to better investigate these differences, exact mineralogy for each sample is necessary, so specific features can be tied to known compositions. Position-sensitive detector X-ray diffraction (PSD-XRD) is a method that has been used to determine modal mineralogy for a number of CI, CM, CV and CR chondrites [20–24]. It is able to directly detect all crystalline phases, and additionally investigate the presence of non-crystalline phases. Further studies are planned to obtain the PSD-XRD patterns for the exact samples used in this study, so modal mineralogy can be established and linked with our lab spectral measurements.

References

- [1] DeMeo F.E. et al. 2009 *Icarus* 202:16 [2] Tholen D.J. 1984 [3] Burbine T.H. et al. in 2002 *Asteroids III* 653. [4] Licandro J. et al. 2007 *Astronomy & Astrophysics* 461:751. [5] Vilas F. et al. 1994 *Icarus* 109:274. [6] Nakamura T. 2005 *Journal of Mineralogical and Petrological Sciences* 100. [7] Tonui E.K. et al. 2014 *GCA* 126:284. [8] Clark B.E. et al. 2010 *Journal of Geophysical Research: Planets* 115. [9] Hiroi T. et al. 1993 *Science* 261:1016. [10] De León J. et al. 2012 *Icarus* 218:196. [11] Perna D. et al. 2017 *A&A* 599. [12] Moskovitz N.A. et al. 2013 *Icarus* 224:24. [13] Salisbury J.W. in 1993 *Remote Geochemical Analysis* 79. [14] Donaldson Hanna K.L. et al. 2012 *Journal of Geophysical Research: Planets* 117. [15] Thomas R. et al. 2014 45th LPSC [16] Donaldson Hanna K.L. et al. 2017 48th LPSC [17] Sears D.W.G. et al. 1990 21st LPSC [18] Lee M.R. et al. 2016 *GCA* 187:237. [19] Alexander C.M.O. et al. 2013 *GCA* 123:244. [20] Howard K.T. et al. 2009 *GCA* 73:4576. [21] Howard K.T. et al. 2010 *GCA* 74:5084. [22] Howard K.T. et al. 2015 *GCA* 149:206. [23] King A.J. et al. 2015 *GCA* 165:148. [24] King A.J et al. 2015 *Meteoritics & Planetary Science* 50:A194.

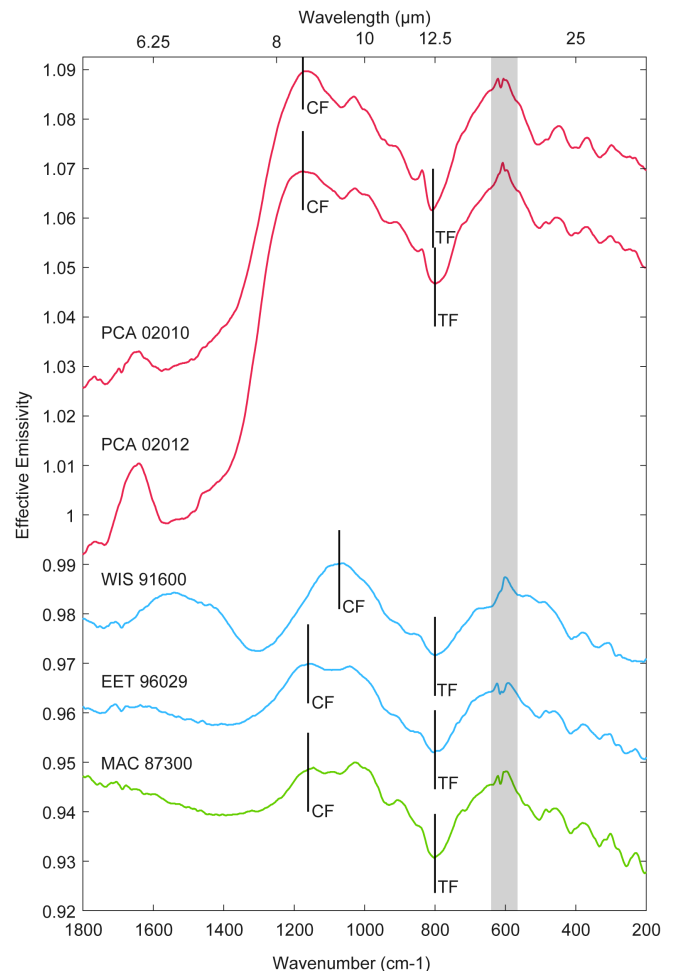


Figure 1: Emissivity spectra for the thermally metamorphosed CM and ungrouped chondrites investigated here. Green spectra are stage I, blue spectra are the stage II samples and red spectra are the stage IV samples. Data are normalized to unity and offset for clarity. The positions of the CF and TF are indicated. The grey box near 600 cm^{-1} indicates noise related to poor signal-to-noise resulting from the beam splitter.

The Jbilet Winselwan CM chondrite: an analogue for C-type asteroid sample return

Ashley J. King¹, Paul F. Schofield¹ and Sara S. Russell¹

¹*Department of Earth Science, Natural History Museum, London, SW7 5BD, UK*

E-mail: a.king@nhm.ac.uk

In June 2018 JAXA's Hayabusa-2 mission reached its target, the C-type asteroid Ryugu, and in December 2018 NASA's OSIRIS-REx spacecraft will arrive at the B-type asteroid Bennu. The C-complex class of asteroids have been linked to the carbonaceous meteorites, in particular the aqueously altered CI and CM chondrites, and are therefore expected to be chemically pristine and contain volatile and organic species [1]. A major aim for both missions is to collect and return to Earth samples from the asteroid surfaces in order to learn about the formation and evolution of the Solar System.

The Jbilet Winselwan meteorite was found on the 24th May 2013 near Smara in Western Sahara, and with a total recovered mass of ~6 kg is currently the fourth largest CM chondrite (the largest find) [2]. Its bulk C, N and O isotopic compositions and major element abundances are within the range of other CM chondrites [2, 3]. Petrographic observations show that it consists of chondrules and calcium-aluminium-rich inclusions (CAIs, <1 vol%) surrounded by dusty rims and set within a matrix of phyllosilicates, oxides and sulphides [2–5]. Like many CM chondrites, Jbilet Winselwan is a breccia with distinct lithologies that underwent varying degrees of aqueous alteration [2–5]. In most lithologies the chondrules and CAIs are partially altered and the abundance of metal is low (<1 vol%), consistent with petrologic sub-types 2.7 – 2.4, whereas in others the chondrules and CAIs are completely altered suggesting more extensive hydration to petrologic sub-types ≤ 2.3 [2–5]. The brecciated nature of Jbilet Winselwan is also highlighted by variations in H₂O and carbonate abundances when analysing different aliquots of the meteorite [3].

Following aqueous alteration some lithologies in Jbilet Winselwan suffered a period(s) of thermal metamorphism. The matrix often has a “spongy” appearance and melted Fe-sulphide masses are present [4]. Bulk X-ray diffraction (XRD) indicates that the phyllosilicates are dehydrated to a highly disordered phase (~70 vol%) and the abundance of tochilinite, which breaks down at temperatures of ~120°C, is low relative to other CM chondrites [3]. Depletions of volatiles such as He and Cd in Jbilet Winselwan are consistent with a peak metamorphic temperature of 400 – 500°C [3]. However, Göpel et al. [6] found no depletions in volatile trace elements and not all of the phyllosilicates are dehydrated [2], suggesting that the heating was heterogeneous and did not affect all regions within Jbilet Winselwan equally.

The Jbilet Winselwan CM chondrite records a complex history of aqueous and thermal processing on a C-type asteroid. It is one of >20 CM chondrites identified as having experienced both hydration and thermal metamorphism [7]. Aqueous alteration took place when accreted ices melted on the parent body and reacted with the original anhydrous mineral assemblage. The presence of a dehydrated phyllosilicate phase in Jbilet Winselwan implies that thermal metamorphism occurred either simultaneously with, or more likely after, aqueous alteration had ceased. Mineral textures and organic structures in heated CM chondrites indicate that the metamorphism was short-lived, perhaps on the order of hours to several years, consistent with either impacts and/or solar radiation on asteroid surfaces [8]. We favour impacts because depending on the size, velocity and composition of the impactor and target rocks it could produce regions on the parent body with different thermal histories [9], as appears to be the case for Jbilet Winselwan.

Many of Jbilet Winselwan's key properties are similar to Y-793321, which is a sample of dehydrated regolith from the surface of a water-rich asteroid [10]. The visible and near-infrared (IR) reflectance spectra of Jbilet Winselwan, Y-793321 and other heated CM chondrites share a number of features with some low albedo, C-complex asteroids, including Ryugu [11, 12]. This suggests that the surfaces of C-complex asteroids are likely to host a diverse mixture of hydrated and dehydrated phases, and that heated CM chondrites such as Jbilet Winselwan are excellent analogues for the types of materials that will be encountered by the Hayabusa-2 and OSIRIS-REx sample-return missions.

References

- [1] Cloutis E. et al. 2011. *Icarus* 216:309.
- [2] Ruzicka A. et al. 2015. *M&PS* 50:1662.
- [3] King A. et al. 2018. *M&PS in review*.
- [4] Zolensky M. et al. 2016. Abstract #2148. 47th LPSC.
- [5] Friend P. et al. 2018. *M&PS in press*.
- [6] Göpel C. et al. 2015. *GCA* 156:1.
- [7] Nakamura T. 2005. *JM&PS* 100:260.
- [8] Nakato A. et al. 2008. *EP&S* 60:855.
- [9] Bland P. et al. 2014. *Nat. Comm.* 5:5451.
- [10] Nakamura T. 2006. *E&PSL* 242:26.
- [11] Hiroi T. et al. 1993. *Science* 261:1016.
- [12] Vilas F. 2008. *Astronom. J.* 135:1101.

Sulfide mineralogy of heated CM/CI-like chondrites as indicator of asteroidal processes

Dennis Harries¹

¹*Friedrich Schiller University Jena, Institute of Geosciences, Carl-Zeiss-Promenade 10, 07745 Jena, Germany
(dennis.harries@uni-jena.de)*

Introduction. Thermal alteration of C-type asteroidal regoliths may induce mineralogical and spectral changes and is therefore of interest to ongoing missions such as Hayabusa2 or OSIRIS-REx. Heating effects superposed on earlier aqueous alteration of CM/CI-like chondrites have been described from multiple meteorites beginning in the late 1980s (e.g., [1], [2], [3]) and continue to be found and systematically classified into heating stages (HS I to IV with increasing temperatures [4]). Yet, it is not clear what kind of process is responsible for the thermal overprint and whether it specifically operated on CM/CI-like parent bodies or can be generally expected to affect asteroids and their regolith surfaces. Clearly, the hydrated mineralogy of CM/CI-like meteorites is highly susceptible to changes via thermal processes, and their effects, such as the amorphisation and recrystallization of phyllosilicates, can be readily observed. However, similar thermal events may go unnoticed in non-hydrated meteorite types due to a lack of suitable mineral indicators if heating persisted only for a relatively short time as indicated by CM/CI-like chondrites.

Sulfide minerals such as pyrrhotite (Fe_{1-x}S), troilite (FeS) and pentlandite [$(\text{Fe,Ni})_9\text{S}_8$] are particularly sensitive to heating and, even before melting, may decompose by loss of sulfur and textural changes [5]. Therefore, they potentially may serve as an alternative indicator of thermal events not only for C-type asteroidal surfaces but also for S-type asteroids such as 25143 Itokawa visited by Hayabusa.

Samples and Methods. TEM studies of the sulfide mineralogies of Yamato (Y-)791198 (CM2, HS I), Y-793321 (CM2, HS II), Y-86720 (CM/CI-like, HS IV), Belgica (B-)7904 (CM-like, HS IV) have been described by [5] and will be summarized here. Additionally the meteorites Y-980115 (CI-like, HS II; [6]) and North West Africa (NWA) 11024 (CM-like, HS III/IV; [7]) have been investigated by SEM and TEM using FIB preparation. Study of the mildly heated CM2 chondrite Jbilet Winselwan (HS II; [8]) is ongoing.

Observations. Compared to the pristine Y-791198 the slightly heated regolith breccia Y-793321 [9] shows only subtle changes in sulfide mineralogy, mostly limited to increased grain sizes of exsolved pentlandite and troilite lamellae in pyrrhotite-bearing, former monosulfide solid solution (MSS) grains. Nanocrystalline phosphorus-bearing pentlandite, occasionally carrying chromium nitride in both meteorites [10] also shows an increase in grain size.

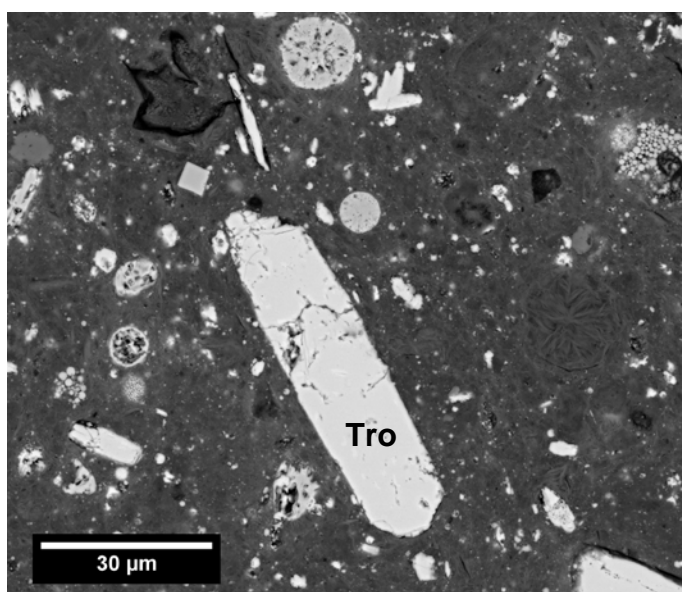


Figure 1. Euhedral sulfide crystals in Y-980115 are replacements of troilite (Tro) after hydrothermally formed pyrrhotite.

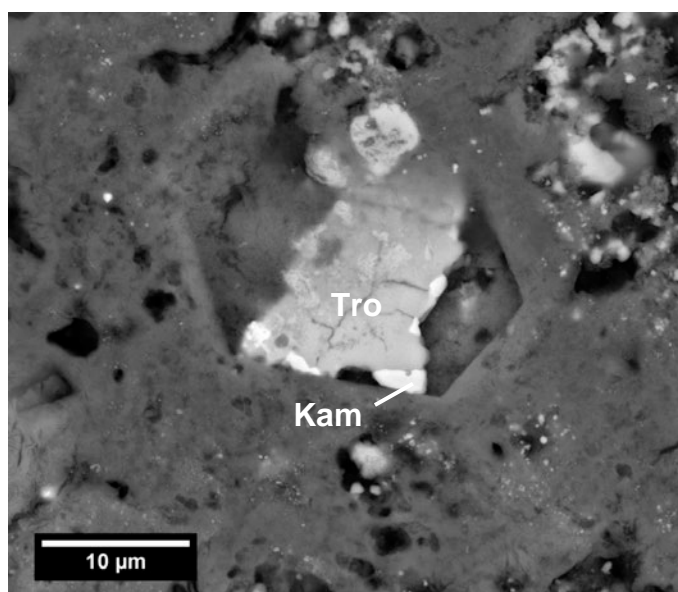


Figure 2. Formerly euhedral sulfide crystal in Y-86720 replaced by troilite (Tro) and partially converted to low-Ni kamacite (Kam).

Substantial mineralogical changes are observed in Y-86720 and B-7904, which contain almost exclusively troilite, which in part has been converted to low-Ni metallic iron (kamacite). Pentlandite appears to be absent in Y-86720, but B-7904 contains rare grains of Fe-rich pentlandite. Both contain small grains of Ni-rich metal (approaching 50 at% Ni in some cases).

Y-980115 shows a brecciated texture with internally fine grained clasts rich in phyllosilicates, magnetite and sulfides. The textures and particularly the morphology of magnetite and sulfide crystals are typical of CI chondrites. Large sulfides grains account for up to 2.8 vol% of the rock. Fe sulfide grains frequently show euhedral platelet shapes and reach sizes up to 70 μm . TEM-SAED patterns obtained from two apparently euhedral sulfide platelets extracted by FIB indicate that the sulfide is polycrystalline troilite and TEM imaging shows that the 'crystals' internally contain abundant grain boundaries meeting in 120° triple junctions. Pentlandite is present as internal grains within the platelets and SAED shows that it does not have a topotactic relationship with the surrounding polycrystalline troilite. The adjacent matrix is poorly crystalline but shows typical fibrous or scaly textures of phyllosilicates. EDS analyses of such aggregates indicate a typical serpentine composition, but SAED only showed diffuse rings with the largest d -value located at 0.465 nm. One better crystalline aggregate gave a diffraction pattern with largest d -value of 0.97 nm consistent with a talc group mineral; another showed polycrystalline rings consistent with olivine.

NWA 11024 displays typical fine-grained rims (FGRs) around chondrules. One rim sampled by FIB shows abundant Ni-rich metal grains < 1 μm in diameter with a composition centered about $\text{Fe}_{50}\text{Co}_3\text{Ni}_{47}$. The only present sulfide is troilite; Ni-poor metal and pentlandite are absent. The phyllosilicates originally present in the FGR have been converted to nanocrystalline olivine as indicated by SAED patterns. A second FIB obtained from a coarse phyllosilicate aggregate shows it to be a pseudomorph consisting entirely of nanocrystalline, Fe-rich olivine and minor amounts of Fe sulfide (probably troilite).

Discussion. The observations collected on a number of meteorites indicate that progressive thermal overprinting of CM/CI-like chondrites results in sulfur loss of pyrrhotite to form nearly stoichiometric troilite. Because pyrrhotite (Fe_{1-x}S) can be considered as an 'omission' solid solution between FeS and a hypothetical vacancy endmember VaS (Va = vacancy), the reaction can be written as $\text{VaS} \rightleftharpoons 0.5\text{S}_2$. Thus, sulfur loss progressively decreases the non-stoichiometry of Fe_{1-x}S until FeS is reached. The preservation of pentlandite in Y-980115 suggests that it is stable at least until about this point. Further heating and increasing loss of sulfur probably leads to the decomposition of pentlandite to form Ni-rich metal as observed in NWA 11024. Preliminary thermodynamic calculations in the Fe-Ni-S system indicate that pentlandite with the composition $\text{Fe}_{4.5}\text{Ni}_{4.5}\text{S}_8$ is not stable with respect to $\text{Fe}_{50}\text{Ni}_{50}$ metal at temperatures above ~280 °C and a sulfur fugacity buffered by the presence of troilite. This needs further refinement for variable Ni/Fe ratios of pentlandite and the resulting metal. At highest temperatures troilite decomposes to form Ni-poor metal via the reaction $\text{FeS} \rightleftharpoons \text{Fe} + 0.5\text{S}_2$ as observed in B-7904 and Y-86720 of heating stage IV. Besides temperature the sulfur fugacity is therefore an important parameter that controls the decomposition. In all cases, the change of sulfide mineralogy requires at least partially open-system behavior such that S_2 (or H_2S) is lost from the rock, suggesting heating in a near-surface regolith or within a small meteoroid.

Potentially, the thermal decomposition of sulfide minerals can serve as another indicator of thermal processing on asteroid surfaces beside the dehydration of phyllosilicates. S-type chondritic regoliths that do not contain phyllosilicates may show heating effects by the presence of decomposed sulfides. However, the direct irradiation of sulfide surfaces by solar wind ions may produce similar effects at lower temperatures [11] and further investigations must establish differentiating criteria.

Acknowledgements. NIPR and S. Ebert/A. Bischoff/S. Wengert/S. Vasilev are gratefully acknowledged for providing the samples. This work was supported by the DFG (LA 830/14-1 to F. Langenhorst) and FSU Jena (DRM/2016-01).

References

- [1] Akai, J. (1988) *Geochim. Cosmochim. Acta*, 52, 1593-1599.
- [2] Tomeoka, K. et al. (1989) *Proc. National Institute of Polar Research Symposium on Antarctic Meteorites 2*, 55-74.
- [3] Ikeda Y. (1992) *Proc. National Institute of Polar Research Symposium on Antarctic Meteorites 5*, 49-73.
- [4] Nakamura, T. (2005) *J. Min. Pet. Science*, 100, 260-272.
- [5] Harries, D. and Langenhorst F. (2013) *Meteoritics & Planetary Science*, 48, 879-903.
- [6] Kikuchi, K. et al. (2017) 8th Symposium on Polar Science/Antarctic Meteorites XXXX (abstract 00272).
- [7] Ebert, S. et al. (2018) submitted to *Meteoritics & Planetary Science*.
- [8] Nakamura T. et al. (2014) 5th Symposium on Polar Science/Antarctic Meteorites XXXVII (abstract 00315).
- [9] Nakamura, T. (2006) *Earth and Planetary Science Letters*. 242, 26-38.
- [10] Harries, D. et al. (2015) *Nature Geoscience*, 8, 97-101.
- [11] Matsumoto, T. et al. (2018) 81st Annual Meeting of The Meteoritical Society (abstract 6096).

Operation Status of Hayabusa2 in the Proximity of Asteroid Ryugu

Yuichi Tsuda¹, Takanao Saiki¹, Fuyuto Terui¹, Satoru Nakazawa¹, Makoto Yoshikawa¹, Sei-ichiro Watanabe²
and Hayabusa2 Project Team

¹*Institute of Space and Astronautical Science, Japan Aerospace Exploration Agency*

²*Nagoya University*

The Japan Aerospace Exploration Agency launched an asteroid sample return spacecraft "Hayabusa2" on December 3, 2014 by the Japanese H2A launch vehicle. Following the successful return back of Hayabusa from the asteroid 25143 Itokawa, Hayabusa2 aims at the round trip mission to the asteroid 162173 Ryugu. Ryugu is a near-Earth C-type asteroid, which is believed to contain organic and hydrated minerals. Thus it is expected that its successful sample return may provide fundamental information regarding the origin and evolution of terrestrial planets as well as the origin of water and organics delivered to the Earth.

On June 27, 2018, Hayabusa2 successfully arrived at Ryugu and began the asteroid-proximity operation, which is to last for 18 months. The spacecraft established "Home Position (HP)-hovering" at 20km distance from the asteroid using optical navigation. In-situ instruments check-out and the initial characterization of Ryugu were all performed as planned.

The first attempt to bring the spacecraft to low altitude is in "Box-C operation", with which the lowest altitude of 6.5km was achieved, providing the first close-up view of Ryugu. From July 31 until August 2, the first fine-guided descent was attempted in the "Mid-altitude Descent Operation". This operation applied the asteroid shape/landmark-based optical navigation called "GCP-NAV" and achieved 8 hour (i.e. >one rotation period of Ryugu) continuous hovering at 5km altitude. From August 5 until 7, the "Gravity Measurement Descent Operation" was conducted. This operation includes the free-fall down to the altitude of 851m (above surface), and thus identified the gravity of the asteroid. Meanwhile number of Ryugu images taken by ONC-T and other important scientific observation data by LIDAR, TIR and NIRS3 are down-linked to the ground in timely manner using Hayabusa2's X/Ka-band high-speed downlink capability. All these data were effectively used for the landing site selection (LSS) activity conducted from July to August, 2018. The LSS decision meeting was held on August 17 participated by the whole international project team, and concluded to select three landing site candidates (1 primary, 2 backups), 1 MINERVA-II-1 landing site and 1 MASCOT landing site.

From September through November 2018, Hayabusa2 is to attempt two rover release operations (MINERVA-II, MASCOT), and two touch-down rehearsal descents, and one touch-down based on the conclusion of the LSS decision meeting. Hence at the time of the Hayabusa2 symposium, we expect to be able to report some results of these critical milestones for the Hayabusa2 missions.

A reshaped rubble-pile asteroid Ryugu as observed by Hayabusa2

Sei-ichiro Watanabe^{1,2}, Joint Hayabusa2 Science Team³

¹*Earth and Environmental Studies, Nagoya University*

²*ISAS, JAXA*

³*Hayabusa2 project*

After a 3.5 year outbound journey the Hayabusa2 spacecraft arrived at C-type near-Earth asteroid (162173) Ryugu on June 2018. This presentation reviews the scientific results from the first half year proximity operation around the asteroid. After a month approach phase in June, the spacecraft reached its home position (HP), about a 20 km altitude from the sub-Earth point of the asteroid's surface, and hovered. The onboard remote-sensing instruments for science are a multi-band visible camera ONC-T, a thermal infrared camera TIR, a NIR spectrometer NIRS3, and a LIDAR altimeter. The most of the science observations are performed from HP, but several observations from lower altitudes (5-7 km altitude) as well as a tour campaign to look into the pole regions of the asteroid was done. Shape models using Stereo-photoclinometry and Structure-from-Motion were constructed from ONC-T images.

The observations from HP revealed that the bulk mean density of Ryugu is as low as 1.2 g cm^{-3} , indicating a very porous and strengthless interior. The low bulk density and the abundant boulder appearance (largest one near the south pole is ~130 m across) suggest Ryugu is a rubble-pile body having accumulated impact fragments from the parent planetesimal. The prominent feature of Ryugu is its top-shape with a circular narrow equatorial ridge of ~500 m radius. There are several top-shaped asteroids have been identified from ground radar observations. Bennu, the target of OSIRIS-Rex mission is one of them. Contrary to Ryugu having a rotation period of 7.632 hr, however, most of the top-shaped asteroids are rapid rotators with rotation periods less than 4.3 hr. Thus, it has been unexpected that Ryugu has a top shape. After the formation Ryugu should be reshaped by the past rapid rotations, the state of which may be obtained by the initial accretion of fragments of the parent body or YORP-induced spin-up. The internal failure of the early Ryugu by rapid rotation made the circular equatorial ridge. Ryugu spins retrogradely around an axis almost perpendicular to the orbital plane (obliquity is $\sim 172^\circ$), which is consistent with one of the final spin states of the YORP evolution.

The most of the surface has very low reflectance and flat featureless reflection spectra in visible and NIR wavelength ranges, and no clear 0.7- μm and 3- μm absorption bands indicating the presence of hydrated minerals have been found so far. Such features may possibly correspond to meteorites like moderately dehydrated carbonaceous chondrites by heat or shock. The equatorial ridge is bright and bluish compared with mid-latitudinal zones, suggesting its freshness or less organic materials.

After the landing site selection Hayabusa2 will try to touch-and-go the surface and collect materials as a return sample. Landers MASCOT and MINERVA-II will descend and land on the surface performing in-situ various observations. The many boulders on the surface of Ryugu would make the sampling difficult. Thus, in-situ information obtained from the landers as well as low-altitude observations of the surface during descents to deploy landers are very important to develop a strategy to get a sample safely from the "fort of boulders". The remote-sensing and in-situ observations of Hayabusa2 and laboratory analyses of the return sample will clarify the origin and history of this small body, early solar system environment around the snow-line, and material supply inventory from the Main Belt to Earth.

The first detailed visible multi-band imaging observations of asteroid Ryugu

S. Sugita¹, R. Honda², T. Morota³, S. Kameda⁴, H. Sawada⁵, E. Tatsumi¹, C. Honda⁶, Y. Yokota⁵, M. Yamada⁶, T. Kouyama⁷, N. Sakatani⁵, H. Suzuki⁸, K. Yoshioka¹, M. Hayakawa⁵, Y. Cho¹, M. Matsuoka⁵, Naru Hirata⁷, Naoyuki Hirata⁸, D. Domingue⁹, H. Miyamoto¹, K. Kikuchi¹, R. Hemmi¹, T. Michikami¹⁰, O. S. Barnouin¹¹, P. Michel¹², M. Hirabayashi¹³, R. Jaumann¹⁴, N. Schmitz¹⁴, S. Schröder¹⁴, T. Hiroi¹⁵, T. Nakamura¹⁶, L. Le Corre⁹, Y. Tsuda⁵, M. Yoshikawa⁵, S. Tanaka⁵, K. Shirai⁵, S. Watanabe³

¹*University of Tokyo*

²*Kochi University*

³*Nagoya University*

⁴*Rikkyo University*

⁵*JAXA/ISAS*

⁶*University of Aizu*

⁷*AIST*

⁸*Kobe University*

⁹*PSI*

¹⁰*Kindai University*

¹¹*Johns Hopkins University/Applied Physics Laboratories*

¹²*Observatoire de la Côte d'Azur*

¹³*Auborn University*

¹⁴*DLR*

¹⁵*Brown University*

We have conducted multi-band visible imaging observations of asteroid Ryugu covering its entire disk from 20 km of distance and covering equatorial regions with higher spatial resolution at 5 – 7km of distance. These observations revealed a number of important properties of Ryugu: 1) a classic bi-cone top shape with upright spin axis, 2) equatorial ridge encircling the entire body, 3) the presence of large boulders particularly around the poles, 4) Gradual latitudinal decrease in number density of large boulders toward equator [1], 5) General uniformity in visible spectra on the entire globe [2], 6) The presence of bright spots and bright surfaces on a large boulder, which exhibit bluer spectra [2], 7) Circular depressions with bowl-shaped profiles and raised rimes, consistent with impact craters [3], 8) The number density of these depressions is on the same order of magnitude as that of crater candidates on Itokawa [4]. 9) Preferential deficiency in small circular depressions with a similar size frequency slope as Itokawa and Eros, suggesting the presence of granular medium subject to seismic shaking and crater erasure. 10) Boulder size measurements indicate that they are too large to be impact ejecta from observed craters, suggesting that they may be direct fragments from Ryugu's parent body.

The bowl-like shape of large (~200m in diameter) circular depressions, consistent with gravity-controlled craters, and the deficiency in small circular depressions suggest that Ryugu may be mantled with strengthless materials at least 10's meter of thickness. Such mobile interior in Ryugu may have played an important role in forming/modifying the circum-equatorial ridge belt [5] and clustered large boulders around the poles, underling the importance of high-resolution observations for granular flows by both Hayabusa2 and MASCOT lander [6]. Furthermore, variations in spectroscopic properties of large boulders may reflect heterogeneity in Ryugu's parent body, its detailed spectroscopic characterization is of great importance for uncovering the history of asteroid leading to the present state of Ryugu and will be also important for understanding the geologic context for the samples to be obtained from Ryugu.

Acknowledgements: This study was supported by JSPS International Planetary Network.

References: [1] Honda, C. et al. (2018), DPS mtg [2] Tatsumi, E. et al., (2018) DPS mtg, [3] Cho et al. (2018), DPS mtg, [4] Morota et al., DPS mtg, [5] Michel et al., DPS mtg, [6] Jaumann et al. (2018) DPS mtg.

First Global Thermal Images of Asteroid 162173 Ryugu and Implications to Its Surface Thermal Inertia, Grain Size and Roughness

T. Okada^{1,2}, T. Fukuhara³, S. Tanaka¹, M. Taguchi³, T. Arai⁴, H. Senshu⁵, N. Sakatani¹, Y. Shimaki¹, H. Demura⁶, Y. Ogawa⁶, K. Suko⁶, T. Sekiguchi⁷, T. Kouyam⁸, J. Takita⁹, T. Matsunaga¹⁰, T. Imamura², T. Wada¹, S. Hasegawa¹, J. Helbert¹¹, T.G. Mueller¹², A. Hagermann¹³, J. Biele¹¹, M. Grott¹¹, M. Hamm¹¹, M. Delbo¹⁴, N. Hirata⁶, Y. Yamamoto¹, F. Terui¹, T. Saiki¹, S. Nakazawa¹, M. Yoshikawa¹, S. Watanabe^{15,1}, Y. Tsuda¹

¹Japan Aerospace Exploration Agency (JAXA), Japan, ²University of Tokyo, Japan, ³Rikkyo University, Japan,

⁴Ashikaga University, Japan, ⁵Chiba Institute of Technology, Japan, ⁶University of Aizu, Japan,

⁷Hokkaido University of Education, Japan, ⁸National Institute of Advanced Industrial Science and Technology (AIST), Japan,

⁹Hokkaido Kitami Hokuto High School, ¹⁰National Institute for Environmental Studies (NIES),

¹¹German Aerospace Center (DLR), Germany, ¹²Max-Planck Institute for Extraterrestrial Physics, Germany,

¹³University of Stirling, UK, ¹⁴Observatoire de la Côte d'Azur, CNRS, Nice, France

The Thermal Infrared Imager TIR [1] onboard the Japanese asteroid explorer Hayabusa2 [2], investigating the thermo-physical properties of the surface of asteroid 162173 Ryugu, a C-type near-Earth asteroid. The asteroid was observed by TIR almost daily during the approach in June 2018, finding the asteroid rotation period of about 7.6 hours to be consistent with the ground observations [3]. After arrival at the Home Position, 20 km earthward from the asteroid, Ryugu was imaged by the TIR on 30 June 2018, with about 50 pixels size, covering its rotation in steps of 6 degrees. This is the first set of high-resolved global thermal images of an asteroid. The temperatures on the sunlit area varied from 300 to 370K at 0.986 AU from the Sun. A north-south hemispheric difference in temperature was found, which is a seasonal variation due to the pole declination and consistent with the results of numerical simulations using a high-resolved thermo-physical model of Ryugu [4]. Global maps of thermal inertia and grain size were estimated [5] from the temperature profile at each site on the asteroid, especially prepared for the landing site selection. Diurnal temperature profile shows rather flat pattern, indicating the effect of surface small-scale roughness. Several models with surface roughness have been investigated to interpret the flat pattern, and we estimated the most suitable thermal inertia and consequently the grain size. For the safety assessment of touchdown for sampling, the highest temperatures at the time of touchdown have been predicted using the best fit thermal model, suggesting no critical temperature (below 370K) for the spacecraft. Higher-resolved thermal images were obtained during the descent to the lower altitude: 5km during the “Mid-Altitude” observation, 1 km during the “Gravity Measurement”, 60 m during the MINERVA and MASCOT lander release operations, and 10 m for “Touchdown”. The surface physical state and temperature at the landing site of MASCOT will be verified by MARA onboard the lander [6]. We also estimated the highest temperatures ever experienced in the past asteroid trajectory, to investigate the possible existence of organic materials in the surface layer of Ryugu. Large scale geologic features such as craters and boulders are also identified in the thermal images by the temperature difference, indicating the physical state of them. Temperature profiles of several large boulders are basically the same as those of the surrounding surface, which implies the materials with high porosity, which is consistent with the rubble-pile asteroid that formed by recretion and sedimentation of impact fragments from a larger parent body, and with the desiccated and vacuum-dried surface of originally volatile-rich materials.

Acknowledgments

This study was supported by JSPS Grant-in-Aid for Science Research (B), No. 26287108, JSPS Innovative areas (Aqua Planetology), No. 17H06459, and JSPS International Planetary Network.

References

[1] Okada, T. et al. 2017. *Space Sci. Rev.*, 208, 255-286. [2] Tsuda, Y., et al. 2016. *Acta Astronaut.* 127, 702-709. [3] Mueller, T.G. et al., 2017. *A&A*, 599, A103. [4] Takita, J., et al. 2017. *Space Sci. Rev.*, 208, 287-315. [5] Sakatani N. et al. 2017. *AIP Adv.*, 7, 015310. [6] Grott, M., et al., 2017. *Space Sci. Rev.*, 208, 413-431.

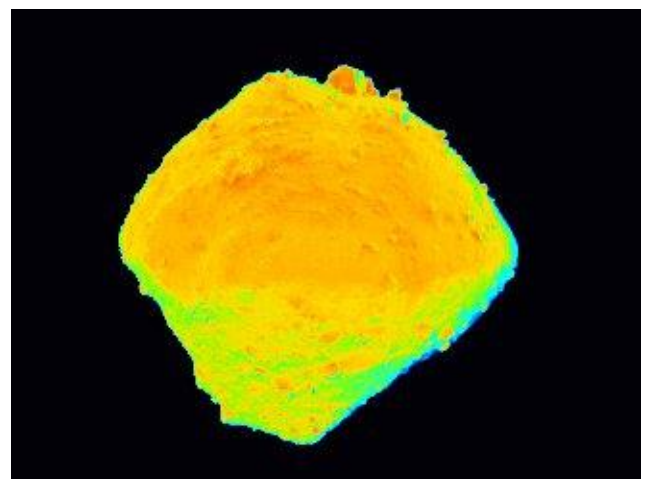


Figure 1 Thermal image of Ryugu observed at 5 km altitude on 1 Aug 2018 (modified from `hyb2_tir_20180801_152656_12a`)

Infrared spectra of asteroid 162173 Ryugu obtained by Near-infrared Spectrometer (NIRS3)

Moe Matsuoka¹, Kohei Kitazato², Takahiro Iwata¹, Masanao Abe¹, Tomoki Nakamura³, Takahiro Hiroi⁴, Takahito Osawa⁵, Makiko Ohtake¹, Shuji Matsuura⁶, Takehiko Arai⁷, Yusuke Nakauchi¹, Mutsumi Komatsu⁸, Hiroki Senshu⁹
¹Japan Aerospace Exploration Agency, ²University of Aizu, ³Tohoku University, ⁴Brown University, ⁵Japan Atomic Energy Agency, ⁶Kwansei Gakuin University, ⁷Ashikaga University, ⁸Graduate University for Advanced Studies, ⁹Chiba Institute of Technology

The asteroid explorer Hayabusa2 was launched in December 2014, and arrived at the target asteroid 162173 Ryugu in June 2018. Near-infrared Spectrometer (NIRS3) onboard Hayabusa2 successfully obtained infrared spectra of Ryugu globally at ~20 km and ~5–7 km above Ryugu surface. The spectroscopic observations of Ryugu are important for estimating the compositional and physical properties of surface material, selecting the landing sites for sampling, and understanding the link between primitive asteroids and carbonaceous chondrites.

NIRS3 is composed of two units: the spectrometric unit (NIRS3-S) and the analog electric unit (NIRS3-AE), which are connected with a harness cable (NIRS3-HNS). A 128-channel indium arsenide (InAs) photodiode sensor is installed in the spectrometric unit and cooled down to 188 K (-85 °C) using a passive radiator. The detectable wavelength range of the spectrometer is 1.8–3.2 μm , and the spectral resolution is ~18 nm. The field of view (FOV) is 0.11° [1, 2] corresponding to the spatial resolutions of 40 m at 20 km altitude and 2 m at 1 km.

We found that Ryugu spectra obtained by NIRS3 are almost homogeneous between places, showing very low albedo (~2% reflectance at phase angle 30°), flat but slightly red slope, and no large absorption features at ~2.7 and ~3.1 μm in wavelength. However, the spectra exhibit slight variety from brighter and bluer spectra on the equatorial ridge to darker and redder spectra in the other areas. No carbonaceous chondrite spectrum collected so far matches exactly with Ryugu spectra. However, some spectra of experimentally-heated hydrous carbonaceous chondrites are similar in terms of their flat shape and low albedo. Ryugu surface might not be totally hydrated because of (1) dehydration due to heating and/or space weathering, or (2) the lack of hydration process.

It is expected that further NIRS3 observations at a lower altitude, at a solar distance larger than 1.027 AU, ONC and NIRS3 observation of the SCI impact crater, MicrOmega observation of the surface regolith, and returned sample analysis will give us more detailed information on the spectral and mineralogical characteristics of Ryugu.

References

[1] Kitazato K. et al. 2015. Abstract #2158. 46th LPSC. [2] Iwata T. et al. 2017. Space Science Reviews 208: 317-337.

Scientific Evaluation on the Asteroid Ryugu in Hayabusa2 Landing Site Selection

H. Yabuta¹, S. Watanabe², T. Nakamura³, N. Hirata⁴, S. Sugita⁵, T. Okada⁶, K. Kitazato⁴, Y. Ishihara⁶, T. Morota², N. Sakatani⁶, K. Matsumoto⁷, K. Wada⁸, S. Tachibana⁵, M. Komatsu⁹, E. Tatsumi⁵, M. Matsuoka⁶, C. Honda⁴, T. Hiroi¹⁰, S. Senshu⁸, R. Honda¹¹, S. Kikuchi⁶, S. Tanaka⁶, A. Miura⁶, T. Yamaguchi⁶, Y. Yamamoto⁶, T. Saiki⁶, Y. Tsuda⁶, LSSAA and LSS-IDS Teams (Hayabusa2 Project)

¹Hiroshima University, ²Nagoya University, ³Tohoku University, ⁴University of Aizu, ⁵Tokyo University, ⁶ISAS/JAXA, ⁷NAOJ, ⁸Chiba Institute of Technology, ⁹Sokendai, ¹⁰Brown University, USA, ¹¹Kochi University

On June 27, 2018, the spacecraft of the Japanese C-type asteroid sample return mission, Hayabusa2, has arrived at the asteroid Ryugu. During its 18-month stay, remote-sensing observations will be carried out with the on-board instruments, Optical Navigation Camera (ONC), Near Infrared Spectrometer (NIRS3), Thermal Infrared Imager (TIR), and Laser Altimeter (LIDAR). Hayabusa2 plans to collect asteroid samples from up to three sites. Based on the remote-sensing data, we will carry out the landing site selection (LSS) in the end of August 2018, for the first touch down (TD1) and for releasing a hopping lander, MASCOT, in the beginning of October 2018. Based on the mission's scientific goals, the most scientifically valuable site for TD1 will be a less altered region where water and/or carbon are abundant.

Seven potential landing sites including equatorial regions (L5, L7, L8, L12) and mid-latitude regions (M1, M3, M4) were proposed based on spacecraft safety and boulder size-frequency by the system engineering team and ONC team. The data products will be obtained at 20 km, 5-7 km and at 5 km in altitude. Shape modeling team produced polygon shape models of Ryugu by two different methods; Shape-from-Motion (SfM) and Stereophotoclinometry (SPC). ONC produces the six types of spectral indices: (i) 0.7 μm absorption depth, (ii) spectral slope from 0.39 μm to 0.95 μm , (iii) spectral slope in ultraviolet, (iv) 0.95 μm absorption depth, (v) scores of PC1 to PC5. NIRS3 produces the spectral feature maps: (i) 3- μm band depth/center, (ii) spectral slope, and (iv) near-infrared albedo. TIR provides the maps of thermal inertia, grain size, and maximum temperature for TD1.

Based on the data products, evaluation and scoring was performed from the three perspectives; Science, Safety, and Sample recovery. Scientific evaluation included the seven topics; 1. Physical properties of surface, 2. Surface age and morphology, 3. Organic carbon compositions and contents, 4. Hydrous minerals distributions, 5. Degrees of heating dehydration, 6. Other minerals and 7. Surface secondary processes.

Distributions of temperature and grain sizes were mostly homogeneous for all the potential landing sites. L7, 8, 12 and M4 are more rough than others. L regions were evaluated as highlands and M regions were evaluated as low lands. The density of craters of Ryugu were comparable to those of Itokawa and Eros, and the surface age of 0.1 to 1 billion years was evaluated. Regarding boulder distributions, L8 and M4 contain less density of large boulders than others.

There was no large variation in the UV-Vis and NIR spectral patterns between all the potential landing sites. Based on the unusual excess of reflectance at 390 nm, the presence of extensively graphitized carbonaceous material is indicated. Assuming that the correlation between v-band albedo (550 nm) and carbon contents is directly applicable, it is estimated that carbon contents of Ryugu is higher than 3%. However there remains uncertainties on the effects of grain size, porosity, and space weathering. Small absorption at 2.7 μm was identified from the NIR spectra of Ryugu, indicating the presence of phyllosilicates. Comparison between the NIR spectra of Ryugu and those of meteorites indicated that the abundances of phyllosilicates are low for all the regions of Ryugu surface. Ryugu could be composed of similar materials to dehydrated C chondrites containing darkening materials, or dark anhydrous material.

The correlation was observed between v-band albedo and b-x slope (480-860 nm). L regions show bluer spectra, while M regions show redder spectra. M1 was particularly red. In the individual regions, L regions are more heterogeneous compared to M3 and M4 regions, showing that wider variety of materials are collected from L regions compared to M regions.

Safety evaluation was complementarily conducted with engineering safety evaluation, based on the area occupied by boulders, median filter, SPC topograph, Hapke roughness parameter, sigma roughness parameter, and grain sizes. Evaluation of samplability was conducted based on the grain sizes and boulder distributions. Summarizing each evaluation, we selected L8, L7 and M4, as the regions that meet both the safety and scientific value for TD1. A variety of topography and geology of Ryugu revealed by the remote sensing observations and LSS scientific evaluation indicates that the mixed samples with different origins would be collected from the selected sites. This would provide the initial sample analysis a great advantage that the origin and chemical evolution of the solar system as well as the formation process and structure of the asteroid Ryugu are comprehensively investigated.

MASCOT's first sight of Ryugu

David Hercik¹, Tra-Mi Ho², Jean-Pierre Bibring³, Karl Heinz Glassmeier¹, Matthias Grott⁴, Ralf Jaumann⁴,
and the MASCOT Team

¹*Technische Universität Braunschweig, Mendelssohnstraße 3, 38106 Braunschweig, Germany*

²*Institute of Space Systems, DLR, Robert-Hooke-Str. 7, 28359 Bremen, Germany*

³*IAS, Université Paris Sud, Bat 121, 91405 Orsay cedex, France*

⁴*Institute of Planetary Research, DLR, Rutherfordstrasse 2, 12489 Berlin-Adlershof, Germany*

Japan Aerospace Exploration Agency's (JAXA) Hayabusa2 successfully arrived to the asteroid Ryugu on 27th of July. In October, a small lander, developed by German Aerospace Center (DLR) and Centre National d'Etudes Spatiales (CNES), called MASCOT is planned to be released from Hayabusa2 to land on Ryugu. MASCOT is equipped with four instruments: MARA - a radiometer (DLR Berlin), MASCAM - a camera (DLR Berlin), MASMAG - a magnetometer (TU Braunschweig), and MicrOmega - an IR imaging spectrometer (IAS Paris). Hereby we will present the first observations and results from the surface of Ryugu as seen by the MASCOT instruments.

Quick-look results for the surface/regolith mechanical properties of Ryugu based on MASCOT bouncing analyses

Jens Biele¹, Patrick Michel², Hajime Yano³, Laurence Lorda⁴, Elisabet Canalias⁴, Thierry Martin⁴, Romain Garmier¹¹, Florian Thuillet², David Hercik⁵, Hans-Ulrich Auster⁵, Nicole Schmitz⁶, Seiji Sugita⁷, Shingo Kameda⁹, Simon Tardivel⁴, Lars Witte⁸, Ralf Jaumann⁶, Stephan Ulamec¹, Tra-Mi Ho⁸, Aurélie Moussi⁴, Friederike Wolff¹⁰, Stefaan van Wal³

¹*DLR - German Aerospace Center, RB-MSC, 51137 Köln, Germany, email: Jens.Biele@dlr.de*

²*Université Côte d'Azur, Observatoire de la Côte d'Azur, CNRS, Laboratoire Lagrange, Nice, France*

³*Institute of Space and Astronautical Science, Japan Aerospace Exploration Agency, Sagami-hara, Japan*

⁴*CNES, 18 Avenue E. Belin, Toulouse 31401, France*

⁵*Technische Universität Braunschweig, Mendelssohnstraße 3, 38106 Braunschweig, Germany*

⁶*DLR - German Aerospace Center, Institute for Planetary Research, 12489 Berlin, Germany*

⁷*Dept. of Earth and Planetary Science, School of Science, University of Tokyo, 7-3-1 Hongo, Bunkyo-ku, Tokyo 113-0033, Japan*

⁸*DLR - German Aerospace Center, RY, 28359 Bremen, Germany*

⁹*Department of Physics, Rikkyo University, 3-34-1 Nishi-Ikebukuro, Toshima, Tokyo 171-8501, Japan*

¹⁰*DLR SR, 82234 Weßling, Germany*

¹¹*CS-SI - rue Brindejone des Moulinais, Toulouse 31500, France*

We present quick-look results and constraints on the mechanical properties of the regolith on asteroid 162173 Ryugu, based on expected data regarding the mechanical interactions by the lander MASCOT as well as data from MINERVA nano-landers and possibly from the first sampling touchdown by Hayabusa2.

MASCOT is going to be deployed from an altitude of ~55 m and has a touch-down velocity of ~0.2 m/s. It is expected to bounce several times before coming to rest [3]. The descent trajectory and the larger bouncing arcs can be captured by optical imaging from the spacecraft (ONC [5]) giving constraints on MASCOT in-flight trajectories. Moreover, direct images of footprints as well as data from MASCOT's magnetometer MASMAG [4] on bounce times (and possibly rotation rates or changes thereof), images by MASCOT's camera MASCAM [2] during bouncing and their fusion with ONC images projected to the shape, and finally MASCAM images after rest offer a rich database that allows us to constrain Ryugu's surface mechanical properties, with implications on the asteroid's surface history. Variations of the radio-frequency signal all along MASCOT's trajectory and day/night detection by MASCOT's photoelectric cell sensors can also contribute to the analysis.

The measured total linear energetic coefficient of restitution (CoR), i.e. the fraction of energy dissipated at each bounce, can be compared to the CoR values measured for the MASCOT structure bouncing against a hard wall [6] and soft-sphere DEM simulations of MASCOT landing on a bed of granular material [7,8]. Footprint images of the bounce imprints in loose granular material also constrain the granular frictional properties and the regolith depth.

Preliminary conclusions on the mechanical properties of Ryugu's surface material will be drawn.

References

- [1] Ho, Tra-Mi, et al. "MASCOT—the mobile asteroid surface scout onboard the HAYABUSA2 mission." *Space Science Reviews* 208.1-4 (2017): 339-374. MASCAM
- [2] Jaumann, R., Schmitz, N., Koncz, A., Michaelis, H., Schroeder, S. E., Mottola, S., ... & Kachlicki, J. (2017). The camera of the MASCOT asteroid lander on board Hayabusa 2. *Space Science Reviews*, 208(1-4), 375-400.
- [3] Garmier R. et al: "MASCOT landing on Asteroid Ryugu : flight dynamics team contribution to the landing site selection process", 2018 SpaceOps Conference, SpaceOps Conferences, (AIAA 2018-2645)
- [4] Hercik, D., Auster, H. U., Blum, J., Fornaçon, K. H., Fujimoto, M., Gebauer, K., ... & Matsuoka, A. (2017). The MASCOT magnetometer. *Space Science Reviews*, 208(1-4), 433-449.

[5] Kameda, S., Suzuki, H., Takamatsu, T., Cho, Y., Yasuda, T., Yamada, M., ... & Sato, M. (2017). Preflight calibration test results for optical navigation camera telescope (ONC-T) onboard the Hayabusa2 spacecraft. *Space Science Reviews*, 208(1-4), 17-31.

[6] Biele, Jens, et al. "Experimental Determination of the Structural Coefficient of Restitution of a Bouncing Asteroid Lander." arXiv preprint arXiv:1705.00701 (2017).

[7] Maurel, C., Michel, P., Biele, J., Ballouz, R. L., & Thuillet, F. (2017). Numerical simulations of the contact between the lander MASCOT and a regolith-covered surface. *Advances in Space Research*.

[8] Thuillet, Florian, et al. "Numerical modeling of lander interaction with a low-gravity asteroid regolith surface-Application to MASCOT on board Hayabusa2." *Astronomy & Astrophysics* 615 (2018): A41.

Brightness and Color Variations on the Surface of 162173 Ryugu: Space Weathering, Thermal Fatigue and Mass Movement

Sho Sasaki¹, Seiji Sugita², Eri Tatsumi², Hideaki Miyamoto², Chikatoshi Honda³, Tomokatsu Morota⁴, Olivier S Barnouin⁵, Masatoshi Hirabayashi⁶, Masanori Kanamaru¹, Naru Hirata³, Takahiro Hiroi⁷, Tomoki Nakamura⁸, Takaaki Noguchi⁹, Rie Honda¹⁰, Tatsuhiro Michikami¹¹, Seiichiro Watanabe⁴, Noriyuki Namiki¹², Patrick Michel¹³, Shingo Kameda¹⁴, Toru Kouyama¹⁵, Hidehiko Suzuki¹⁶, Manabu Yamada¹⁷, Hiroshi Kikuchi², Deborah Lorin Domingue¹⁸, Yuichiro Cho², Kazuo Yoshioka², Masahiko Hayakawa¹⁹, Moe Matsuoka¹⁹, Naoya Sakatani¹⁹, Hirotaka Sawada¹⁹ and Yasuhiro Yokota¹⁹

¹*Osaka University, Earth and Space Science, Toyonaka, Japan,*

²*The University of Tokyo, Bunkyo-ku, Japan,*

³*University of Aizu, Aizu-Wakamatsu, Japan,*

⁴*Nagoya University, Nagoya, Japan,*

⁵*JHU Applied Physics Lab, Laurel, MD, United States,*

⁶*Auburn University, Aerospace Engineering, Auburn, AL, United States,*

⁷*Brown University, Providence, RI, United States,*

⁸*Tohoku University, Sendai, Japan,*

⁹*Kyushu University, Fukuoka, Japan,*

¹⁰*Kochi University, Kochi, Japan,*

¹¹*Kinki University, Higashi-Hiroshima, Japan,*

¹²*NAOJ National Astronomical Observatory of Japan, Mitaka, Japan,*

¹³*UNS-CNRS-Observatoire de la Cote d'Azur, Nice, France,*

¹⁴*Rikkyo University, Tokyo, Japan,*

¹⁵*National Institute of Advanced Industrial Science and Technology, Tsukuba, Japan,*

¹⁶*Meiji University, Kawasaki, Japan,*

¹⁷*Chiba Institute of Technology, Planetary Exploration Research Center, Narashino, Japan,*

¹⁸*Planetary Science Institute Tucson, Tucson, AZ, United States,*

¹⁹*JAXA/ISAS, Sagami-hara, Japan*

162173 Ryugu is a dark body with overall visible albedo is 4.6% and photometry standard reflectance is lower than 2% (Tatsumi et al., 2018, DPS&AGU). Ryugu is the one of the darkest body in the solar system. However, there is striking brightness (and associated) color difference on the surface. Bright, large boulders are on polar regions and smaller ones with similar brightness are scattered globally. Regionally, the equatorial ridge and some of undulated crater rim zones are brighter. Some boulders shows brightness variation within their surface, suggesting brightness/color difference may not be due to compositional variation but to the differences of space weathering maturity. Two types of space weathering are advocated for carbonaceous asteroids: darkening (and reddening) or brightening (and bluing) with time. On Ryugu, probably thermal fatigue and/or local impacts should have brightened the boulder surface (i.e., large boulders on both poles). Ridge/crater brightness can be ascribed to movement of fine darker materials to potentially lower region. In high-resolution images (<1m), Ryugu's surface is covered with fine (and darker) regolith materials that would cover and bury boulders. Like the large boulders on both poles, bright boulders usually have smooth surface and brightness is affected by darker regolith and shadow (Fig.1). There observed also darker boulders with rough/undulated surface, which would have experienced longer exposure and thus more erosion and weathering. We can observe the relation between brightness and surface roughness also in close-up images (Figs.2). In the left figure, there is a large (40m) relatively darker boulders with rough and layered surface. This is partially covered with much darker regolith materials. In the right figure, we observe bright layered boulders with smooth surface. Some feature (e.g., Fig. 3) would be explained by conglomerate or breccia, rather than regolith coverage.

Acknowledgements: This study was supported by JSPS International Planetary Network (S. Sugita) and Grant-in-Aid for Scientific Research (B) (S. Sasaki).

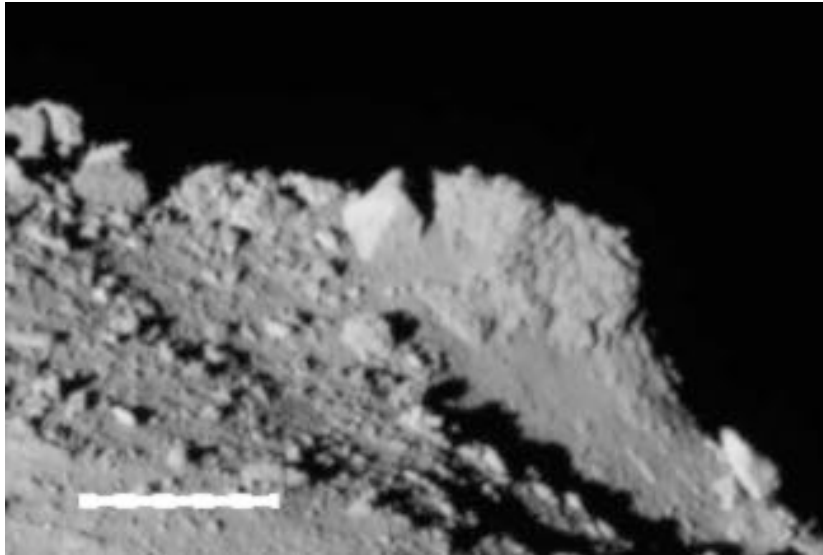
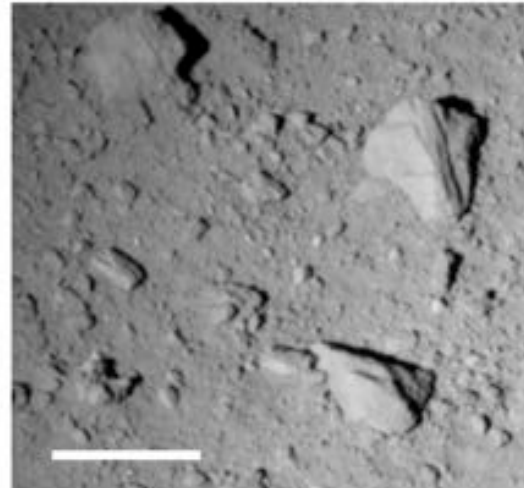
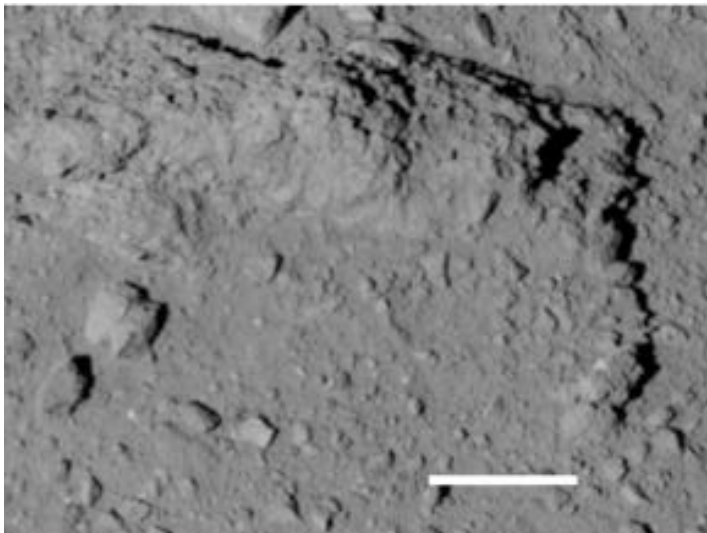


Figure1 Bright/smooth and dark/rough boulders on the polar region of Ryugu, Both are partly covered by darker regolith. The length of the white scale is 50m.



Figures 2 The surface of Ryugu where ONC-T camera captured from about 1km height. Length of white scales is 10m.

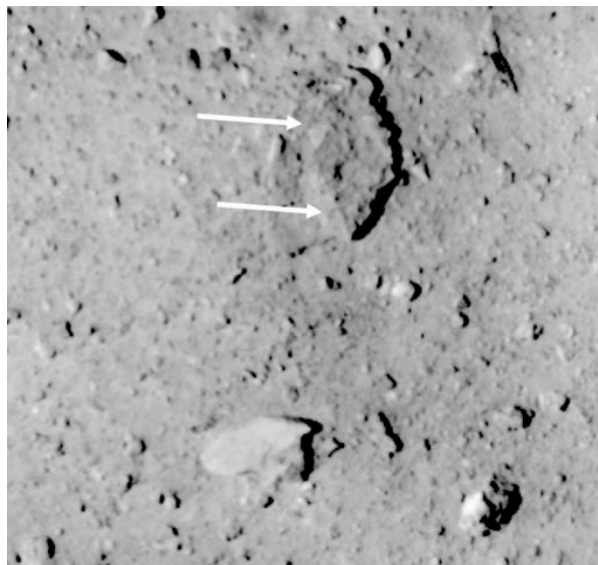


Figure 3 The surface of Ryugu (at relatively boulder poor region). Arrows show possible breccia

Gaussian Deconvolution of the 2.7- μ m Absorption Band of Type 1 and 2 Carbonaceous Chondrites for Interpreting Hayabusa2 Near-Infrared Spectrometer (NIRS3) Data

T. Hiroi¹, R. E. Milliken¹, K. M. Robertson¹, H. Kaiden², K. Misawa², H. Tanaka³, S. Sasaki³, M. Matsuoka⁴, T. Nakamura⁵,
¹Department of Earth, Environmental and Planetary Sciences, Brown University, ²Antarctic Meteorite Laboratory, National Institute of Polar Research, ³Department of Earth and Space Sciences, Osaka University, ⁴JAXA Institute of Space and Astronautical Science, ⁵Department of Earth and Planetary Materials Sciences, Tohoku University

Introduction: Continuing our previous work of deconvolving the composite 3- μ m absorption band of type 1 and 2 carbonaceous chondrites (CCs) to derive the correlation between the 2.7- μ m hydroxyl absorption band characteristics and CC types [1], in this study we have expanded the number of CC reflectance spectra, and also converted them into simulated Hayabusa2 Near-Infrared Spectrometer (NIRS3) [2] in an attempt to help interpreting data of the asteroid 162173 Ryugu.

Experimental: In addition to the previously studied reflectance spectra (2.5-4 μ m) of powder or pressed pellet samples of CCs (CI mix: Ivuna-Orgeuil mixture, Murchison and Y-793595 (CM2), Renazzo (CR2), and Tagish Lake) [1], spectra of UV-irradiated Murchison and laser-irradiated Y-793595 pellet samples, powder samples of Kaidun and 15 CM2 chondrites including MET 00639 (probably shocked), and a chip sample of MIL 13005 (CM1/2) have been either newly measured or taken from the RELAB database [3].

Method: Following our previous study [1], natural log reflectance spectrum of each sample was deconvolved into a linear continuum background and Gaussians (both in wavenumber) over a wavelength range from 2.67 μ m to around 3.8 μ m. Gaussians centered beyond about 2.8 μ m were regarded as due to adsorbed water or organics [4] and removed from the natural log reflectance spectrum, the remaining portion was restored to the reflectance space, and resampled to the NIRS3 bands.

Results: Examples of those Gaussian deconvolutions of simulated NIRS3 spectra of the CC samples are shown in Fig. 1. These deconvolution calculations used only two Gaussians for the hydroxyl bands, although the original laboratory spectra may have taken three to fit. The band centers and the relative strength of these two bands are plotted in Fig. 2. There seems to be a trend that aqueous alteration, shock, and space weathering all shift band centers toward shorter wavelength.

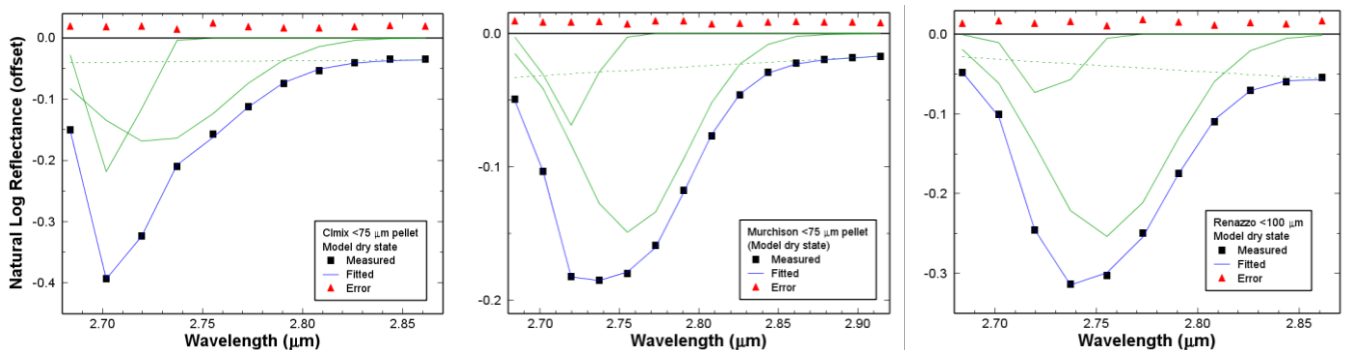
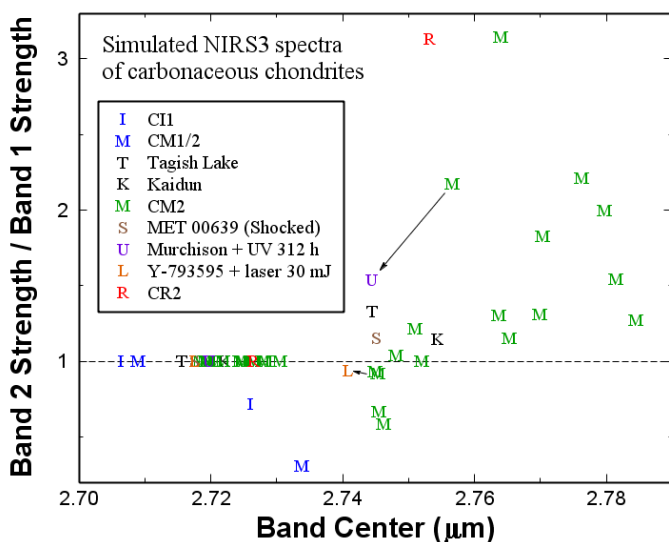


Figure 1. Examples of Gaussian deconvolutions of NIRS3-simulated spectra of type 1 and 2 carbonaceous chondrites.



Acknowledgment: Antarctic meteorite samples were loaned from National Institute of Polar Research or NASA Johnson Space Center. RELAB is a multiuser laboratory supported by NASA SSERVI. T. H. was supported by NASA PDART grant.

References: [1] Hiroi T. et al. 2018. Abstract #1056. 49th LPSC. [2] Iwata T. et al. 2017. Space Sci. Rev. 208, 317. [3] RELAB database: <http://www.planetary.brown.edu/relabdata/>. [4] Takir D. et al. 2013. Meteoritics Planet. Sci. 48, 1618.

Figure 2. Band centers and relative strength of two hydroxyl bands of model spectra of CCs such as those shown in Fig. 1.

Abrasion experiments of mineral and meteorite grains: Application to grain abrasion of Itokawa, Ryugu and lunar regolith particles.

A. Tsuchiyama¹, M. Ogawa¹, H. Yamaguchi¹, and A. Nakamura²

¹*Division of Earth and Planetary Sciences, Graduate School of Science, Kyoto University, Kyoto, JAPAN*

²*Department of Planetology, Graduate School of Science, Kobe University, Kobe, JAPAN*

Introduction: The external 3D shapes of Itokawa regolith particles by X-ray microtomography showed that some particles have rounded edges, which should be formed by mechanical abrasion [1]. Abraded surfaces were confirmed by detailed observation using SEM [2]. Mechanical abrasion of lunar regolith particles was also recognized by X-ray microtomography and SEM as well [3]. Seismic wave induced by micrometeoroid impacts [1], YORP effect and tidal motion [4] were proposed for the abrasion process on Itokawa.

In order to understand detailed process of the abrasion, abrasion experiments have been carried out [5]. In these abrasion experiments, quartz, olivine (Fo₉₀ from San Carlos), corundum and calcite (marble) as mineral samples and Sayh al Uhaymir 001 (L5) and Murchison (CM2) as meteorite samples were used. They were crushed into particles 1-2 mm in size except for corundum (~1mm). These particles (~6.5g) were put into a vessel (10 mL) (filling fraction of 50%) without any crushing tool, and the vessel was vibrated in a mill (Multi-beads-shocker: YASUIKIKAI Co.). Time changes of the amounts of powders produced by abrasion and their external shapes using X-ray microtomography were measured. In addition, the external shapes of marked particles were traced using X-ray nanotomography in a series of abrasion experiments. Based on the experiments, two modes of abrasion were recognized; gradual wearing and chipping of particle edges. The 3-axial ratios of particles almost unchanged by gradual wearing while they changed by chipping. It was proposed that the former process is responsible for Itokawa particle abrasion and later for lunar particle abrasion. However, the grain size used in the experiments (~1 mm) is larger than the regolith particle size (~0.1 mm).

In this study, additional experiments were made to understand the size effect and the abrasion rates were applied to abrasion on Itokawa and Moon by considering the size effect. Abrasion of Ryugu regolith particles, which will be returned by the Hayabusa2 spacecraft, was also discussed.

Experiments and analytical procedure: Quartz particles with three different sizes (0.5-1 mm, 1-2 mm and 2-4 mm) were used in the experiments on the size effect. The abrasion experiments were made at vibration rate of 2000 rpm only for 1 min. The other conditions are the same as those in the previous experiments. After the experiments, the mass of powder (<250 μm) produced by abrasion was measured.

Figure 1 shows the result in the previous experiments using olivine grains [5], where proportion of abraded powder in the total mass as the amount of abrasion, P , is plotted against the duration, t . We used the proportion at first 1 min., P_1 , as the representative of the abrasion rate for comparison among different samples and sizes.

Results: In the present experiments, the P_1 value is almost proportional to the average of particles size, d ; P_1 (%) = $0.849(12) \times d^{0.987(15)}$ (Fig. 2). By using this relation, we can correct P_1 values of a different size to that of 1-2 mm particle. Figure 3 shows the P_1 values for different samples with 1-2 mm as a function of the vibration rates, ω . P_1 increases with increasing ω in a power law with the power index of ~2 to 3. These relations may correspond to $E_{vib} \propto \omega^2$, where E is the vibration energy. The abrasion rate decreases from corundum, olivine ~

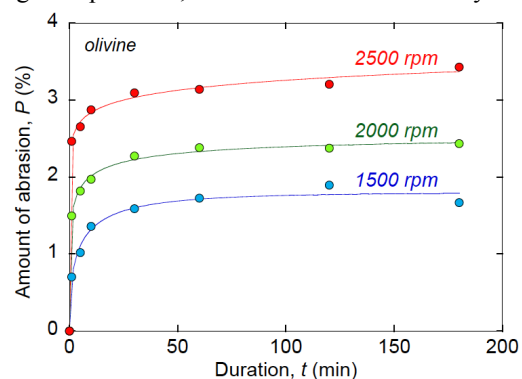


Figure 1. Amount of abrasion, P , plotted against duration, t , for different vibration rates, ω , using olivine samples.

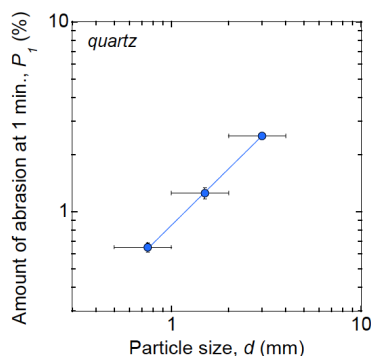


Figure 2. Amount of abrasion at 1 min., P_1 , plotted against particle size, d , of quartz at $\omega = 2000$ rpm.

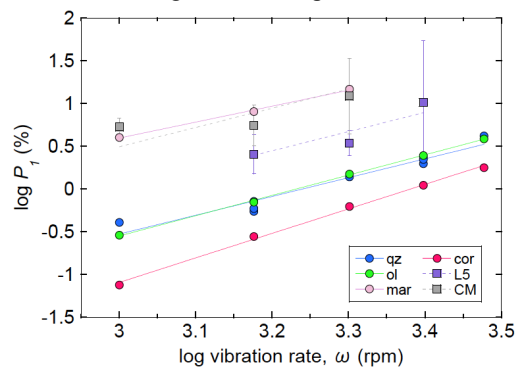


Figure 3. Amount of abrasion at 1 min., P_1 , for 1-2 mm grains plotted against vibration rates, ω .

quartz to calcite (marble), and this order is consistent with their mechanical strengths. The data of L5 and CM chondrites were obtained from only six particles in each run and thus have large errors.

Discussion: The degrees of abrasion of regolith particles on Itokawa and Moon were roughly estimated from the present experiments. Figure 4 shows P_I in a wide range of ω , where the values of P_I of SaU 001 (L5) and Murchison (CM) grains obtained in the experiments are extrapolated with the log slop of 2 by considering $E_{vib} \propto \omega^2$. The following three types of estimation were made; (1) abrasion by impact-induced convection in a regolith layer, (2) abrasion in an ejecta during impact and (3) abrasion in a regolith layer during impact. In order to compare the grain velocity, v , and acceleration, a , in the models with those of the experiments, we used the means of absolute velocity and acceleration ($\langle |v| \rangle$ and $\langle |a| \rangle$, respectively) by assuming simple harmonic motion of the sample vessel in the experiments (amplitude; 0.015 m). The corresponding values of $\langle |v| \rangle$ and $\langle |a| \rangle$ to ω are shown in Figure 4.

(1) *Abrasion by impact-induced convection:* Yamada and Katsuragi [6] estimated the convection velocity, v_{conv} , in a regolith layer of Itokawa due to impact-induced seismic shaking [1]. The typical value at the time of impact is ~ 6 mm/s. The corresponding P_I for L5 is only $10^{-4} \sim 10^{-5}$ %, and if the size effect ($P_I \propto d^{-1}$) is taken into consideration P_I with a few 100 μm grains should be $10^{-4} \sim 10^{-5}$ %. These values indicate that abrasion cannot effectively occur by this process on Itokawa.

(2) *Abrasion in an ejecta during impact:* In order to evaluate the possibility of abrasion by contact of grains during excavation and ejection by impact, the ejecta velocity, v_{eject} , was estimated as a function of the launch position of ejecta from the crater center, x , and the crater radius, R , using the model of [7]. On Itokawa, $v_{eject} \sim 0.001 \sim 0.1$ m/s (corresponding $\omega \sim 1 \sim 100$ rpm) for $R=1$ cm \sim 100 m at $x/R \sim 1$. The corresponding P_I values for 1-2 mm L5 grains are $\sim 0.01 \sim \sim 10^{-6}$ % (Fig. 4) ($\sim 0.001 \sim \sim 10^{-7}$ % for a few 100's μm grains). This indicates that effective abrasion is not expected. It should be also noted that only grains with v_{eject} less than the escape velocity of Itokawa, $v_{esc} \sim 0.2$ m/s, can survive, suggesting $P_I < \sim 0.01$ % for 1-2mm grains (Fig.4). In contrast, on Moon, $v_{eject} > 1$ m/s ($\omega > \sim 1000$ rpm) for $R > 1$ m at $x/R \sim 1$, indicating that abrasion is possible on Moon by this mechanism.

(3) *Abrasion in a regolith layer during impact:* In order to evaluate the possibility of abrasion by contact of grains in a regolith layer during impact, the maximum acceleration of the first peak on impact-induced seismic wave, g_{max} , was estimated as a function of distance from the impact point, x , for different impactor radius, r , using the model of [8] and the crater size model using the π -scaling theory [9]. The estimated g_{max} values on Itokawa and Moon are ~ 2 and ~ 100 m/s² irrespective of the impact conditions. The corresponding P_I values for 1-2 mm L5 grains are ~ 0.01 and ~ 1 % (~ 0.001 and ~ 0.1 % for a few 100's μm grains) on Itokawa and Moon, respectively (Fig. 4). Therefore, abrasion on Itokawa is not possible while it is possible on Moon.

The above discussion suggests that abrasion by impact is almost impossible on Itokawa while it is possible on Moon. Mechanical abrasion is so high energetic process that this cannot occur on small asteroids, like Itokawa. Accordingly, Itokawa regolith particles with rounded surfaces by abrasion should originate from the parental body of Itokawa, where abrasion occurred by impact on the body. For the case of Ryugu, v_{conv} may be also small and thus abrasion is not expected even for materials with smaller strength, like CM, by the process (1). In the process (2), if v_{eject} is slightly less than v_{esc} (~ 0.4 m/s), the maximum values of P_I for CM grains are estimated to be ~ 1 % (1-2 mm) and ~ 0.1 % (a few 100's μm) (Fig.4). Similar values of P_I are expected in the process of (3) although we cannot estimate g_{max} with good precision at this moment. These P_I values may suggest that a small degree of abrasion of regolith particles on Ryugu is possible.

References: [1] Tsuchiyama A. et al. 2011. Science, 333: 1121. [2] Matsumoto T. et al. 2016. GCA 187: 195. [3] Tsuchiyama A. et al. 2016. 4th Symp. Solar System Materials. [4] Connolly H. et al. 2015. EPS 67: 12. [5] Tsuchiyama A. et al. 2018. Abstract #1844. 49nd LPSC. [6] Yamada T. M. and Katsuragi H. 2016. Planetary and Space Science 100: 79. [7] Housen & Holsapple, 2011. [8] Yasui, M. et al. 2015, Icarus 260: 320. [9] Holsapple, K. A. 1993. Annu. Rev. Earth Planet. Sci. 21: 333.

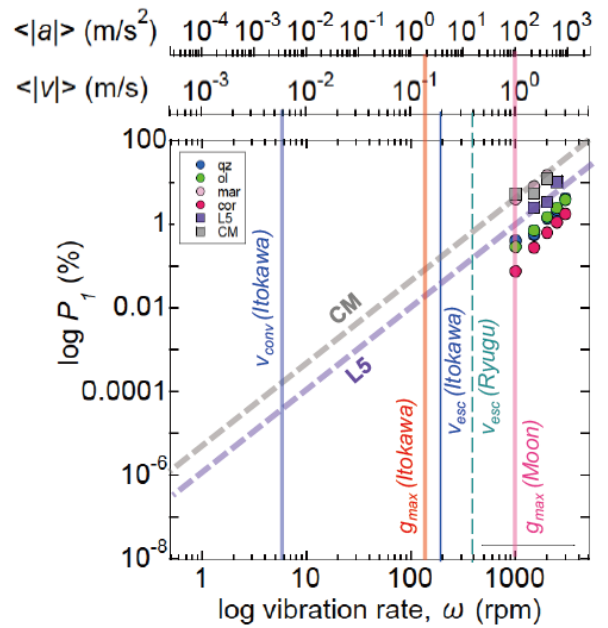


Figure 4. Estimation of the amount of abrasion at 1 min., P_I , with 1-2 mm grains for Itokawa, Ryugu and Moon.

Comparison of solar wind He implantation profiles between Genesis collectors separately implanted fast-speed flow, low-speed flow, and coronal mass ejection flow components

K. Bajo¹, A. Tonomani¹, C. T. Olinger², A. J. G. Jurewicz³, D. S. Burnett⁴, I. Sakaguchi⁵, T. T. Suzuki⁵, S. Itose⁶, M. Ishihara⁷, K. Uchino⁸, R. Wieler⁹, and H. Yurimoto^{1,10}

¹*Department of Earth and Planetary Sciences, Hokkaido University, Sapporo 810-0060, Japan.*

²*Applied Modern Physics Group, Los Alamos National Laboratory, Los Alamos, NM 87545, USA.*

³*CMS/SESE, Arizona State University, Tempe, AZ 85287-1404, USA.*

⁴*Division of Geological and Planetary Sciences, California Institute of Technology, CA 91125, USA.*

⁵*National Institute for Materials Science, Tsukuba, Ibaraki 305-0044, Japan.*

⁶*JEOL Ltd., Akishima, Tokyo 196-8558, Japan.*

⁷*Department of Physics, Osaka University, Toyonaka, Osaka 560-0043, Japan.*

⁸*Graduate School of Engineering Sciences, Kyushu University, Kasuga, Fukuoka 816-8580, Japan.*

⁹*Institute for Isotope Geology and Mineral Resources, ETH Zurich, 8092 Zurich, Switzerland.*

¹⁰*Institute of Space and Astronautical Science, Japan Aerospace Exploration Agency, Sagami-hara 252-5210, Japan*

NASA's Genesis mission collected samples of solar wind that can be analyzed with high precision in laboratories. Sputtered neutral mass spectrometry (SNMS) with tunneling ionization has been applied to measure ⁴He profiles in Genesis Bulk collector [1], of which apparatus was Laser Ionization Mass nAno Scope (LIMAS). The instrument can quantify ⁴He presented at tens of ppma from an area of few-microns across of a solid surface. Depth profiling was carried out for isotope analysis of He and Ne of solar wind from a Genesis diamond-like carbon film on a silicon (DOS) substrate, which was irradiated by bulk solar wind for 2.3 years. The depth profile of ⁴He in deep (>100 nm) was comparable with a background ⁴He as residual gas a sample chamber of LIMAS [1]. The residual gas corresponded to $\sim 3 \times 10^{-4}$ He⁺ count per mass scan (cpms). Here we analyzed Genesis H, L, and E collectors of Genesis irradiated by high-speed or coronal hole flows, low-speed or interstream flows, and coronal mass ejection (CME), respectively.

Helium depth profiles for the three collectors should be different each other on the basis of ACE/SWICS data [2]. A measurement condition for the depth profiling was improved to distinguish each depth profile of the target isotopes. An ion pump of 410 l/s (Agilent VacIon plus 500) and a non evaporation getter (NEG) pump were replaced to reduce residual noble gases in the sample chamber. To increase ion intensity, we installed high power Ti-sapphire fs laser (Astrella, Coherent, Inc.) of 6 mJ per 30 fs pulse to increase ionization efficiency for He [3]. As a result, the background He abundance, which was the same measurement for sample without the primary beam pulse for sputtering, decreased from $\sim 3 \times 10^{-4}$ He⁺ cpms to $\sim 2 \times 10^{-5}$ cpms. The ion intensity of 2×10^{-5} cpms corresponds atom concentration of $\sim 10^{17}$ cm⁻³ (~ 1 ppma) under the same measurement condition. A useful yield of He are increased from 9×10^{-5} [1] to 5×10^{-4} . Control timing for the mass spectrometer [3] were also refined to measure multi-isotopes at the same time. Mass resolving power for He depth profiling was $\sim 13,000$ in 99% valley after 95 multi-turn of $m/z = 4$ in MULTUM II to separate ⁴He⁺ from ¹²C³⁺ of the main element of the DOS.

Depth profiles for ⁴He and ^{20,22}Ne of the DOS samples from the three Genesis collectors were measured at the same time. A ⁴He depth profile of the H collector showed relatively symmetric with a peak of 35 nm. A profile of the L array showed that ⁴He was concentrated less than 40 nm and the peak was 10–20 nm, which was close to the limit of the depth resolution of 30 keV Ga⁺ beam. The E array demonstrated broad ⁴He profile and observed ⁴He in deep (>100 nm) as well as the bulk collector. On the other hand, He in deeper than 150 nm of the Genesis H and L arrays were equivalent to the background level. This He in deep indicates that the ⁴He in deep should be derived from the questionable very high-speed flows (Halloween event of 2003) during October 23–November 3 2003 [2]. The depth of the 35 nm for the H collector corresponds to the speed of 600 km s⁻¹. The L collector profile should be corresponded to 400 km s⁻¹ of the solar wind. The ⁴He deeper than 100 nm of the E collector represents faster than 1000 km s⁻¹ derived from the Halloween event of 2003.

References

- [1] K. Bajo et al. (2015) *Geochem. J.*, 49, 559-566. [2] D. B. Reisenfeld et al. (2013) *Space Sci. Rev.* 175, 125-164. [3] A. Tonomani et al. (2016) *Surf. Interface Anal.*, 48, 1122-1126. [4] K. Bajo et al. (2018) *Surf. Interface Anal.*, accepted.

Hayabusa2 sample recovery and phase-1 curation

M.Abe^{1,2}, T. Yada¹, K. Yogata¹, T. Okada^{1,3}, K. Sakamoto¹, M. Yoshitake¹, S. Furuya¹, M. Nishimura⁴, K. Kumagai⁴,
and H. Yurimoto^{5,1}

¹*Institute of Space and Astronautical Science,*

²*SOKENDAI,*

³*University of Tokyo,*

⁴*Marinen Works Japan LTD,*

⁵*Hokkaido University*

Hayabusa2 spacecraft will bring back the C-type asteroid Ryugu sample to the Earth in the end of 2020. Astromaterials Science Research Group (ASRG) of ISAS/JAXA will execute re-entry capsule recovery at landing site, sample extraction from sample container, initial description of the sample, distribution the samples to succeeding detail analysis, and storage the sample for future generation. In this presentation, we report the current plan of sample recovery and phase-1 curation of our group.

10 % amount of Hayabusa2 returned sample will be delivered to NASA according to MOU between NASA and JAXA. The rest of the sample will be used for detail analysis operated by initial analysis team directed by Hayabusa2 project and phase-2 curation teams collaborated with ASRG, and after that, will be open for international AO. Schedule of curatorial work and sample distribution plan for Hayabusa2 will be shown in Fig.1 as below.

Initial analysis will be done by the Hayabusa2 mission to maximize the scientific achievement of the project for 12 months after the phase-1 curation (sample description at the ISAS curation facility). The initial analysis should be a good showcase to prove the potential of the rest of samples. Along with the initial analysis, the phase-2 curation of returned samples will be done for integrated thorough analysis and description of samples to build a sample database and to obtain new scientific perspective from thorough analysis of samples. The phase-2 curation will be done both in ISAS and also in several research institutes outside JAXA led by the ISAS curation facility.

After the recovery of the re-entry capsule, the sample container will be extracted from the re-entry capsule at the landing site like Hayabusa mission. In Hayabusa2 mission, residual gas sampling from the sample container will be done at the landing site moreover. After that the sample container will be transported to ISAS curation facility, and outer lid extraction and cleaning of the outer surface of the sample container will be done in the clean room. Opening operation of the inner lid of the sample container and picking up operation of a few samples from sample container will be done in the clean chamber in vacuum environment.

The rest sample will be handled in the another clean chamber in ultra pure nitrogen environment. Returned sample will be stored in the sample catcher connected with inner lid of the sample container. Sample catcher is consisted in 3 rooms. The samples obtained from 3 touch down sites of the spacecraft at the asteroid Ryugu is stored in each rooms. In the clean chamber, we will observe inside of each rooms using optical scope, and remove the samples of each rooms to the each quartz dishes. After extraction of the sample from sample catcher, we will initial description of bulk sample at first. These procedure will be used by optical microscope, infrared spectroscope, and weighing device. After bulk observation, we will pick up each particles of larger than 1 mm (TBD) size and storage into each quartz dishes separately.

In the phase-1 curation will be done within 6 months after the re-entry capsule recovery. After phase-1 curation, we will delivered some portion of the returned sample to detail analysis, which is operated by initial analysis team and phase-2 curation team. The amount of the sample for the initial analysis will be 15%(TBD) of the recovered samples. Representative and unprocessed sample will be desired by the initial analysis. Initial analysis also desires coarse and fine particle. ISAS curation will be delivered the fine particle in one bundle. The samples delivered to phase-2 curation will be selected by ISAS curation considering the result of the initial description. The amount of the samples will be 15%(TBD) including detail analysis at phase-1 curation and outreach sample. The purpose of phase-1 detail analysis is confirmation of the sample origin (the return sample is originated from Ryugu or not), ascertainment of the sample heterogeneity, and discrimination of the contamination by composition analysis of some portion of the returned sample using SEM (TBD) at ISAS curation.

In principle, during phase-1 curation, it is based on nondestructive and uncontaminated description, however, for conducting composition analysis, we will allow the contamination for some portion of the sample by SEM observation.

New clean room and clean chamber for receiving Hayabusa2 returned sample will be established by the end of this year. We are currently preparing the observation instrument and handling tool of returned sample. From this year we started the operational test of the clean chamber, and we will start to the rehearsal operation including handling test of the analog sample from next year. We will finish rehearsal and reharbush of the clean chamber by earth return of the spacecraft in the end of 2020.

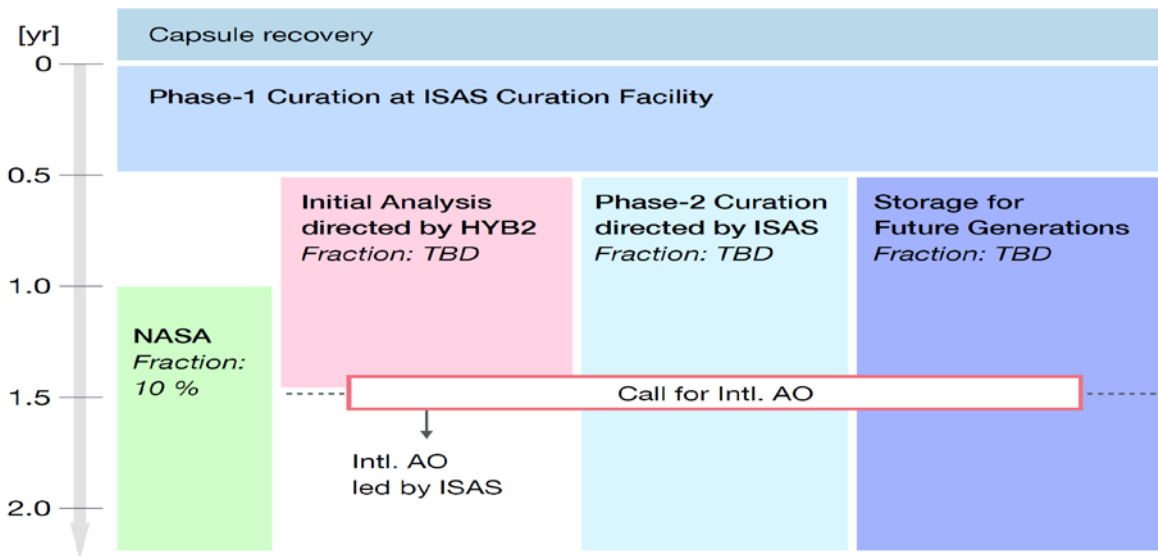


Fig.1 Shcedule of curatorial work and sample distribution plan for Hayabusa2

A perspective of Phase 2 Curation “Team Kochi” for Hayabusa2 returned sample: *in-depth* analysis of a single grain utilizing linkage microanalytical instruments

M. Ito¹, N. Tomioka¹, M. Uesugi², K. Uesugi², T. Ohigashi³,
A. Yamaguchi⁴, N. Imae⁴, Y. Karouji⁵, N. Shirai⁶, T. Yada⁷ and M. Abe⁷

¹Kochi Inst. for Core Sample Res., JAMSTEC, ²JASRI/SPring-8, ³UVSOR, Inst. Molecular Science,
⁴National Inst. Polar Research, ⁵JSEC/JAXA, ⁶Tokyo Met. Univ., ⁷ISAS/JAXA

Analyses of returned samples from asteroid [1] and comet [2] were essential to understand their origin and nature as well as increasing our knowledge about the Solar System. The most recent returned sample was from the S-type asteroid Itokawa by Hayabusa mission in 2010. The results by series of researches provided new insights for the connection to meteorites, space weathering processes, small asteroidal body formation in the Solar System [e.g., 1, 3, 4]. JAXA Hayabusa2 and NASA Osiris-REx are both current sample return missions from the organic-rich asteroids, Ryugu (C-type) and Bennu (B-type), respectively [5, 6]. Both missions have complementary scientific goals that are to understand the Solar System evolution in the point of view of organics, water, and associated minerals.

Phase 2 curation teams will be acting under the scientific direction and strong ethic of the Astromaterial Science Research Group (ASRG) of JAXA and was authorized 2 institutes by the steering committee of the ASRG in 2017: (1) Kochi Inst. for Core Sample Research, JAMSTEC in collaboration with JASRI/SPring-8, UVSOR/Inst. Molecular Science, National Inst. Polar Research and Tokyo Metropolitan University, and (2) the Inst. for Planetary Materials, Okayama University at Misasa. The JAXA Curation requested us to make an *in-depth* analysis of few grains by our *state-of-the-art* instruments/techniques and nationwide corroborative research abilities. We will conduct on analyses in parallel with the initial analysis team led by the Hayabusa2 project.

Here are our policies as Phase 2 curation team:

- 1) We will analyze Hayabusa2 samples utilizing the *state-of-the-art*, original analytical and research in collaboration with several institutes and universities to acquire petrological and chemical characteristics to the utmost. Our results and developed techniques are fed back to the initial analysis teams, and will be a benchmark that contributes to the international announcement of opportunity and curation works.
- 2) We will acquire a 2D / 3D high resolution texture of a single grain, molecular structures, chemical species identifications, light element isotopic ratios, major and trace elemental abundances, microtextural features, and crystal structures. To make this successfully we will apply the sequential analysis protocol from non-destructive analyses at synchrotron radiation facility such as 3D-CT and XRD, STXM-XANES to destructive analyses such as FIB sample preparations, TEM observations and mass spectrometry with SIMS, LA-ICP MS.
- 3) We will explore *in-depth* of Hayabusa2 samples from the viewpoint of similarities or different characteristics with the current knowledge of extraterrestrial materials (meteorites, micrometeorites, Hayabusa samples) in Antarctic Meteorite Center of National Inst. Polar Research and JAXA curation facility. Primary objective will focus on studying of extraterrestrial water and primordial organic components in Hayabusa2 samples.

Avoiding terrestrial contaminations (i.e., atmospheric water/air, organics) during sample curation, transportation and analysis are important to obtain original chemical characteristics of Hayabusa2 samples. We, then, have developed novel and universal sample holders for a linkage analysis utilizing micro-analytical instruments of FIB, TEM, STXM and NanoSIMS minimizing terrestrial contaminations and sample damages of lost or broken. We also made an additional sample holder (namely Okazaki cell) for STXM analysis (Ohigashi T. et al. *in preparation*), and a sample transport vessel (FFTC: facility to facility transfer container) under vacuum or inert gas (Uesugi K and Uesugi M. et al. *in preparation*) in parallel.

We will report current status of “Team Kochi” of Phase2 Curation and our developed universal sample holders for FIB, TEM, NanoSIMS, STXM, and a sample transport vessel under vacuum or inert gas among nationwide/international universities and institutes.

References

- [1] Nakamura T. et al. (2011) Science 333, 1113–1116. [2] Brownlee D.E. et al. (2006) Science 314, 1711–1716. [3] Yurimoto H. et al. (2011) Science 333, 1116–1119. [4] Noguchi T. et al. (2018) Science 333, 1121–1125. [5] Tachibana S. et al. (2014) Geochemical J. 48, 571–587. [6] Lauretta D.S. et al. (2014) Meteorit. Planet. Sci. 50, 834–849.

DESTINY⁺: Flyby to Asteroid (3200) Phaethon and in-situ dust analyses

Tomoko Arai¹, M. Kobayashi¹, K. Ishibashi¹, F. Yoshida¹, H. Kimura¹, K. Wada¹, H. Senshu¹, M. Yamada¹, O. Okudaira¹, T. Okamoto¹, S. Kameda², R. Srama³, H. Krüger⁴, M. Ishiguro⁵, H. Yabuta⁶, T. Nakamura⁷, J. Watanabe⁸, T. Ito⁸, K. Ohtsuka⁸, S. Tachibana⁹, T. Mikouchi⁹, M. Komatsu¹⁰, K. Nakamura-Messenger¹¹, S. Messenger¹¹, S. Sasaki¹², T. Hiroi¹³, S. Abe¹⁴, S. Urakawa¹⁵, N. Hirata¹⁶, H. Demura¹⁶, G. Komatsu^{1,17}, T. Noguchi¹⁸, T. Sekiguchi¹⁹, T. Inamori²⁰, H. Yano²¹, M. Yoshikawa²¹, T. Ohtsubo²¹, T. Okada²¹, T. Iwata²¹, K. Nishiyama²¹, H. Toyota²¹, Y. Kawakatsu²¹ and T. Takashima²¹

¹Planetary Exploration Research Center, Chiba Institute of Technology, Chiba 275-0016, Japan (tomoko.arai@it-chiba.ac.jp), ²Rikkyo University, Japan, ³Institut für Raumfahrtssysteme, Stuttgart University, ⁴Max Planck Institute for Solar System Research, ⁵Seoul National University, South Korea, ⁶Hiroshima University, Japan, ⁷Tohoku University, Japan, ⁸National Astronomical Observatory of Japan, ⁹The University of Tokyo, Japan, ¹⁰The Graduate University for Advanced Studies, Japan, ¹¹NASA Johnson Space Center, TX, U.S.A, ¹²Osaka University, Japan, ¹³Brown University, RI, U.S.A, ¹⁴Nihon University, Japan, ¹⁵Japan Spaceguard Association, Japan, ¹⁶Aizu University, Japan, ¹⁷Università d'Annunzio, Italy, ¹⁸Kyushu University, Japan, ¹⁹Hokkaido University of Education, ²⁰Nagoya University, Japan, ²¹ISAS, JAXA, Japan.

Introduction: More than 40,000 metric tons per year of extraterrestrial dust accrete onto the Earth [1]. While carbonaceous meteorites are rare (less than 5%) among meteorite collection, interplanetary dust particles (IDPs) generally include carbon and organic materials and their carbon contents are 5-10 times richer than those for carbonaceous meteorites. Dust particles are likely major carriers of carbon and organic matters to the Earth and potentially be precursors to the terrestrial life. Extraterrestrial dust particles are derived either from cosmic dust background or from meteor showers. The former consists mostly of IDPs which originate from miscellaneous comets and asteroids, with minor interstellar dusts. The latter are meteoroids transported via dust trails or streams, where dust ejected from specific comets and asteroids, whose orbits cross that of the Earth.

Asteroid (3200) Phaethon is a parent body of Geminid meteor shower [e.g. 2], which is amongst the most active meteor showers. While parent bodies of meteor showers are mostly comets, Phaethon is an Apollo type asteroid with carbonaceous, B-type reflectance spectra [e.g. 3]. Recurrent dust ejection at its perihelion (0.14 au) are reported [4-6], while no coma was observed around 1.5 au [7]. The dust ejection mechanism of the active asteroid remains unknown. Na depletion is reported for Geminid meteor shower [8] and higher dust density (2.9g/cm³) is estimated [9], both of which hints volatile depletion possibly by solar heating. Phaethon is of great interest and significance because it is a carbonaceous asteroid providing dust to the Earth via dust stream, has a break-up body, 2005 UD [10], is possibly a breakup from main-belt asteroid 2 Pallas [11], experiences extensive solar heating at a small perihelion distance, and among the largest potentially hazardous body. Due to its scientific importance, Phaethon was a potential target for previous missions, such as Deep Impact and OSIRIS-REx. However, sample return, impact experiment, as well as rendezvous are difficult for Phaethon with a large relative velocity due to its large eccentricity and inclination. Only viable approach for Phaethon is flyby.

Mission overview: DESTINY⁺ (Demonstration and Experiment of Space Technology for INterplanetary voYage, Phaethon fLyby and dUst Science) is a mission proposed for JAXA/ISAS Epsilon class small program, currently in the pre-project phase (Phase-A) with a launch targeted for 2022. DESTINY⁺ is a joint mission of technology demonstration and scientific observation. It will demonstrate high performance electric propelled vehicle technology and high-speed flyby exploration of asteroid (3200) Phaethon. DESTINY⁺ aims to realize high-resolution imaging during close proximity flyby, high-accuracy navigation and wide-range observation, and these implemented for multiple small bodies (multi-flyby). Engineering challenges include proximity fly-by navigation with adequate risk of collision, radio-optical hybrid navigation guidance and control, and autonomous imaging based on optical information for target tracking. System design of DESTINY⁺ is summarized in Table 1.

Science goal of DESTINY⁺ is to understand the nature and origin of cosmic dust brought to the Earth, in the context of exogenous contribution of carbon and organics to the origin of terrestrial life. The science mission objectives are to measure physical properties (velocity, orbit, mass) and chemical composition of interplanetary and interstellar dust particles around 1 au during deep space cruising phase, and to conduct geological observation of Phaethon to understand dust ejection mechanism of active asteroid, surface compositional variation, and analyze dust particles from Phaethon during high-speed flyby (33 km/sec).

Mission profile: DESTINY⁺ spacecraft is injected into an elliptical orbit around the Earth by an Epsilon launch vehicle and then the electric propulsion is used to raise the orbit to reach the moon. Subsequently, it escapes from the Earth's gravity sphere through multiple lunar gravity assists, and heads for Phaethon after cruising by electric propulsion in deep space, and finally conducts flyby observation. A flyby point is around descending node of Phaethon with a geocentric distance of 1.72 au and a heliocentric distance of 0.87 au. After Phaethon fly-by, DESTINY⁺ may head for another target asteroid such as 2005 UD, a breakup body of Phaethon, as an extended mission. The summary of mission profile is shown in Table 2.

Science payloads: DESTINY⁺ has three science payloads, panchromatic telescopic camera (TCAP), VIS-NIR multiband camera (MCAP) and dust analyser (DDA) for science observation. The three payloads in relation to science requirements are shown in Fig. 1. Dust analyzer is developed with a heritage of Cosmic Dust Analyzer (CDA) onboard Cassini and provided by a team led by Stuttgart University [12]. TCAP and MCAP are developed by a team led by Planetary Exploration Research Center, Chiba Institute of Technology. TCAP is equipped with a tracking mirror. The observation profile during flyby and the current design of the cameras are presented by Ishibashi et al. [13].

Observation campaign for Phaethon and 2005UD: Phaethon approached the Earth as close as 10,000,000 km in December 2017. Variable observation of Phaethon, such as photometric, spectroscopic, polarimetric and radar observation were successfully conducted over the world [e.g.14, 15]. Asteroid 2005UD, which is a likely breakup body and a target candidate for multi-flyby of DESTINY⁺ will approach the Earth as close as 0.2 au in October 2018. Another observation campaign for 2005UD is currently organized. These observation data are crucial to better characterize Phaethon for further mission plan and detailed payload design for DESTINY⁺.

References:

[1] Love S. G. and Brownlee D. E. (1993) Science 262, 550. [2] Williams I. P. and Wu Z. (1993) Mon. Not. R. Astron. Soc. 262, 231-248. [3] Licandro J. et al. (2007) A&A 461, 751-757. [4] Jewitt D. and Li J. (2010) AJ, 140, 1519. [5] Jewitt D. et al. (2013) Astrophys. J. Lett. 771, L36. [6] Li J. and Jewitt D. (2013) AJ. 145: 154. [7] Jewitt D. and Hsieh H. (2006) AJ, 132, 1624. [8] Kasuga T. et al. (2006) A&A 453, L17. [9] Borovicka J. et al. (2009) Icy Bodies of the Solar System, Proc. IAU symp. No 263. 218. [10] Ohtsuka K. et al. (2006) A&A 450, L25. [11] De Leon J. et al. (2010) A&A 513, A26. [12] Kobayashi M. et al. (2018) LPS 49th, abstract#2050. [13] Ishibashi K. et al. (2018) LPS 49th, abstract#2126. [14] Takir D. et al. (2018) LPS 49th, abstract#2624. [15] Taylor P. A. et al. (2018) LPS 49th, abstract#2509.

Table 1. System design of DESTINY⁺ spacecraft.

Mission Period	> 4 years
Mass	480 kg (including 60 kg Xenon and 15.4 kg Hydrazine)
Launcher	Epsilon rocket + kick motor
Trajectory	230 km x 49913 km, 30 deg. → Lunar swing-by → Phaethon transfer
Attitude control	3-axis (Error < 1 arc-min.)
Communication	X band (GaN SSPA, HGA 4 kbps, MGA 1 kbps, LGA 8 bps at 1.9 AU)
Solar Array	High-specific power light-weight paddle (138 W/kg, 4.7 kW (BOL), 2.6 kW (EOL))
Battery	Li-ion (42 Ah, 11s1p)
Propulsion	RCS (Hydrazine) + Ion thrusters (μ10 x 4)
Thermal control	Loop heat pipes, Reversible Thermal Panels
Radiation dose	Approx. 30 krad (with aluminum shield of 3-mm thick)

Table 2. Mission profile of DESTINY⁺.

	Period	Operation
1	1 month	Launched into a highly elliptic orbit (230 x 49913 km) by Epsilon rocket
2	0.5-2 years	Spiraled orbit raising by electric propulsion
3	0.5 years	Lunar swing-by
4	2 years	Phaethon transfer orbit (Aphelion 1.16 au)
5	Several days	Phaethon flyby
6	0.5-1 years	Earth swing-by transfer orbit (Perihelion 0.83 au)
7	Several days	Earth swing-by
8	T.B.D.	Transfer orbit to next target

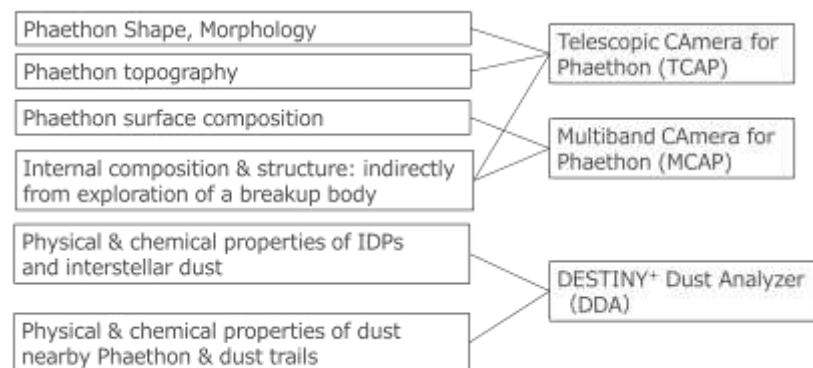


Fig. 1. Science goals and related instruments for DESTINY⁺.

Martian Moons eXploration (MMX)

Tomohiro Usui¹, Yasuhiro Kawakatsu¹, Kiyoshi Kuramoto², MMX Science Board, JAXA MMX Pre-Project Team

¹*Institute of Space and Astronautical Science, JAXA*

²*Department of CosmoSciences, Hokkaido University*

Martian Moon eXploration (MMX) is the 3rd Japanese sample return mission followed by Hayabusa [1] and Hayabusa-2 [2]. The MMX spacecraft is scheduled to be launched in 2024, orbit both Phobos and Deimos (multi-flyby), and retrieve and return >10 g of Phobos regolith back to Earth in 2029 [3]. The origins of Phobos and Deimos are still a matter of significant debate: capture of asteroids versus in-situ formation by a giant impact on Mars. In either case, MMX will definitely provide clues about their origins and offer an opportunity to directly explore the satellite building blocks or juvenile crust/mantle components of Mars. MMX will also aim to understand physical processes in the circumplanetary environment of Mars. The new knowledge of Phobos/Deimos and Mars will be further leveraged to constrain the initial condition of the Mars-moon system and to gain vital insights regarding the sources and delivery process of water (and organics) into the inner rocky planets.

We select seven nominal science payloads for the remote sensing observations: 1) wide-angle multi-band camera (OROCHI), 2) telescope camera (TENGOO), 3) near-infrared spectrometer (MacrOmega), 4) gamma-ray and neutron spectrometer (MEGANE), 5) light detection and ranging (LIDAR), 6) circum-Martian dust monitor (CMDM), and 7) mass spectrum analyzer (MSA) (Table 1). The spacecraft also carries a sampler system equipped with a robotic manipulator and corers, which enables the acquisition of Phobos regolith >2 cm beneath the surface.

The spacecraft consists of propulsion, exploration, and return modules (total launch mass = ~3,500 kg). The chemical propulsion system is utilized for Mars orbit injection and escape maneuver. The outward interplanetary flights take ~1 year by the most efficient Hohmann-like transfer. The spacecraft stays at circum-Mars orbits ~3 years for exploration followed by the ~1 year homeward interplanetary flight to Earth. The Phobos exploration includes multiple landing/sampling operations; each takes ~2.5 hours. The spacecraft employs ballistic descent to reach the space right above a landing site before the final free-fall descent without a thruster jet to prevent whirling wind from blowing regolith particles.

Table 1. Nominal science payload

Payload	Measurements
Wide-angle multiband camera (OROCHI)	<ul style="list-style-type: none">Global mapping of hydrated minerals, organics, and the spectral heterogeneity of the Martian moons
Telescopic camera (TENGOO)	<ul style="list-style-type: none">Determine the global topography and surface structure of the Martian moonsCharacterize the topography around the sampling sites
Gamma-ray, neutron spectrometer (MEGANE)	<ul style="list-style-type: none">Determine the bulk elemental abundance and compositional variability of Phobos
Near-infrared spectrometer (MacrOmega)	<ul style="list-style-type: none">Global mapping of minerals, molecular H₂O and organics of the Martian moonsCharacterize the material distribution around the sampling sitesMonitor the transport of H₂O vapor, H₂O/CO₂ clouds, and dust in the Mars atmosphere
Light detection and ranging (LIDAR)	<ul style="list-style-type: none">Determine the Phobos shape and topography
Circum-Martian dust monitor (CMDM)	<ul style="list-style-type: none">Detect and monitor: 1) the circum-Martian dust ring; 2) interplanetary dust; 3) Interstellar dust
Mass spectrum analyser (MSA)	<ul style="list-style-type: none">Determine the mass and energy of ions from Phobos, Mars and Sun

References

[1] Fujiwara, A. et al. 2006, Science 312: 1330-1334. [2] Tsuda, Y. et al. 2013. Acta Astronautica 9: 356-362. [3] Usui, T. et al. 2018, Abstract# B4.2-0007-18, 42nd COSPAR.

HERACLES – The exploration of the Moon including sample return mission

Y. Karouji¹, H. Hiesinger², P. Martin³, M. Abe¹, J. Haruyama¹, M. Ohtake¹, W. Carey⁴, S. Hosseini⁴, J. Carpenter⁴ and M. Landgraf⁴

¹Japan Aerospace Exploration Agency, 3-1-1 Yoshinodai, Chuo-ku, Sagami-hara-shi, Kanagawa 252-5210, Japan

²Institut für Planetologie, Westfälische Wilhelms-Universität, Wilhelm-Klemm-Str. 10, 48149 Münster, Germany

³Canadian Space Agency, 6767 Route de l'Aéroport, St Hubert, QC, J3Y 8Y9, Canada

⁴European Space Agency/European Space Research and Technology Centre, Keplerlaan 1, 2201 AZ Noordwijk, Netherlands

Inspired by the Global Exploration Roadmap (GER), the HERACLES (Human-Enhanced Robotic Architecture and Capability for Lunar Exploration and Science) is designed to demonstrate key elements and capabilities for sustainable human exploration of the Moon while maximizing opportunities for unprecedented scientific knowledge gain. To enable human lunar exploration, which is one of the four cornerstones of the European Exploration Envelope Program, it is planned to launch a sub-scale demonstration mission in the mid-2020's timeframe to test key components of lunar vehicles, including a lander, rover and ascent vehicle. European Space Agency (ESA) will coordinate and undertake the study of the ascent module, Japan Aerospace Exploration Agency (JAXA) will study the lander, and the Canadian Space Agency (CSA) will investigate the rover element. In parallel, we are developing surface operational scenarios that reflect the input from the international lunar science community. This will include the selection and characterization of a potential landing site with a large scientific potential and return of lunar samples of high scientific value before conducting a long distance traverse that will provide further opportunities for in-situ science and exploration. The coordination of the planning of science opportunities is performed by the multi-agency HERACLES Science Working Group (SWG). This working group is also responsible for developing a mission science management plan to describe science team and science payload selection processes, and data and sample policies. In the next steps, we will engage the science communities of the study agencies and install an international HERACLES Science Definition Team (iSDT). The iSDT will generate a prioritized list of investigations and will provide input for the landing site selection. In the initial phase of mission planning, the HERACLES study team has developed a nominal scenario with Schrödinger basin as the reference landing site with the purpose of driving engineering requirements. On the basis of studies by the Lunar Planetary Science Institute in 2015 and preliminary studies by the HERACLES team, Schrödinger basin might be a potential landing site that could satisfy many science objectives although other sites may also be considered. The iSDT will provide the report on candidate landing sites in mid-December 2018.

The current mission planning foresees a 70-day surface sample return mission, followed by a 1-year traverse encompassing one or more additional potential human exploration landing sites. We plan to return maximum of 15 kg of samples. A possible mission scenario to accomplish these objectives is shown in Fig. 1. The first HERACLES mission starts with the launch of a mid-sized launch vehicle (baseline Ariane 64) to lunar transfer orbit (LTO). The lunar descent element (LDE) will perform the landing to the lunar surface carrying the Lunar Ascent Element (LAE) and the rover. It is assumed that the landing is to occur during daylight conditions. On the surface, the rover egresses the LDE and starts the surface campaign. Initial exploration of the surface by the rover is supported by ground control and time-tagged commanding until the crew arrives on the Lunar Orbital Platform-Gateway (LOP-G). Once the crew is present, the crew-supported surface mobility operations will start. The rover then is commanded to drive, to perform sample collection and to transfer the sample container to the LAE. The sample collection phase can take multiple lunar day-night cycles and ends with the deposition of the samples into the LAE. The LAE will ascend from the surface, and initiates the transfer to the LOP-G. The sample container will be removed from the LAE by the LOP-G robotic arm. HERACLES's rover remains functional on the surface and is driven by ground-control along the planned traverse to demonstrate long-life, long-range surface mobility and exploration activities (in-situ investigations and sampling).

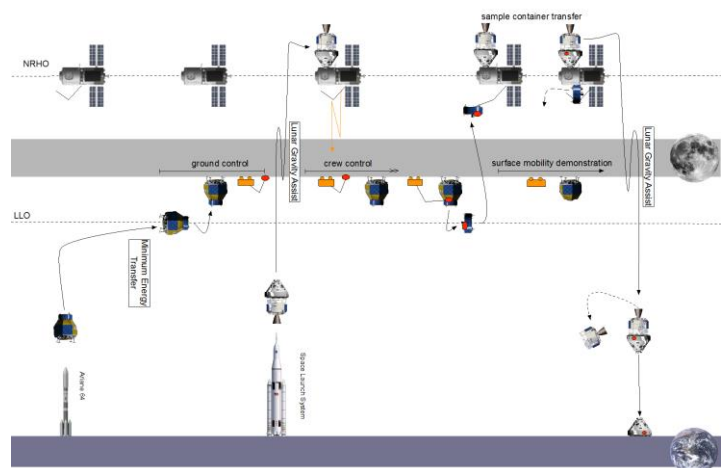


Figure 1. Baseline Mission Operations Scenario (left to right).

The OKEANOS: Small Body Exploration to a Jupiter Trojan Asteroid

M. Ito¹, T. Okada^{2,3}, Y. Kebukawa⁴, J. Aoki⁵, Y. Kawai⁵, T. Iwata², J. Matsumoto², T. Chujo², S. Kikuchi², J.-P. Bibring⁶, S. Ulamec⁷, R. Jaumann⁷, R. Nakamura⁸, H. Yano², S. Yokota⁵, M. Toyoda⁵, H. Yurimoto^{2,9}, Y. Saito², C. Okamoto¹⁰, S. Matsuura¹¹, K. Tsumura¹², D. Yonetoku¹³, T. Mihara¹⁴, A. Matsuoka², R. Nomura², T. Hirai², N. Grand¹⁵, H. Cottin¹⁵, A. Buch¹⁶, L. Thirkell¹⁷, C. Briois¹⁷, T. Saiki², H. Kato², O. Mori², and J. Kawaguchi²

¹JAMSTEC, ²ISAS-JAXA, ³University of Tokyo, ⁴Yokohama National University, ⁵Osaka University, ⁶IAS, Orsay, France, ⁷DLR, Germany, ⁸AIST, ⁹Hokkaido University, ¹⁰Hosei University, ¹¹Kwansei Gakuin University, ¹²Tohoku University, ¹³Kanazawa University, ¹⁴RIKEN, ¹⁵LISA, Univ-Paris-XII, ¹⁶Ecole Centrale Paris, ¹⁷CNRS, Orleans

Introduction: The OKEANOS (Oversize Kite-craft for Exploration and AstroNautics in the Outer Solar system), which is also known as the Solar Power Sail (or SPS), mission is one of the candidates of the strategic middle-class space exploration to the outer Solar System lead by JAXA [1]. The mission will be launched in late 2020s, and rendezvous for spectral observations and landing for *in-situ* isotope/elemental measurements to a D or P type Jupiter Trojan asteroid of ~20-30 km in diameter on or about 2040. Unique scientific instruments of a high-resolution mass spectrometry (HRMS) together with suits of remote-sensing instruments will be on board. Currently we consider three mission plans for the OKEANOS, plan A is a rendezvous and landing for single asteroid, plan A' is multi-rendezvous and landing for single asteroid, and plan B is a rendezvous, landing for single asteroid and sample return. Note that the sample return is not yet fully developed. More detailed developments of the sample return canister, a plan to prevent sample heating and degradation during capsule reentry will be required.

Scientific Goals: Through in-depth scientific observations with HRMS and spectroscopy, the OKEANOS will provide critical input to the key questions of (1) constraining planet formation/migration theories, (2) inventory and distribution of volatiles (water and organics) in the Solar System.

In-situ HRMS analysis: The HRMS is one of the flagship instruments on the OKEANOS, conducting critical measurements towards the scientific goals of the mission. D/P-type asteroids likely consist of dominant of organics (carbonaceous materials) and anhydrous silicates (hydrated silicates cannot be excluded), possibly with water (ice) in its interiors [2]. We, therefore, plan to analyze volatile materials on the Jupiter Trojan, for their isotopic and elemental compositions using a HRMS (MULTUM: multi-turn ToF mass spectrometer [3]) with a combination of pyrolysis ovens and gas chromatography [4]. This HRMS system allows to measure H, N, C, O isotopic compositions and elemental compositions of molecules. Analyses of light isotopes and molecules of materials on a Trojan asteroid may permit deciphering if the Trojan bodies originate from the cometary reservoir or share similarities with asteroids (or meteorites) from the inner Solar System. Especially isotopic analysis may provide insight into the migration model of giant planets (Jupiter, Saturn) at the early Solar System.

The sample return from the Trojan asteroid: Beside *in-situ* HRMS analysis of isotopic ratios, elements and molecules in surface and subsurface samples on the Trojan asteroid, analysis of returned samples from Trojan asteroidal objects containing non-volatile materials (organics and minerals) as well as water (ice) will open a new insight of the detailed scientific objectives for the Solar System evolution. Since *in-situ* analysis is limited in terms of sample preparations, lack of relationship among components, and mineralogical/petrological contexts, the *state-of-the-art* microanalysis techniques on the Earth will provide these additional information such as isotopic ratios of individual component (organics and associated minerals), trace amount of gaseous species (e.g., Noble gases, CO, CO₂, NH₃, CH₄ gasses in ice), and organic compounds that are hard to be detected under the current *in-situ* HRMS system (e.g., amino acids).

Relationship to other missions: Collaboration with LUCY (multi-rendezvous) of NASA Discovery mission [5] will be enhanced an understanding of origin and nature of a Jupiter Trojan asteroid. Indeed, detailed chemical analysis of single Trojan asteroid by the OKEANOS will support to understand the diversity among other Trojan asteroids by LUCY. The sample return missions of C-type asteroid by Hayabusa2 [6], B-type asteroid by OSIRIS-REx [7] and comet by CAESAR [8] will provide chemical and physical properties of comets and asteroids. These may contribute better understanding of Trojan asteroids in combination with the OKEANOS's *in-situ* analysis and sample return from D/P-type asteroid.

References: [1] Okada T. et al. (2018) Planetary and Space Science, 161, 99, 2018. [2] Guilbert-Lepoutre A. (2014) Icarus, 231, 232–238. [3] Shimma S. et al. (2010) Anal. Chem., 82, 8456. [4] Goesmann F. et al. (2017) Astrobiology, 17, 655. [5] Levison H. et al. (2016) LPSC 47, abst#2061. [6] Tachibana S. et al. (2014) Geochemical J., 48, 571-587. [7] Loretta D. S. et al. (2014) Meteorit. Planet. Sci., 50, 834-849. [8] Nakamura et al. (2018) in this meeting.

Project overview of CAESAR comet sample return mission

Tomoki Nakamura¹, Steve W. Squyres², Keiko Nakamura-Messenger³, Yoshihiro Furukawa¹,
Yuki Kimura⁴, Aki Takigawa⁵, Dante Lauretta⁶, Scott Messenger³, CAESAR project team

¹ *Tohoku University*, ² *Cornell University*, ³ *NASA Johnson Space Center*, ⁴ *Hokkaido University*,
⁵ *Kyoto University*, ⁶ *University of Arizona*

The Comet Astrobiology Exploration Sample Return (CAESAR) mission will acquire both rocks and ice with a minimum amount of 80 g from the surface of short-period comet 67P/Churyumov-Gerasimenko and recover the samples to the Earth for laboratory analysis [1]. Since comets preserve the records of the early evolution of solar-system material, analysis of returned samples by CAESAR is expected to uncover the origin of the Solar System starting materials and how these components came together to form planets and give rise to life. ESA's Rosetta mission visited comet 67P and carried out detailed remote sensing observations, which provides us geomorphological information and composition of surface material. Infrared spectra of comet 67P show a large 3 μm absorption band from water ice, while no apparent 2.7 μm absorption band from phyllosilicates [2], which suggests minimum aqueous alteration and thus preservation of intact solid material. CAESAR can take the advantage from the Rosetta results to maximize science return and to reduce the risk for landing. CAESAR preserves much of the science of a cryogenic sample return by retaining volatiles in a dedicated reservoir securely separated from the solid sample.

Analyses of returned samples will determine the nature and abundances of interstellar materials that are present in the solar-system starting material. They will trace the evolution of volatile reservoirs, delineate chemical pathways that led from simple interstellar species to complex and prebiotic molecules, and constrain the geological and dynamic evolution of 67P. And they will evaluate the potential role of comets in delivering water and organics to the early Earth. These goals will be achieved by sample analyses that link macroscopic properties of the comet with microscale mineralogy, chemistry, and isotopic studies of volatiles and solids. These analyses can be performed in terrestrial laboratories with orders of magnitude greater sensitivity and precision than possible with spacecraft instrumentation.

CAESAR is one of the two finalists selected by NASA for Phase A study in the New Frontiers 4 program and the result of the final selection will be in public in late 2019.

References: [1] Squyres S. W. et al. (2018) 49th LPSC, Abstract #1332. [2] Barucci M. A. et al. (2016) *A&A* 595, A102.

Mars Sample Return – How Should it be Organised Into Science Objectives?

International Mars Sample Return and Objectives Team (iMOST) and Caroline Smith¹

¹*Department of Earth Sciences, The Natural History Museum, London, SW7 5BD, UK. C.L.Smith@nhm.ac.uk*

The analysis in Earth laboratories of samples that could be returned from Mars is of extremely high interest to the international Mars exploration community. IMEWG (the International Mars Exploration Working Group) is currently exploring options to involve the international community in the planning for returned sample science, including the analysis of the returned samples. The Mars 2020 sample-caching rover mission is an essential component of a potential Mars Sample Return campaign, so its existence constitutes a critical opportunity - the prospects for MSR are more real now than they have ever been. The Mars 2020 samples, if returned, would provide the basis for performing a variety of Earth-based experiments including ones related to the search for the signs of life.

PROPOSED MARS SCIENCE OBJECTIVES

Seven objectives have been defined for MSR, traceable to published priorities established over more than two decades by Planetary Science Decadal Surveys in the USA and other international studies [e.g. 1, 2]. For each, their importance to science or engineering is described, critical measurements that would address the objectives are specified, and the kinds of samples that would be most likely to carry key information are identified.

1. Interpret in detail the primary geologic processes that formed and modified the ancient (pre-Amazonian) geologic record.

The objective seeks to investigate the geologic environment represented at a high-priority landing site (whichever site might be selected). All the sites are of ancient (Noachian or Hesperian) age. The intent is to provide definitive geologic context for samples and details that relate to past biologic processes. This objective is divided into sub-objectives that would apply at different landing sites.

1.1 Understand the essential attributes of a martian sedimentary system. The intent is to understand the preserved martian sedimentary record. Most important samples: A suite of sedimentary rocks that span the range of variation. Scientific importance: Basic inputs into the history of water, climate change, and the possibility of life.

1.2 Understand an ancient martian hydrothermal system through study of its mineralization products. The intent is to evaluate at least one potentially life-bearing 'habitable' environment via samples. Most important samples: A suite of rocks formed and/or altered by hydrothermal fluids. Scientific importance: A possibly habitable geochemical environment with high preservation potential.

1.3 Understand the rocks and minerals representative of a deep subsurface groundwater environment. The intent is to definitively evaluate the role of water in the subsurface. Most important samples: Suites of rocks/veins representing water/rock interaction in the subsurface. Scientific importance: May be the longest-lived habitable environments and key to the hydrologic cycle.

1.4 Understand ancient water/rock interactions at the martian surface, or more broadly, atmosphere/rock interactions, and how they have changed with time. The intent is to constrain the time-variable factors necessary to preserve records of microbial life. Most important samples: Regolith, paleosols, and evaporites. Scientific importance: Subaerial near-surface processes could support and preserve microbial life.

1.5 Understand the essential attributes of a martian igneous system. The intent is to provide definitive characterization of igneous rocks on Mars. Most important samples: Diverse suites of ancient igneous rocks. Scientific importance: Thermochemical record of the planet and nature of the interior.

2. Assess and interpret the biological potential of Mars.

The objective seeks to inform our efforts to understand the nature and extent of martian habitability, the conditions and processes that supported or challenged life, the timescales, and how different environments might have influenced the preservation of biosignatures and created non-biological 'mimics'. This objective also has three sub-objectives.

2.1 Assess and characterize carbon, including possible organic and pre-biotic chemistry. Most important samples: All samples collected as part of Objective 1. Scientific importance: Any biologic molecular scaffolding on Mars would likely be carbon-based.

2.2 Assay for the presence of biosignatures of past life at sites that hosted habitable environments and could have preserved any biosignatures. Most important samples: All samples collected as part of Objective 1. Scientific importance: Provides the means of discovering ancient life.

2.3 Assess the possibility that any life forms detected are still alive, or were recently alive. Most important samples: All samples collected as part of Objective 1. Scientific importance: Planetary protection, and arguably the most important scientific discovery possible.

3. Determine the evolutionary timeline of Mars, including calibrating the crater chronology time scale.

This objective seeks to provide a radioisotope-based time scale for major events, including magmatic, tectonic, fluvial, and impact events, and the formation of major sedimentary deposits and geomorphological features.

Most important samples: Ancient igneous rocks that bound critical stratigraphic intervals or correlate with crater-dated surfaces. Scientific importance: Quantification of martian geologic history.

4. Constrain the inventory of martian volatiles as a function of geologic time, and determine the ways in which these volatiles have interacted with Mars as a geologic system.

Comprising the atmosphere and hydrosphere, volatiles play major roles in martian geologic and possibly biologic evolution. The objective seeks to recognize and quantify these roles.

Most important samples: Current atmospheric gas, ancient atmospheric gas trapped in older rocks, and minerals that equilibrated with the ancient atmosphere. Scientific importance: Key to understanding climate and environmental evolution.

5. Reconstruct the history of Mars as a planet, elucidating those processes that have affected the origin and modification of the crust, mantle and core.

The objective seeks to quantify processes that have shaped the planet's crust and underlying structure, including planetary differentiation, core segregation and state of the magnetic dynamo, and cratering.

Most important samples: Igneous, potentially magnetized rocks (both igneous and sedimentary) and impact-generated samples. Scientific importance: Elucidates fundamental processes for comparative planetology.

6. Understand and quantify the potential martian environmental hazards to future human exploration.

The objective seeks to define and mitigate an array of health risks related to the martian environment associated with the potential future human exploration of Mars.

Most important samples: Fine-grained dust and regolith samples. Scientific/engineering importance: Key input to planetary protection planning.

7. Evaluate the type and distribution of in-situ resources to support potential future Mars exploration.

The objective seeks to quantify the potential for obtaining martian resources, including use of martian materials as a source of water for human consumption, fuel production, building fabrication, and agriculture.

Most important samples: Regolith. Scientific/engineering importance: Facilitating long-term human presence on Mars.

References

[1] National Research Council (2003) New Frontiers in the Solar System: An Integrated Exploration Strategy. [2] MEPAG E2E-iSAG (2011) Planning for Mars Returned Sample Science.

ASPECT hyperspectral imager for small interplanetary spacecrafts

Tomas Kohout¹ and Antti Näsilä²

¹Faculty of Science, University of Helsinki, Finland (tomas.kohout@helsinki.fi)

²VTT Technical Research Centre of Finland Ltd, Espoo, Finland

The ASPECT Hyperspectral Imager is developed as a payload for APEX CubeSat to be deployed by Hera (ESA) spacecraft at asteroid Didymos. Hera (ESA) together with DART (NASA) will perform the first-ever kinetic impactor deflection test of an asteroid within the joint AIDA (Asteroid Impact & Deflection Assessment) project.

ASPECT is a miniaturized, CubeSat-sized, hyperspectral imager with primary scientific task of high resolution compositional mapping of Didymos surface and detailed characterization of impact crater created by impacting DART (NASA) spacecraft. Thanks to its modular design, ASPECT hyperspectral imager range and resolution can be easily modified to match specific objectives of different missions.

The ASPECT Hyperspectral Imager allows for global compositional mapping and imaging of the target asteroid with sub-meter resolution. The spectral range of 500-2500 nm covers most common silicate mineral (olivine, pyroxene, and plagioclase) absorption bands related to Fe²⁺ ions in their structure. Additionally, hydrated minerals as serpentine can be detected using ~700 nm Fe³⁺ absorption features. Direct presence of -OH and H₂O can be detected at 1400 and 1900 nm respectively. Observations at various phase angle allows for estimation of surface roughness. An extension of the spectral range into MIR (mid-infrared) region is being currently investigated. This spectral range allows for direct detection of hydrated materials and water/ice in 2700-3000 nm region as well as organic materials at 3200-3600 nm (Fig. 1).

In contrast to more traditional spatial scanning imaging spectrometers, ASPECT takes 2D snapshots at a given wavelength. When multiple snapshots are combined, a spectral datacube is formed, where the wavelength bands are separated in the time domain. The spectral separation is done by a tunable Fabry-Perot Interferometer (FPI).

The ASPECT asteroid hyperspectral imager is split into three measurement channels, one in the visible (VIS), and two in the infrared (NIR1 and NIR2). The parameters of each channel as well as possible extensions are summarized in Table 1. Sub-meter imager resolution can be achieved at orbital distances of 3 km or lower. All three channels have dedicated FPIs optimized for the desired wavelength range and are independent on each other. The imaged wavelengths are freely selectable within these ranges, and the targeted spectral resolution is 10-50 nm. Recently, a feasibility study of additional MIR channel with spectral range of 2500-4000 nm was launched. An extension in other direction towards UV (ultraviolet) is also currently under development for ESA ALTIUS mission and can be potentially integrated into the ASPECT Hyperspectral Imager.

The number of ASPECT imager channels, spectral range and resolution can be customized to meet specific mission objectives. Spectral resolution can be increased using FPI's higher orders of interference. However, this will result in smaller spectral range of the single channel and subsequent need to increase number of the imager channels. For example, improving the spectral resolution from 20 to 10 nm in NIR1 channel, the range will decrease from 900-1400 nm to approx. 900-1100 nm. Cascading the FPI will also result in better spectral resolution, however, the throughput and sensitivity will be decreased. Thus, there is a possibility for customization of ASPECT hyperspectral imager configuration satisfy mission requirements.

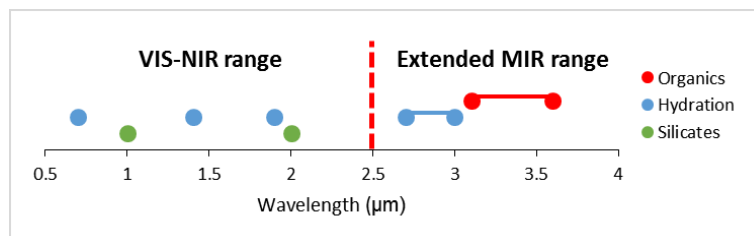


Figure 1. Spectral features detectable with ASPECT hyperspectral imager.

Table 1. ASPECT Hyperspectral Imager configuration with optional extensions.

Range	VIS	NIR1	NIR2	UV (optional)	VIS (optional)	MIR (optional)	VNIR mini
Size	0.5U	0.5U	0.25-0.5U	0.5-1U	0.5U	0.25U	1 cubic inch
FoV [deg]	10 × 10	5.3 × 5.3 10 × 10	5.3 × 5.3	TBD	2.5 × 2.5	TBD	10 × 10
Spectral range [nm]	500-900	900-1600	1600-2500	250 - 400	430-800	2500-4000	500-800 or 700-1000
Image size [px]	1024 × 1024	512 × 512	256 × 256	Single point	2048 × 2048	Single point	512 x 512
Spectral resolution [nm]	10-15 nm	20-40 nm	20-30 nm	< 2.5 nm	< 2.5 nm	30-50	20 nm
TRL	9	7	5	5	8	3	3-4
Flight heritage	Aalto 1 (in orbit, 2017)	Reaktor Hello World (FM delivered, launch 2018)	Under development, prototype in 2018	ESA ALTIUS (under development)	VISION (FM delivered, launch 2019)	Concept	Under development with ESA
Note			2 FPI cascade. With a single FPI the range is 1600 - 2100	4 FPI cascade. Can also be used with imaging detector		2 FPI cascade. With a single FPI the range is 2500 - 3500	Based on MEMS technology

Effect of viscosity on propagation of MHD waves in astrophysical plasma

- [ALEMAYEHU MENGESHA](#) (a1) (a2) (a3) and [S. B. TESSEMA](#) (a2) (a3)
- <https://doi.org/10.1017/S0022377813000020>
 - Published online: 25 January 2013

We determine the general dispersion relation for the propagation of magnetohydrodynamic (MHD) waves in an astrophysical plasma by considering the effect of viscosity with an anisotropic pressure tensor. Basic MHD equations have been derived and linearized by the method of perturbation to develop the general form of the dispersion relation equation. Our result indicates that an astrophysical plasma with an anisotropic pressure tensor is stable in the presence of viscosity and a strong magnetic field at considerable wavelength.

Ragged Phobos and coated Deimos: two satellites with various relations to the Roche limits

Gennady G. Kochemasov

IGEM of the Russian Academy of Sciences, 35 Staromonetny, 119017 Moscow,
kochem.36@mail.ru

As all cosmic bodies in Universe move in several periodic orbits of wave nature with very different orbiting frequencies, they are affected by modulated waves. They appear as predicted by radio wave physics. The modulation is division and multiplication of the higher frequency by the lower one. As a result, along with main frequencies appear two side frequencies with corresponding them tectonic granules. Examples are on surfaces of Saturn, Jupiter (cloudy covers), Pluto, the Moon, Titan, Ceres, Churyumov-Gerasimenko comet core [2, 3]. Now we show the modulation effects on Phobos and Deimos.

On Phobos a series of crossing troughs and crater chains is well presented. They cover the entire satellite surface by a kind of wavy cloak – a drying apple (Fig. 1). This shrinkage of the gaining speed falling on Mars satellite is due to necessity to keep the angular momentum [4]. Thus, the body's radius must diminish and the body shrinks and abundantly degases (numerous craters witness this). This occurs not chaotically but in form of regular crossing in four directions waves inscribed in a drying diminishing its surface sphere. Smallest wave forms concordant with the highest orbital frequency of the satellite (1/7.65 hours) still are not visible. However, modulated side waves and corresponding them forms (troughs and “craters «chains) are visible. $1/7.65 : 1/16488$ (circummartian frequency) gives the side frequency $1/2155$ and corresponding granule size 16.5 m (the scale is the Earth with the orbital frequency 1/1 year and the corresponding wave length $\pi R/2$ or the granule size $\pi R/4$). The smallest visible features (troughs and “craters”) in Fig.1 are about 15 m. Along with them also are numerous wider troughs marking earlier more distant orbits of the satellite with the lower frequencies.

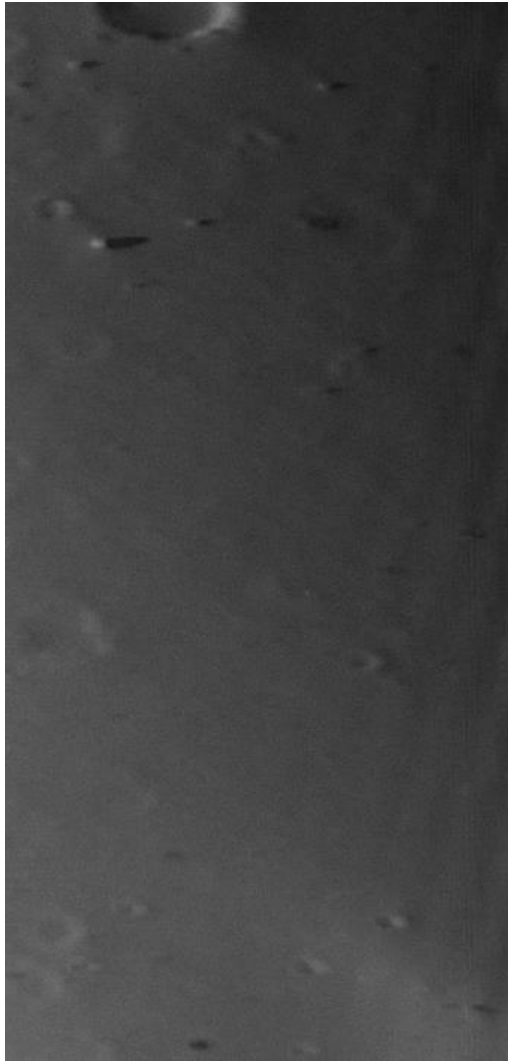
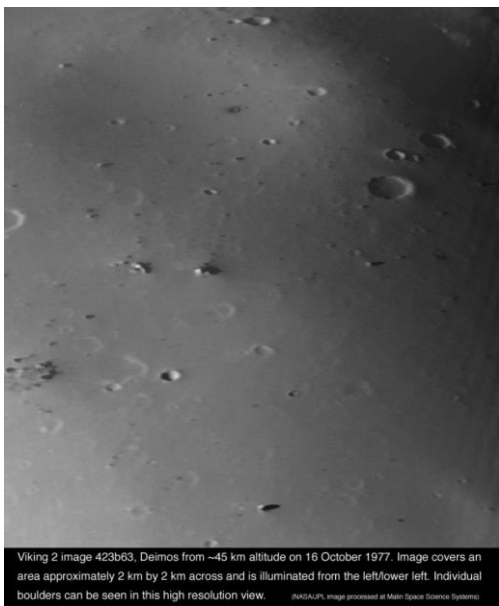
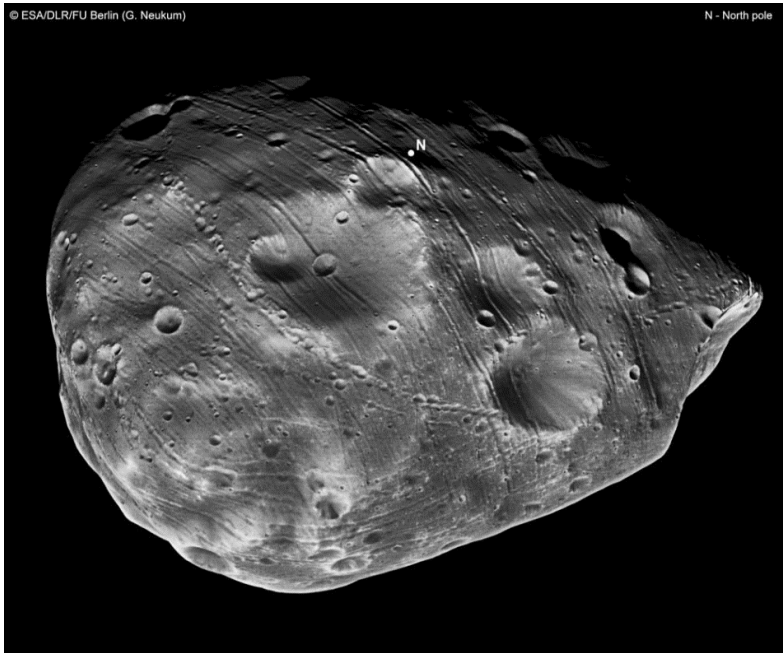
Two modulated frequencies of Deimos are interesting in that the corresponding them granules are: for the smallest (0.038 m), too fine and making smooth surface and, for the large (34.6 m), hardly visible as grids under the soft damping cover of fine dust material and blocks (Fig. 2, 3, 4). These grids are better visible along brinks of the image (Fig. 2-4). Presence of mainly two sizes of fragments (dust and blocks-bifurcation of sizes) also proves an action of two distinct modulated structuring frequencies. The dust cover is mainly discarded on shrinking Phobos and grows on Deimos. The first diminishes orbit radius, the second, in contrast, keeps it or slowly increases (different tendencies of angular momenta development).

Phobos diminishes the radius of its orbit eventually crossing the Roche limit for the “liquid” (actually porous dusty) cover and losing it. The squeezed folded peeled bedrock outcrops (Fig. 1). Deimos, on the contrary, far from the limit, keeps its dusty cover (Fig. 2-4) [6].

Striped off Phobos dispersed (dust) material finds its way towards Mars making a part of the planet atmosphere dust and the surface regolith. A significant part of the martian dust is replenished by eroded highly standing continents but a certain part could derive from the Phobos' dust. A thin coat of light (not dark) material on the martian surface is revealed due to impacts from inside (degassing) or hits of meteorites (less possible) (Fig.5). In any case, a dark basaltic(?) inside material uncovers itself (spiders, Fig. 5). Contrasting composition of the bedrock (dark probably basaltic) and aeolian lighter in color dusty coat is obvious. This lighter surface material is made mainly of eroded highlands with some participation of disappearing dusty cover of Phobos. Formation of bifurcated (blocks-dust) surface materials is observed also on the Churyumov-Gerasimenko comet core [3] and on Deimos.

References:

- [1] Duxbury T.C., Veverka J. Viking imaging of Phobos and Deimos: An overview of the primary mission // *J. Geophys. Res.*, 1977, v. 82, # 28, p. 4203-4211.
- [2] Kochemasov G.G. Wave modulation in the Solar system bodies and their radio emissions // *Geophya. Res. Abstr.*, v. 10, EGU2008A-01272, 2008. SRef-ID: 1607-7962/gra/EGU-2008-A-01272; EGU General Assembly 2008.
- [3] Kochemasov G.G. A wave modulation nature of the 3D structural lattice of the Churyumov-Gerasimenko comet icy core// 46th LPSC, 2015, Abstr. # 1088.
- [4] Kochemasov G.G. (2016) The Moon and Phobos: specific responses of two satellites moving off and nearer their respective planets // *DPS 48/EPSC 11*, Pasadena, Oct. 16-21, 2016, *Bulletin of the American Astronomical Society*, 2016, vol. 48, # 7, p. 175, Abstract 318.08, Session 318: Formation and Evolution of Planets and Satellites Posters.
- [5] Veverka J., Duxbury T.C. Viking observations of Phobos and Deimos: preliminary results // *J. Geophys. Res.*, 1977, v. 82, # 28, p. 4213-4223.
- [6] Mars'orbital frequency modulates orbital frequencies of its satellites and determines their characteristics tied to their position relative to the Roche limits (ragged Phobos and swelling Deimos) // *Late Mars Workshop 2018 (LPI contrib. # 2088, abstract #5001.pdf.*



3
 Fig.1. Phobos. ESA/DLR/FU Berlin (G. Neukum). Radii 14 x 11 x 10 km.
 Fig.2. Deimos. PIA11826-Deimos.jpg. Radii 8 x 6 x 6 km.
 Fig. 3-4. Deimos (Fig. 4-an enlarged portion of Fig. 3).
 Fig. 5. Mars-spiders.jpg.

4

5

In situ oxygen three-isotope analysis of carbonates with 15 μ m and 3 μ m beam: Preliminary results

Takayuki Ushikubo¹ and Wataru Fujiya²

¹Kochi Institute for Core Sample Research, JAMSTEC

²Faculty of Science, Ibaraki University

Introduction

Carbonates are common secondary minerals in carbonaceous chondrites and they precipitated from fluids during the aqueous alteration in carbonaceous chondrite parent bodies at ca. 4563Ma [1-3]. Occurrence of carbonates with distinct textures (e.g. monocrystalline type 1 calcite vs. porous and polycrystalline type 2 calcite [4]) within the same chondrite and/or existence of chemical zoning in individual crystals [e.g. 5] indicate that carbonates formed at multiple stages of thermal evolution of chondritic parent bodies. Oxygen and carbon isotopic compositions of carbonates very likely record information of physicochemical evolution of aqueous solutions and carbonaceous chondrite parent bodies [e.g. 1]. However, since the presence of H₂O significantly increases the oxygen diffusivity in carbonate [6,7], careful investigations are needed to distinguish primary isotopic signatures recorded in fine-scale structures of carbonate from later isotopic disturbance after carbonate formations. Here, we report results of oxygen isotope test analyses of standard carbonates by SIMS with different primary beam settings. We also measured oxygen isotope ratios of carbonate in Nogoya CM2 chondrite.

Analytical Conditions

Oxygen three-isotope ratios of carbonate (Calcite and Dolomite) were measured with the large-radius multi-collector SIMS (MC-SIMS), CAMECA IMS 1280-HR at Kochi Institute for Core Sample Research, JAMSTEC. Test measurements of the terrestrial standards, UWC-3 calcite [8] and UW-6220 dolomite [9], were performed using two distinct primary beam conditions: one is the normal Cs beam condition (¹³³Cs⁺, total accel. voltage 20 kV, 2.5 nA, and 15 μ m in diameter) and the other is the small beam condition (¹³³Cs⁺, total accel. voltage 20 kV, 30 pA, and 3 μ m in diameter). Three Faraday Cup (FC) detectors were used to detect secondary O⁻ ions for the normal beam condition, and one FC (for ¹⁶O⁻) and two electron multiplier (EM, for ¹⁷O⁻ and ¹⁸O⁻) detectors were used for the small beam condition, respectively. Analytical conditions are basically same as those reported in [10,11]. For the measurements of calcite in Nogoya (CM2), the small beam condition was employed.

Results and Discussion

With the normal Cs beam condition (15 μ m in diameter), the reproducibility (2 SD) of the spot-to-spot analyses was $\pm 0.26\%$ (for $\delta^{18}\text{O}$) and $\pm 0.38\%$ (for $\Delta^{17}\text{O}$) for UWC-3 calcite (N=10), and $\pm 0.49\%$ (for $\delta^{18}\text{O}$) and $\pm 0.52\%$ (for $\Delta^{17}\text{O}$) for UW-6220 dolomite (N=10), respectively. Since the reproducibility of the $\Delta^{17}\text{O}$ value is mainly constrained by the S/N of ¹⁷O⁻ signal, we expect that better reproducibility can be achieved with a higher intensity primary beam. With the small beam condition (3 μ m in diameter), that was $\pm 0.70\%$ (for $\delta^{18}\text{O}$) and $\pm 0.84\%$ (for $\Delta^{17}\text{O}$) for UWC-3 calcite (N=8), and $\pm 1.7\%$ (for $\delta^{18}\text{O}$) and $\pm 1.3\%$ (for $\Delta^{17}\text{O}$) for UW-6220 dolomite (N=10), respectively.

A typical reproducibility (2 SD, N=8 to 10) of the bracketing analyses of UWC-3 during the Nogoya carbonate measurement session was $\pm 1.4\%$ for $\delta^{18}\text{O}$ and $\pm 1.0\%$ for $\Delta^{17}\text{O}$, respectively. Oxygen isotope data of Nogoya calcite show that (1) the type 1 (solid and monocrystalline) and the type 2 (porous and polycrystalline) calcite grains in Nogoya have distinct oxygen isotopic compositions, and (2) their oxygen isotope ratios are distributed along a trend line with the slope of ~ 0.67 (Figure 1). These are consistent with previously reported CM chondritic carbonate data [4]. The MC-SIMS has capability to investigate oxygen three-isotope ratios of carbonate down to a few μ m in size.

References

- [1] Alexander C. M. O'D. et al. 2015. *Meteoritics & Planetary Science* 50: 810. [2] Fujiya W. et al. 2012. *Nature Communications* 3: 627. [3] Fujiya W. et al. 2013. *Earth & Planetary Science Letters* 362: 130. [4] Lindgren P. et al. 2017. *Geochimica et Cosmochimica Acta* 204: 240. [5] Fujiya W. et al. 2015. *Geochimica et Cosmochimica Acta* 161: 101. [6] Farver J. R. 1994. *Earth & Planetary Science Letters* 121: 575. [7] Labotka T. C. et al. 2000. *American Mineralogist* 85: 488. [8] Kozdon R. et al. 2009. *Chemical Geology* 258: 327. [9] Śliwiński M. G. et al. 2016. *Geostandard & Geoanalytical Research* 40: 157. [10] Kita N. T. et al. 2009. *Chemical Geology* 264: 43. [11] Ushikubo T. et al. 2017. *Geochimica et Cosmochimica Acta* 201: 103.

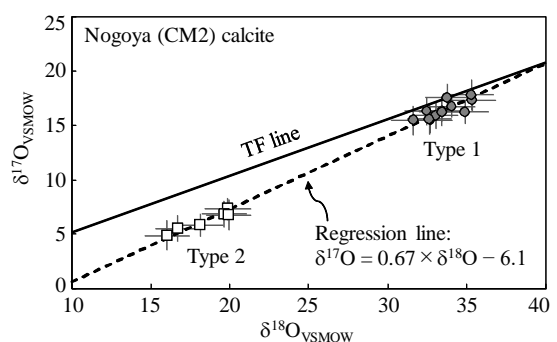


Figure 1. Oxygen three-isotope ratios of type 1 (monocrystalline) and type 2 (polycrystalline) calcite grains in Nogoya CM2 chondrite. Errors are 2 SD.

Electrical properties of Itokawa grains returned by Hayabusa

F. Cipriani¹, D. Koschny¹, N. Drozdovski¹, L. Colangeli¹, B. Shortt¹, B. Butler¹, S. Sanders¹, D. C.v.d. Luijt¹, D. Breeveld¹, M. Ferrari^{2,3}, V. Della Corte², M. Accolla^{2,3}, A. Rotundi^{2,3}

¹ ESA/ESTEC, Keplerlaan 1, 2200AG, Noordwijk, The Netherlands E-mail : fabrice.cipriani@esa.int

² INAF-Istituto di Astrofisica e Planetologia Spaziali, Via Fosso del Cavaliere 100, 00133 Roma, Italy

³ Dip. Scienze e Tecnologie, Università degli Studi di Napoli "Parthenope", Centro Direzionale I C4, 80143 Napoli, Italy

A wealth of data exists on the properties of lunar regolith samples returned by Apollo missions e.g. [1,2] as well as on terrestrial minerals. However such experimental data have not yet been collected on asteroids material. In this study we present measurements of secondary electron emission characteristics from areas of samples RA-QD02-0126-02 and RA-QD02-0136-14 returned by Hayabusa [3] under electronic irradiation in the range 200eV to 5keV. Secondary emission yields are found to be strongly dependent on surface composition and roughness and orientation of Itokawa particles. We compare them to reference measurements including grains and powders of reference materials such as terrestrial Frosterie and JSC-1 planetary analog. In addition we observe the build-up of local electric field patterns arising from surface electrostatic charging in relation with grains morphology. Consequences on our understanding of regolith properties and electrostatic effects on planetary regolith will be discussed.

References:

[1] B. Feuerbacher et al , *Proceedings of the Third Lunar Science Conference*, 1972: Vol. 3, pp. 2655-2663

[2] D.W. Strangway et al, *Earth and Planetary Science Letters*, 1972, Volume 16, Issue 2, pages 275-281,

[3] Nakamura et al. , 2014, *Meteorit Planet Sci*, 49: 215–227. 10.1111/maps.12247

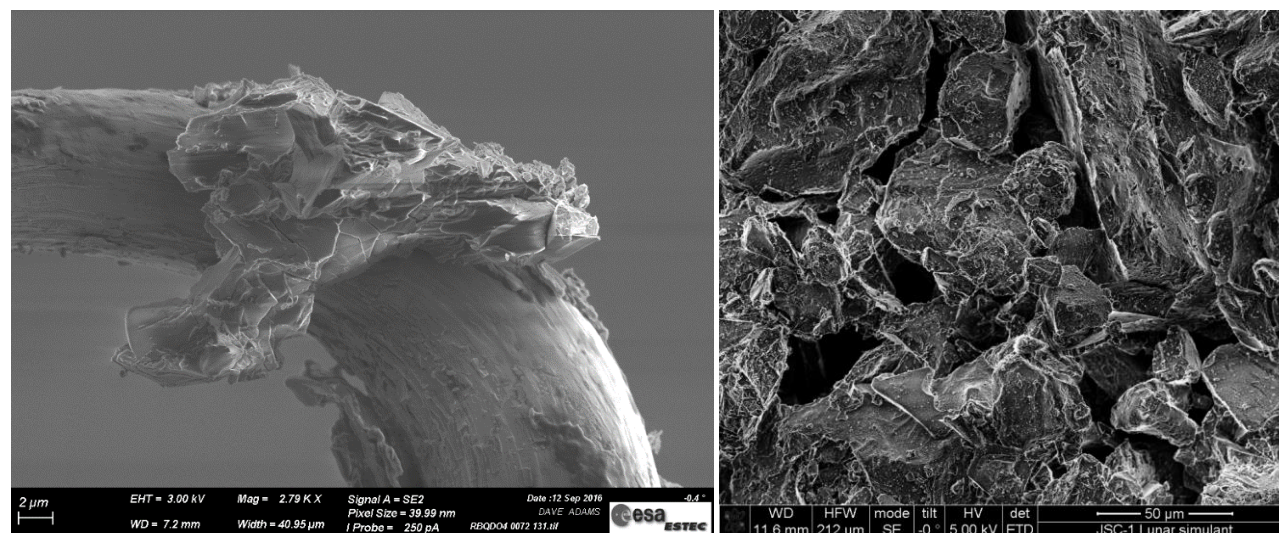


Figure 1: Left panel : Hayabusa sample RB-QD04-0072 observed at 3keV in Zeiss Sigma SEM. Right panel : mapping of a JCS-1 analog layer in FE-SEM Quanta 650.

The boron isotopic composition of the implanted solar wind in Itokawa grains: Technical development

Ming-Chang Liu

Department of Earth, Planetary, and Space Sciences, UCLA

The Sun accounts for ~99.8% of the total Solar System mass. Therefore, knowledge of the elemental and isotopic abundances of the Sun, and thus by inference those of the solar nebula, are of fundamental importance, as such information sheds light on the astrophysical processes that took place during Solar System formation. The importance of the solar boron isotopic composition is that it provides a basis for understanding the evolution of this element in the Galaxy and in the Solar System. Since stellar nucleosynthesis processes destroy boron, the presence of this element in the universe is primarily derived from non-thermal nuclear reactions between energetic (>GeV) particles (protons and alphas) in the Galactic cosmic rays (GCRs) and C, N, and O nuclei in the interstellar medium (ISM) (e.g., [1]). However, the $^{11}\text{B}/^{10}\text{B}$ ratio of 2.5 in the GCRs, first predicted by [2] and then later confirmed by spacecraft measurements (e.g., [3]), falls short of the CI-chondrite value (4.04; [4]). Moreover, the boron isotopic compositions in the solar neighborhood determined by spectroscopy, albeit with large uncertainties ($^{11}\text{B}/^{10}\text{B} = 3.4 \pm 0.7$ in local diffuse clouds and $^{11}\text{B}/^{10}\text{B} = 3.7\text{--}4.7$ in the atmospheres of two nearby stars; e.g., [5–6]), are similar to that of the CI chondrites, implying that GCRs cannot be the sole source of boron and additional production mechanism(s), such as low-energy irradiation (e.g., [7]) and/or neutrino-spallation of ^{12}C during supernova explosions (e.g., [8]), are needed to account for the ^{11}B overabundance observed in the Solar System and elsewhere.

A wealth of bulk-chondrite data has shown that the average $\delta^{11}\text{B}$ value of each chondrite group (carbonaceous, ordinary, and enstatite) is only within a few permil of the CI-chondrite value (average $^{11}\text{B}/^{10}\text{B} = 4.04$; [4]). However, variations up to 25‰ in $\delta^{11}\text{B}$ are present both within individual chondrite groups and among the different chondritic meteorites ([4]; also see [9] for a detailed review). Large boron isotopic fractionations are known to occur between fluids and B-bearing minerals at low temperatures ([10]), and this might in part be responsible for the observed variations in chondritic meteorites. Given that CI chondrites have undergone severe aqueous alteration, how representative the CI $^{11}\text{B}/^{10}\text{B}$ ratio is of the solar value is called into question. It is therefore necessary to bring additional constraints from direct measurements of solar material. Literature data, albeit only a couple of them which are published in conference abstracts, have pointed to isotopically lighter boron isotopic compositions in the solar wind compared to that of CI chondrites, with $^{11}\text{B}/^{10}\text{B} = 3.78 \pm 0.06$ ($-64 \pm 15\%$) in a lunar soil sample [11] and 3.47 ± 0.28 ($-141 \pm 69\%$) in the shallow layer of an unpolished Itokawa olivine grain returned by the Hayabusa mission [12]. Although the isotopically light solar wind is expected in the context of Insufficient Coulomb Drag (ICD), the degree to which boron isotopes would fractionate between the bulk Sun and solar wind is only ~40‰/amu (assuming a mean charge state of 5+; e.g., [12–14]), considerably smaller than the observed solar wind values. Given the excellent agreement between the ICD model predictions of oxygen, nitrogen and noble gases and *Genesis* data (e.g., [14–16]), it is reasonable to assume that the actual isotopic fractionation of boron in the solar wind is close to the model estimate. Therefore, the Sun could be marginally lighter than CI chondrites (and the solar nebula) by ~20‰ (after correcting for ICD effects), as was implied by the data of [11], or could be as negative as -100% in $\delta^{11}\text{B}$ (if using the result from [12]). Given the discrepancy in the literature data, a better understanding of the solar $\delta^{11}\text{B}$ would be highly desirable to constrain the origin and evolution of this element in the Solar System.

We will perform boron isotopic analysis of unpolished Hayabusa olivine and pyroxene grains will be performed on the UCLA CAMECA ims-1290 ion microprobe in multicollection depth profiling mode by using a primary O^- beam generated by the Hyperion-II RF oxygen plasma source. Analytical development for such measurements is currently underway. One key issue in determining the solar wind boron isotopic ratios in Hayabusa samples is the instrument sensitivity. A low concentration of solar-wind implanted boron in the Hayabusa surface grains is expected given its natural (cosmic) abundance being ~6 orders of magnitude lower than that of oxygen. Fujiya et al., (2016) [12] provided an upper limit of B fluence of 4×10^{11} ions cm^{-2} based on the surface irradiation ages of 10^2 to 10^5 years inferred from the solar flare track densities [17] and ^{20}Ne flux of the bulk solar wind at 1 AU inferred from the *Genesis* data [14]. Assuming a 200-nm implantation depth from the grain surface, one should anticipate at most ~100 ppb in total (if distributed homogeneously) of solar-wind B in this shallow region of a grain. Therefore, the mass spectrometer needs to be sensitive enough to detect weak secondary ion signals and to measure the isotopic compositions with reasonable precision. We have also performed a sensitivity test with a San Carlos olivine standard in depth profiling mode on the ims-1290. Multicollection of boron isotopes and $^{29}\text{Si}^{3+}$ (used as a matrix normalizing element for estimating the concentration) with electron multipliers is chosen in this application to measure low secondary ion intensities and to improve the analytical precision. A small field aperture (FA) was used to ensure that only

signals from the center ($15 \times 15 \mu\text{m}^2$) of a $25 \times 25 \mu\text{m}^2$ raster square were collected. After summing up the counts over the cycles where signals were stable, we obtained an intrinsic B abundance in the olivine of ~ 30 ppb, which corroborates the result of [18], and we measure chondritic $^{11}\text{B}/^{10}\text{B} = 3.95 \pm 0.24$ (2σ , after correction for instrumental mass fractionation). The error on the isotopic ratio is comparable to those obtained in phases of similar B abundance (e.g., some melilite crystals in CAIs) on other large-radius ion microprobes. We can expect slightly better precision for the solar wind B as the abundance is higher, albeit distributed in very shallow surface layers.

The test result demonstrates that the ims-1290 ion microprobe has the required sensitivity to measure very trace amounts of boron for isotopic ratios. However, there are two issues that must be further addressed to ensure the success of this proposition. First, the boron abundance estimated here is not based on a matrix-matched standard, but rather on a NIST616 glass. This could affect the relative sensitivity factor (RSF), and thus give rise to inaccurate quantification of elemental concentrations. We will follow the method used in [19] to develop proper standards by implanting ^{10}B into terrestrial olivine and pyroxene to better quantify the RSF. In contrast to the elemental RSF, we do not expect that matrix effects on the IMF will be a problem for boron as extensive investigations show at most permil level deviations for various silicate glasses of different chemical compositions [20], which is negligible compared to expected analytical uncertainty. Second, signals from surface contamination on olivine appeared to have lasted 60–80 analysis cycles (the “knock-on effect”). If we perform B isotope analysis on the Hayabusa grains the same way as we did in this test, the SW signals can be significantly diluted by surface contamination. Therefore, we will pre-sputter a large area on the grain surface using an ion beam with low impact energy to remove surface contamination without eroding away much of the material of interest, and has been proven effective in the oxygen analyses of Genesis samples [16]. We will work out the optimum conditions (beam intensity, impact energy, pre-sputtering time) on a ^{10}B -implanted San Carlos olivine standard, and then apply it to cleaning the surface contamination on the Hayabusa samples. Some preliminary data from the development will be presented in the symposium.

References: [1] Reeves et al. 1970, *Nature* 226:727. [2] Meneguzzi et al. 1970, *Astro. Astrophys.* 15:337. [3] Krombel and Wiedenbeck 1998, *ApJ*. 328:940 [4] Zhai et al. 1996, *GCA* 60:4877. [5] Lambert et al. 1998, *ApJ*. 494:614. [6] Proffitt et al. 1999, *ApJ*. 516:342. [7] Ramaty et al. 1996, *ApJ*. 456:525. [8] Woosley and Weaver 1995, *ApJS*. 101:181. [9] Liu and Chaussidon, 2018, *Advances in Isotope Geochemistry: Boron isotopes*. Ch12. [10] Spivack and Edmond 1987, *GCA*, 51:1033. [11] Chaussidon et al. 1998. Abstract #1580, 29th LPSC. [12] Fujiya et al. 2016, *MAPS*. 51:1721. [13] Bochsler 2000, *Rev. Geophys.* 38:247. [14] Heber et al. 2012, *ApJ*. 759:121. [15] Marty et al. 2011, *Science* 332:1533. [16] McKeegan et al. 2011, *Science* 332:1528. [17] Keller and Berger 2014 *EPS*. 66:71 [18] Ottolini et al. 2002 *American Mineralogist* 87:1477. [19] Steele et al. 2017, *GCA*, 201:245. [20] Chaussidon et al. 1997, *Geostand. Newsletter* 21:7

Visualization on XCT data of Hayabusa samples: 3D printings and VR

Junya Matsuno¹ and Akira Tsuchiyama¹
¹*Kyoto University*

It is important to carry out mineralogical and petrological descriptions using non-destructive analysis, especially for precious and small samples such as cosmic dust and returned samples from Itokawa. X-ray CT (XCT) has been used widely for these samples to observe three dimensional (3D) structures. In order to survey the 3D data, it is necessary to project them on a two-dimensional screen or create direct 3D models. Recent developments in 3D technology are remarkable, and various visualization technologies are emerging. Here we introduce two kinds of visualization methods: (1) 3D printings and (2) virtual reality (VR) and demonstrate these products applying XCT data of Hayabusa samples obtained in SPring-8 BL47XU [1].

(1) 3D printings: There are several methods for the 3D printings, basically laying out one layer at a time and outputting a 3D model. Matsumoto et al. [2] introduced a method of laying gypsum powder in layers and printing a liquid adhesive from a printer head. Although this method is relatively inexpensive, the structure inside the 3D model cannot be observed since the gypsum is opaque. In this study, we tried a method of repeating the output of ink-like ultraviolet (UV) curable resin and UV irradiations. Some of the ultraviolet curing resins are transparent under visible light, and by outputting together with opaque color inks, 3D internal structures can be observed directly. The surface rendering image (or called isosurfaces) of each mineral can be extracted only by simple binarization processing from the set of slice images using a plugin of ImageJ [3,4]. Object500 Connex performed a 3D printing of Hayabusa sample (RA-QD02-0024) and three inks of cyan, magenta and transparent were used. By assigning a transparent color to the olivine and low-Ca pyroxene widely distributed in the sample, inclusions such as plagioclase and high-Ca pyroxene could be observed.

(2) VR: In recent years, by preparing two screens for stereoscopic vision on smartphones and passing through lenses for stereoscopic viewing, it is possible to easily recognize 3D images. Stereoscopic goggles for smartphones and the dedicated goggle type devices have been available commercially, and these are called VR technology and VR goggles. It is possible to cause the screen to follow the direction in which the observer points the face due to the line of sight sensor. Since it can be introduced easily at this time, we adopted a web VR that allows you to upload VR data to a web server and run it on the web browser of the smartphone. We used A-Frame [5] for the implementation which is one of web frameworks for building VR based on HTML. The isosurfaces created by ImageJ were converted to an appropriate file format using Blender [6] and placed in the VR space. By entering URL for the VR web server on the web browser such as Firefox and wearing smartphone VR goggles installed an android smartphone, we could easily access the VR space and observe 3D shape of Hayabusa samples.

It was very efficient to actually perform 3D observation on 3D models and via VR space. At the same time, it is not necessary to install special software for accessing 3D information by using these two methods. This means it is also effective for various analysts to share 3D data of future's samples from sample return missions. In addition, it was also very popular as these were used for exhibitions such as open campuses, so these methods were also effective outreaching.

References

[1] Tsuchiyama A. et al. 2011. *Science* 333, 1125 [2] Matsumoto T. et al. 2016. *GCA* 187, 195 [3] Schneider C. et al. 2012. *Nature methods* 9(7), 671 [4] Doube M. et al. 2010. *Bone* 47, 1076 [5] <https://aframe.io> [6] <https://www.blender.org>

Advanced Curation Development of Tools and Methods for Microparticle Processing

Christopher Snead¹, Francis McCubbin², Jeffrey Jang³, Thomas Cowden⁴ and Zia Rahman⁵

^{1,5}*JETS, NASA Johnson Space Center, Houston TX 77058, USA.*

²*NASA Johnson Space Center, Houston, TX 77058, USA.*

^{3,4}*Texas State University, 601 University Drive, San Marcos, TX 78666. USA.*

Introduction: The Astromaterials Acquisition and Curation Office at NASA Johnson Space Center is currently developing new tools and methods for the collection, storage, handling and characterization of particles $<100\mu\text{m}$ in diameter, or microparticles [1]. Astromaterials Curation currently maintains four microparticle collections [2]: Cosmic Dust that has been collected in Earth's stratosphere by ER2 and WB-57 aircraft, Comet 81P/Wild 2 dust returned by NASA's Stardust spacecraft, interstellar dust that was returned by Stardust, and a portion of asteroid Itokawa particles that were returned by JAXA's Hayabusa spacecraft. NASA Curation is currently preparing for the anticipated return of two new astromaterials collections – asteroid Ryugu regolith to be collected by Hayabusa II spacecraft in 2021 (a subset of samples will be provided by JAXA as part of an international agreement) [3], and asteroid Bennu regolith to be collected by the OSIRIS-REx spacecraft in 2023 [4]. In order to maximize the scientific yield from these valuable acquisitions, it will be necessary to develop methods that extend our current microsample handling capabilities. Here we describe recent progress in the development of sample handling techniques that will enhance our microparticle curation capabilities.

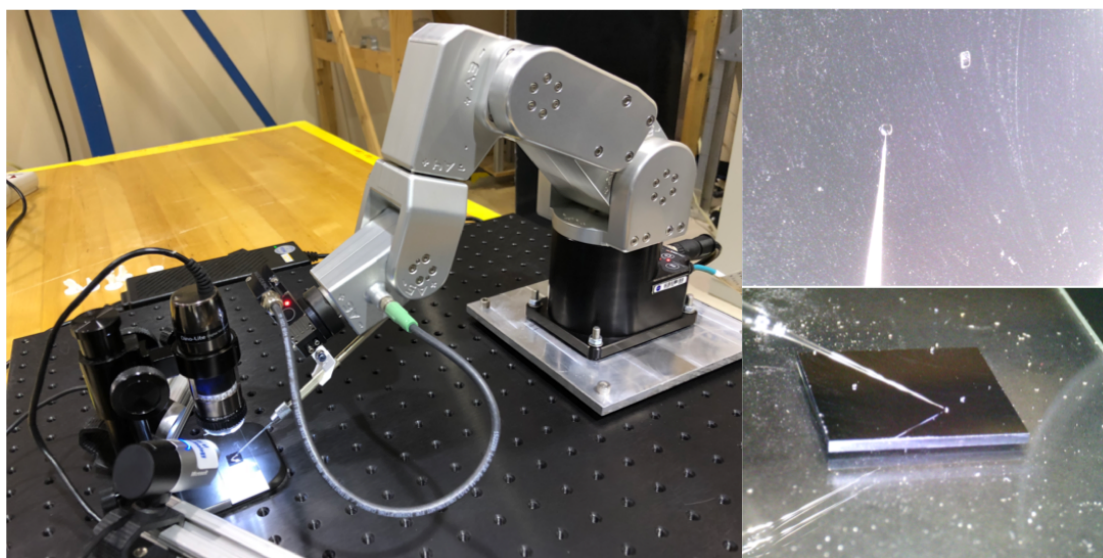


Figure 1: Meca500 robot arm manipulating 0.2mm magnetite particles on 1cm^2 silicon chip.

Six-Axis Robot Arms for Particle Manipulation: We have been investigating the use of compact six-axis robot arms to facilitate microsample handling within gloveboxes. 3-axis micromanipulators are currently in use in the Stardust and Cosmic Dust curation facilities; although they have been extremely successful for activities involving the transfer of isolated particles in the 5-20 μm range (e.g. from microscope slide to epoxy bullet tip, beryllium SEM disk), their limited ranges of motion and lack of yaw, pitch and roll degrees of freedom restrict their utility in other applications. For instance, curators removing particles from cosmic dust collectors by hand often employ scooping and rotating motions to successfully free trapped particles from the silicone oil coatings. While cosmic dust curators have been remarkably successful with these kinds of particle manipulations using handheld tools, operator fatigue limits the number of particles that can be removed during a given extraction session. The challenges of microparticle curation will be exacerbated by dry N_2 environments of sample cabinets (i.e. gloveboxes) in which Hayabusa2 and OSIRIS-REx samples will be processed. We have recently developed a robotic micromanipulation test platform using the Meca500 six-axis robot arm with $5\mu\text{m}$ reproducibility and an observed step resolution of $1\mu\text{m}$. The Meca500 system we designed is controlled via a custom graphic user interface (GUI) either by clicking control buttons within the GUI, or by PC mouse control within a range-of-motion field. Our GUI also includes embedded video feed from a Dino-Lite 5 megapixel USB microscope and a second USB camera mounted at 45 degrees relative to the sample surface for positioning/altitude information. In addition to the GUI control system, we are investigating other means of controlling the Meca500, including videogame controllers and haptic feedback devices.

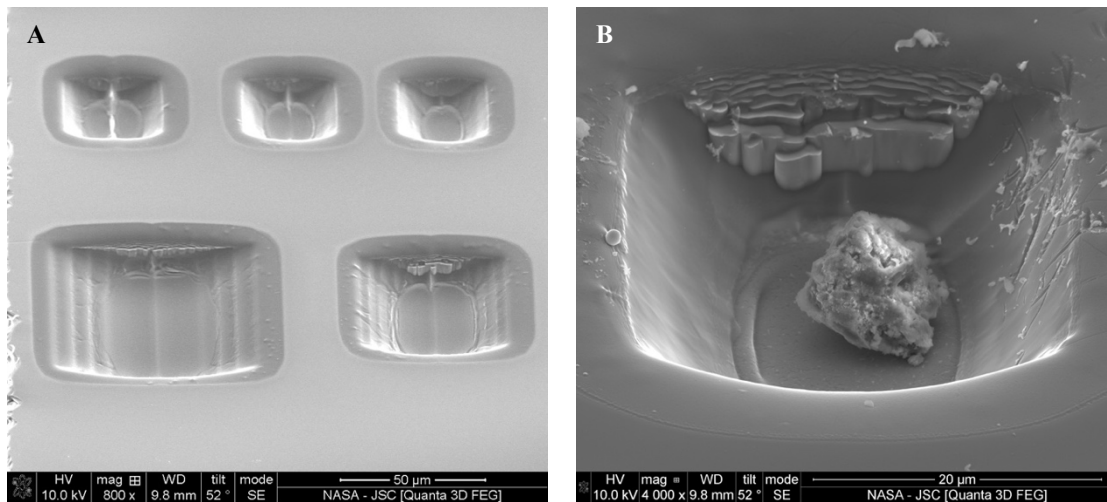


Figure 2: A) Particle receptacles produced via FIB milling. B) Secondary electron image of 10µm particle in well.

Charge-Dissipative Substrates: Microparticles removed from cosmic dust collectors have traditionally been stored and distributed to investigators in glass concavity slides; we have identified friction between these slides and particles as a major source of sample electrification. In cases where substrate transparency is not a curation requirement, the glass slide may be replaced with a charge-dissipative substrate such as silicon. Particles retain a high level of visibility on such substrates, and triboelectric charging [5] is significantly reduced such that microparticles can be reliably manipulated in ambient atmospheric conditions without the use of a Po-210 source. Recently, we have experimented with producing storage receptacles in silicon using focused ion beam (FIB) milling. We used an FEI Quanta 3D-FEG Focused Ion Beam (FIB) to mill several shallow (<20µm) depressions between 30µm² and 80µm² into the surface of a silicon chip; material was sputtered using a 65nA Ga⁺ beam at 30kV. A 10µm particle of CM2 meteorite was placed into one of the FIB-produced wells using a micromanipulator. The charge-dissipative nature of the Si chip enabled us to successfully acquire a secondary electron image of the stored particle using a 190pA beam current at 10kV. Storage substrates that also enable electron beam imaging and characterization are desirable, as they minimize the need for high-risk microparticle transfers between storage and analysis substrates. We are currently investigating this technique to produce storage wells in other charge-dissipative substrates that could enable in-situ elemental analyses.

References:

- [1] McCubbin F. M. and Zeigler R. A. (2017) *Hayabusa 2017 Symposium of the Solar System Materials*. [2] Allen C C, et al. (2011) *Chemie der Erde-Geochemistry*, 71(1), 1-20. [3] Minamino H. et al. (2012) *Asteroids, Comets, Meteors*, Abstract #6188. [4] Lauretta D. S. (2012) *LPS XLIII*, Abstract #2491. [5] Matsusaka S. et al. (2010) *Chemical Engineering Sci.*, 65, 5871-5807.

A chain of events-from cosmic to terrestrial- leading to origin and development of the Homo genus

Gennady G. Kochemasov

IGEM of the Russian Academy of Sciences, 35 Staromonety, 119017 Moscow, Russian Federation, kochem.36@mail.ru

The cosmic pair Earth-Moon (Fig. 1) moves in the elliptical circumsolar orbit with periodically changing accelerations. That is why both bodies are warped by a series of waves of various lengths (harmonics). The mechanical energy of movement is transferred into a heat energy melting the bodies' mantles-making asthenospheres. Produced basaltic liquids are lifted up into crusts for "healing" lost angular momenta because of decreased rotation rates of bodies. The small satellite is heated and melted first. Its crustal basalts have ages 3-4.5 billion years. Much more massive Earth-81 times- is proportionally heated and melted much later: 3-4.5 billion divided by 81 gives 37-55 million y. (the proportion is according to the first Newton's law). This is the Mz-Cz age – age of main oceanic basaltic covers and many other significant geological and biological events.

The Mz-Cz activation ("explosion"), the mantle melting and enormous degassing leads to terrestrial relief sharpening (uplifts to 1-2 kms are measured). This is especially noted at ancient terrains of the Archean platforms (cratons) [1]. Most raising continent is the African one (Fig. 2). It raised to 300 meters in the Early Miocene and to 900 m in the Late Pliocene and Pleistocene [1]. The most actively uplifting is the bulge of the Eastern Africa where remains of ancient hominids are actively searched. There are found numerous remains of australopithecines of several species. The oldest known up to now have an age about 6 million years (Pliocene-Miocene). The first hints to genus *Homo* are in a fossil jaw from Afar having an age about 2.85 million y. BP [2, 3]. The earliest representatives of the genus *Homo* – *Homo habilis* were not perfect (complete) bipedalists (though australopithecines already walked on two legs). The process of taking off hands from earth accompanies tectonic uplift because a human body have to increase its height to diminish a ratio of weight to height required by a raising tectonic block increasing its angular momentum. Thus, a body grows, straightens, a head, brain, and sapientation increase.

The further development of the genus *Homo* – from *H. habilis* through *H. erectus/ergaster* to *H. sapiens* – was on the background of the constantly rising (uplifting) African continent Increasing its angular momentum. This required an anti-action in the anthroposphere – diminishing bodies' mass or a ratio of mass to height (stature). Two strategies were observed showing in real morphological peculiarities. Increased stature of small mass men as in nilotes of the Eastern Africa were the tectonic "bulge" rises most actively. Another striking feature is development of the steatopygism – growing the lower part -buttocks of a body. This redistribution of mass lowers the center of gravity, thus the angular momentum. This body form is observed among ancient and present bushmen and gottentotes populated in the past the whole Africa (Fig. 3, 4, 5).

In brief, to understand origin and evolution of the genus *Homo*, one must consider a tectonical background of an area where this happened (tectonoanthropology). Only in the equatorial rapidly tectonically rising domain it could be realized (angular momentum consideration)- in the African continent. Such tectonic and geographical feature appeared because of a tremendous planetary cosmic event –the Mz-Cz explosion in heating, melting, and degassing the mantle. It was a sequence of the planet Earth moving in keplerian elliptical orbit with periodically changing accelerations. The Earth's mass was a critical parameter determining a time localization of this event (the Newton's law of inertia). A cosmic scale for this event is the Moon with its small mass and the early Archean "basaltic explosion".

References:

- [1] Artyushkov E.V., Hofmann A. The Neotectonic crustal uplift on the continents and its possible mechanisms. The case of Southern Africa // *Surv. Geophys.*, 1998, v. 15, p. 515-544.
- [2] Villmoare B., kimbel W.H., Sayoum C. et al. Early *Homo* at 2.8 Ma from Ladi-Geraru, Afar, Ethiopia // *Science*. 2015. V. 347. P. 1352-1355.
- [3] Derevianko A.P. Three global human migrations in Eurasia. V. II. The original peopling of Northern, Central and Western Central Asia. Ed.-in-chief M.V. Shunkov, Novosibirsk, IAET SB RAS Publishing, 2017. 884 p. (In Russian)



Fig. 1. Earth and Moon in cosmos, PIA17170

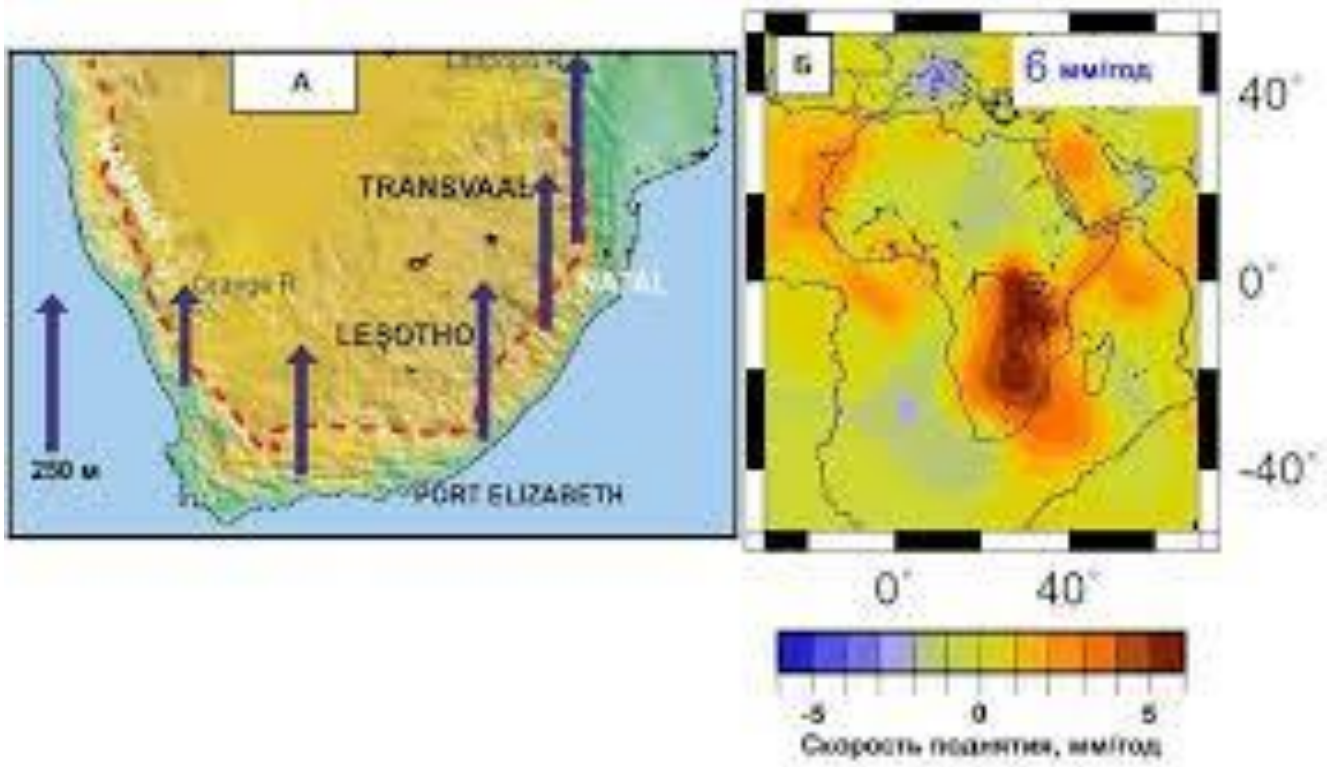


Fig. 2. Uplifting Africa

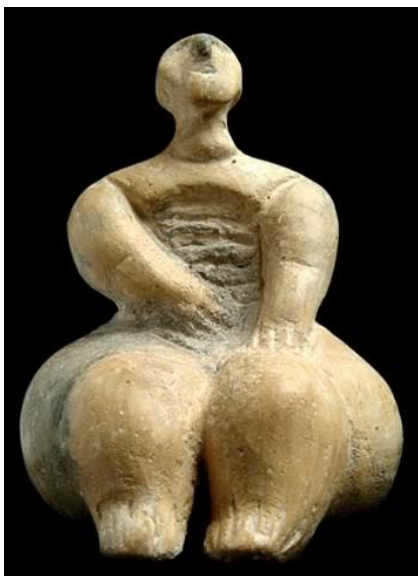


Fig.3. Ancient steatopygie



Fig.4, 5. Present steatopygie



SARTJER, THE HOTTENTOT VENUS.
 Sketched in London in 1801.

A Negroe is 22 years old is 4 feet 10 ins high, broad has (as we are told) a good capacity for food in the proportion of a Cock at the Cape of Good Hope. Her Country is situated not far from 600 Miles from the Cape. The Constitution of several women in this and 1811 has by water for a more perfect, a little of Beauty, or small well of Nature will produce several of these. Their principal trade is in cattle skins & Tallow. They are also a Nation of small stature, very little force; the Dutch could not carry them into Europe; and did them when ever they found them. - 5th Part 1801. - 86

The effect of possible contamination from sample holders on samples returned by Hayabusa2

N. Shirai¹, Y. Karouji², K. Kumagai³, M. Uesugi⁴, K. Hirahara⁵, M. Ito⁶, N. Tomioka⁶, K. Uesugi⁴, A. Yamaguchi⁷, N. Imae⁷,
T. Ohigashi⁸, T. Yada², M. Abe²

¹*Tokyo Metropolitan University*, ²*Japan Aerospace Exploration Agency*, ³*Marine Works Japan Ltd.*, ⁴*Japan Synchrotron Radiation Research Institute*, ⁵*Osaka University*, ⁶*Japan Agency for Marine-Earth Science and Technology*, ⁷*National Institute of Polar Research*, ⁸*Institute for Molecular Science*

Introduction: For technical developments in handling, transfer and analysis of samples returned by the Hayabusa2 spacecraft, special team (Phase 2 curation team) was organized by Extraterrestrial Sample Curation Center of Japan Aerospace Exploration Agency. A sample transfer container among facilities and sample holders which are applicable to multiple analytical instruments such as SR-CT, SEM, TEM, STXM and NanoSIMS were newly developed, and Antarctic micrometeorites were successfully analyzed by using the transfer container and holders minimizing sample lost and sample damages [1]. As sample holder comes into contact with samples, it could cause contamination of metallic elements, organic materials, volatile species such as water and noble gasses. In this study, two materials (gecko tape made by carbon nanotubes, and polyimide film) which were used as the new sample holders were analyzed by instrumental neutron activation analysis (INAA) and/or instrumental photon activation analysis (IPAA). Besides these materials, quartz plate was also analyzed. Quartz plate was used for the preservation and transfer of Hayabusa-returned samples [2]. Based on the elemental abundances of these three materials, any contamination from these three materials was evaluated.

Sample and methods: Gecko tape samples were developed by Nitto Denko Corporation and Osaka University. Quartz plate (7 mmφ x 1 mm) and polyimide film were provided from Fujiwara Scientific Co. Ltd and Protein Wave Co. Ltd, respectively. Before analysis, quartz plate was treated by both full-course and acid-alkali cleanings [3]. Polyimide film was washed by ethanol at an ultrasonic bath. INAA and IPAA were performed at Kyoto University Research Reactor Institute (KURRI). For INAA, the three materials were irradiated for 10s and 4 hrs at the pn-3 and pn-2 of KURRI, respectively. Gecko tape and quartz plate were analyzed by IPAA. The irradiation was carried out using the linear accelerator at KURRI operated at 30 MeV electron beam energy and 102 μA current for 36 hrs.

Results and Discussion: Ten elements (Na, Al, Cr, Mn, Fe, Ni, Eu, W, Au and Th), fourteen elements (Na, Mg, Cl, K, Cr, Mn, Fe, Co, Ni, Y, Zr, Sb, Hf and Au) and fourteen elements (Na, Al, K, Sc, Ti, Cr, Zn, Ga, Br, Sb, La, Eu, Ir, Au) could be determined for gecko tape, quartz plate and polyimide film, respectively. Europium, W, Au and Th contents for gecko tape, and Ti for polyimide film are higher than those for carbonaceous chondrites. Other elements abundances for these three materials are about ten times lower than those for carbonaceous chondrites. Assuming that 1% of contamination (in mass) from these three materials to carbonaceous chondrites, elemental contributions are estimated to be 1.5% for Cl, 7% for Ti, 8% for Eu, 4% for W, 7% for Au and 35% for Th. Elemental contributions of other elements were less than 1% for carbonaceous chondrites, indicating that contaminations of these three materials could be negligible for other elements.

Groups of carbonaceous chondrites can be distinguished from each other based on elemental ratios for refractory elements to moderately volatile and/or volatile elements (e.g., Zn/Cr). In order to define the effect for contamination from sample holders (gecko tape, quartz plate and polyimide film), elemental ratios (Mn/Cr, Zn/Cr, Ga/Cr, Sb/Cr, Ir/Cr and Au/Ir) of CM chondrite as an analogue of Hayabusa2-returned sample contaminated from sample holders were estimated. In the case of quartz plate and polyimide film, 100% by mass contamination could not affect elemental ratios of CM chondrite. In contrast, more than 0.3% by mass contamination from gecko tape may affect Au/Cr ratio of CM chondrite, implying that careful attention is required when the Au/Cr ratio is used for discussion. Although more than 20% by mass contamination from gecko tape could affect elemental ratios (Mn/Cr, Zn/Cr, Ga/Cr, Sb/Cr and Ir/Cr), such contamination is not highly likely and could be optically detected.

References

[1] Uesugi M. et al. (2017) Hayabusa Symp. 2017 [2] Yada T. et al. (2013) MAPS 49, 135-153. [3] Karouji Y. et al. (2014) Chikyukagaku 48, 211-220.

The NASA Cosmic Dust Collection: Current Status and Advanced Curation Planning

Marc Fries¹, Francis McCubbin¹ and Ryan Zeigler¹

¹NASA Curation, Johnson Space Center, Houston, TX USA

Cosmic dust, composed of what is otherwise known as interplanetary dust particles (IDPs), has been collected by NASA U-2, ER-2, and WB-57 aircraft in the stratosphere on oil-coated Lexan surfaces since 1981. This collected material composes the NASA Cosmic Dust collection curated at the Johnson Space Center. Many thousands of 2 – 100 μm particles have been collected, and it is believed that both comet and asteroid samples are present. Several cosmic dust collections have been flown during periods that coincided with prominent meteor streams and low velocity fresh cometary dust trails. These samples therefore have great scientific value. This material is curated by the NASA Curation office and is made available for allocation to the international scientific community through a sample requests with input from the Curation Analysis and Planning Team for Extraterrestrial Materials (CAPTEM).

Collection and curation of the Cosmic Dust collection is now in its 37th year. Material is collected during regularly-scheduled flights of NASA high altitude aircraft at altitudes of ~18-25km on plates coated with silicone oil. Particles are extracted from the oil and rinsed to remove oil in an ISO 5 cleanroom, and then given a preliminary examination. SEM and EDS analysis of each particle facilitates a tentative classification and provides requestors enough information to make an informed sample request. Approximately 1/10th of the collection consists of extraterrestrial particles which may originate from all bodies in the Solar System, with cometary and asteroidal sources predominating. The remaining collection of terrestrial particles includes volcanic debris, rocket exhaust components, aerospace debris, and other material that has been requested for study and is scientifically valuable in its own right.

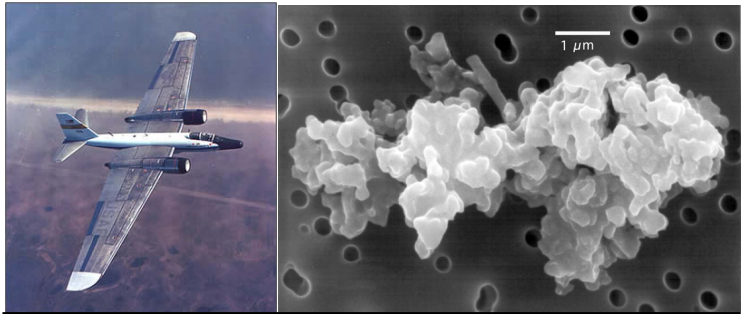


Figure 1: LEFT: One of the NASA WB-57 high altitude research aircraft used to collect Cosmic Dust in the stratosphere. RIGHT: A Cosmic Dust particle of chondritic composition, which was then allocated to a researcher for analysis.

NASA Curation actively strives to improve current collections in order to increase the scientific, historical, and cultural value of NASA's collections through the Advanced Curation program. In accord with this goal, Advanced Curation efforts for improving the Cosmic Dust collection include investigation of expanding Cosmic Dust collection through NASA's high-altitude scientific balloon program, addition of oil-free collection methods as a supplemental collection technique, and investigation of potential improvements in sample processing and preliminary data analysis. Short-term plans include development of a prototype high-altitude balloon collector for Cosmic Dust. This will be an undergraduate student project involving engineering students from Texas A&M University, with at least one balloon flight expected in 2019. "Dry", or oil-free, collection methods will also commence testing. While silicone oil is an efficient collection medium, it introduces contamination that causes interference with some measurements such as analysis of organic compounds, oxygen isotopes, and primitive silicate glasses. The first dry collection trials will use foam collectors on the balloon prototype, as the low air speed collection afforded by a balloon-based system may be especially suitable for foam collectors. Future trials may expand into 3D printed collectors optimized for dry collection, depending on results from the foam trials. In addition, data from the entire history of the Cosmic Dust program will be collated into comprehensive statistics on the types of particles collected, collection efficiency, and other factors.

The NASA Cosmic Dust program has enjoyed almost four decades of successfully sampling the Earth's natural infall of extraterrestrial material. The material has been carefully curated and provided to the international scientific community and this will continue into the indefinite future. NASA's Advanced Curation efforts will continue to improve the collection in response to scientific need, using the most up to date technology and methods available.